Fisheries and Oceans Canada | Pêches et Océans Canada
Ecosystems and Oceans Science | Sciences des écosystèmes et des océans

Canadian Science Advisory Secretariat (CSAS)

Research Document 2023/047

Quebec Region

An Integrated Population Model for St. Lawrence Estuary Belugas (*Delphinapterus leucas*)

M. Tim. Tinker[1], Arnaud Mosnier[2], Anne P. St-Pierre[2], Jean-François Gosselin[2], Stéphane Lair[2], Robert Michaud[2], Véronique Lesage[2]

[1] Nhydra Ecological Consulting
St. Margaret's Bay, NS B3Z

[2] Maurice Lamontagne Institute
Fisheries and Oceans Canada
850, route de la Mer
Mont-Joli, Québec, G5H 3Z4

July 2024

Canada

Foreword

This series documents the scientific basis for the evaluation of aquatic resources and ecosystems in Canada. As such, it addresses the issues of the day in the time frames required and the documents it contains are not intended as definitive statements on the subjects addressed but rather as progress reports on ongoing investigations.

Published by:

Fisheries and Oceans Canada
Canadian Science Advisory Secretariat
200 Kent Street
Ottawa ON K1A 0E6

http://www.dfo-mpo.gc.ca/csas-sccs/
csas-sccs@dfo-mpo.gc.ca

ISSN 1919-5044
ISBN 978-0-660-72095-1 Cat. No. Fs70-5/2023-047E-PDF

Correct citation for this publication:

Tinker, M.T., Mosnier, A., St-Pierre, A.P., Gosselin, J-F., Lair, S., Michaud, R. and Lesage, V. 2024. An Integrated Population Model for St. Lawrence Estuary Belugas (*Delphinapterus leucas*). DFO Can. Sci. Advis. Sec. Res. Doc. 2023/047. iv + 61 p.

Aussi disponible en français :

*Tinker, M.T., Mosnier, A., St-Pierre, A.P., Gosselin, J-F., Lair, S., Michaud, R. et Lesage, V. 2024. Modèle de population intégrée des bélugas (*Delphinapterus leucas*) de l'estuaire du Saint-Laurent. Secr. can. des avis sci. du MPO. Doc. de rech. 2023/047. iv + 65 p.*

TABLE OF CONTENTS

ABSTRACT

St. Lawrence Estuary (SLE) belugas are a relict population from the Wisconsin glaciation that probably numbered 10,000 or more in the mid-1800s. As a result of intensive harvests starting in the 1700s, combined with environmental degradation, the population was greatly reduced by the 1980s, leading to their classification as 'Endangered' by the Committee on the Status of Endangered Wildlife in Canada in 1983 and to the implementation of a series of programs to monitor the health, demography and dynamics of the population. SLE beluga are exposed to multiple stressors, including environmental contaminants, prey reductions, toxic algal blooms, vessel noise, and various other risk factors. We compiled available data sets on abundance trends, mortality patterns, cause of death and age structure, and used these data to develop and fit an integrative population model (IPM) with the aim of assessing the current status and trends of the SLE beluga population, estimating the risk of quasi-extinction under different scenarios, and identifying new recovery targets for this endangered population. The process model consisted of a stage-structured projection matrix model that incorporated age and sex differences in survival and reproduction. We used Bayesian hierarchical methods to estimate time and density varying vital rates by simultaneously fitting to aerial survey data (from visual and photo-based methods), data on the age structure of the living population and the death assemblage (based on age estimation of stranded carcasses) and cause-of-death analyses of the relative frequencies of natural mortality, harvest mortality, and dystocia/postpartum mortality of adult reproductive females. We found evidence for increased density-dependent (DD) and density independent (DiD) mortality over the 20th century that prevented rebound of the population after the cessation of human harvest in 1979. Our model results showed complex patterns of age and sex specific mortality trends over recent decades: for example, DiD hazards affecting older animals declined between 2010-2018, possibly reflecting reduced cancer rates associated with lower contaminant exposure, resulting in an increasing trend in abundance. In contrast, DD mortality of calves increased over that period, along with dystocia/postpartum mortality of pregnant females, with the result that the proportion of young animals in the living population decreased while the proportion of young animals in the death assemblage increased. These demographic shifts, combined with an uptick in DiD hazards after 2018, caused abundance trends to stabilize after 2018 and possibly begin to decline, although the higher level of uncertainty typical of the end of a time series makes the current trend uncertain.

INTRODUCTION

The St. Lawrence Estuary (SLE) beluga (*Delphinapterus leucas*) is a relict population from the Wisconsin glaciation that has likely established itself in the SLE some 10,000—12,000 years ago when the Champlain Sea covered most of the St. Lawrence Lowland (Harington 2008). The population appears to undertake only limited seasonal movements, remaining in the SLE year-round with part of the population moving into the northwestern Gulf of St. Lawrence during winter (see Mosnier et al. 2015 for a review). While maximum population size is uncertain, historical harvest records and modelling suggest a population likely numbering around 8,000—10,000 at the end of the 19th century (Reeves and Mitchell 1984, Mosnier et al. 2015). Intense exploitation has considerably reduced the population, which was estimated at a few hundred individuals in the late 1970s (Pippard and Malcolm 1978, Sergeant and Hoek 1988, Kingsley 1998). These results led to their classification as 'Endangered' by the Committee on the Status of Endangered Wildlife in Canada in 1983 (Pippard 1985), and to the implementation of a series of programs to monitor the health, demography and dynamics of the population (DFO 2014, Lesage 2021; also see below). These programs have been rigorously maintained over time, leading to one of the longest multi-faceted datasets for a cetacean, and making SLE beluga the best monitored beluga population (Norman et al. 2022), and among the best monitored cetacean populations in the world.

Following the ban of beluga hunting in 1979, the population continued to show little signs of recovery. While adult mortality rate appeared comparable to Arctic populations and emigration rate minimal, recruitment rate was deemed to be low, and identified as the likely cause for the apparent stagnation of the population (Hammill et al. 2007). These observations suggested that population growth in the early 1980's was constrained by anthropogenic stressors or sub-optimal environmental conditions associated with local climate, or both (Lesage 2021). In the 1980s, monitoring programs confirmed that the population was small (Kingsley 1998), and amongst the most contaminated marine populations on the planet (Martineau et al. 1987, 1994, Wagemann et al. 1990, Béland et al. 1993, Lebeuf 2009), with an incidence of tumours and other severe lesions much higher than observed in any other wild mammal population (Béland et al. 1993, De Guise et al. 1994).

SLE beluga are exposed to multiple stressors in addition to contaminants, thus identifying a single cause for their apparent lack of recovery might be challenging (Beauchesne et al. 2020, Lesage 2021). SLE beluga live in a major seaway to central North America, and are chronically exposed to noise from shipping, and to multiple ferries, recreational vessels and a highly developed whale-watching industry operating within their habitat (Simard et al. 2010, 2014, McQuinn et al. 2011, Gervaise et al. 2012, Chion et al. 2021). These operations and associated noise may interfere with beluga normal activities, and can reduce the potential for females to maintain contact with their newborn calf (Richardson et al. 2013, Erbe et al. 2018, Southall et al. 2021, Vergara et al. 2021). Overfishing and climate variability and warming have affected community structure of many ecosystems including the Estuary and Gulf of St. Lawrence (Worm and Myers 2003, Savenkoff et al. 2007, Cairns et al. 2014). These factors, and the population increase of potential competitors such as grey (*Halichoerus grypus*) and harp (*Pagophilus groenlandicus*) seals (Hammill and Sauvé 2017), have likely modified the St. Lawrence trophodynamics (Savenkoff et al. 2007) with potential consequences for prey quality and availability to SLE beluga (Lesage et al. 2020). Toxic algal blooms occur sporadically in the St. Lawrence Estuary; in 2008, mortality of multiple marine species, including beluga, following a well-documented event, highlighted the vulnerability of the population to such stochastic events (Starr et al. 2017).

A large die-off of newborn calves (5 to 6-fold typical values) in 2012 raised new concerns over the status of the population, triggering a thorough review of the multiple time series available to document the evolution of their health, population dynamics, and various threats over time (DFO 2014). As part of this exercise, a population dynamics model integrating multiple data sources issued from long-term monitoring programs was implemented in a Bayesian framework to provide a biologically plausible context to observed changes in demography (Mosnier et al. 2015). This analysis indicated that several aspects of SLE beluga demography had changed over time. The population had shifted from a stable to unstable state around 1999, when an increased interannual variability was estimated in calf mortality. The proportion of juveniles in the population was also estimated to be smaller during the latter period (33% vs. 42% pre-1999), whereas female reproductive cycles were estimated to have changed toward the end of the time series (when calf mortality was abnormally high), with peaks every two years and about 50% of the females being pregnant, instead of the normal three-year cycle and one-third of the females being annually pregnant. As a result, and given the low abundance estimate obtained in 2009 (Gosselin et al. 2014), the model predicted a population shifting from a stable or slightly increasing trend between 1990-2002 (~0.13% yr^{-1}), toward a declining trend (~ –1.13% yr^{-1}) between 2003-2012 (Mosnier et al. 2015).

Reasons for this apparent decline and increased calf mortality were uncertain (DFO 2014, Lesage 2021). The model-predicted decline coincided with periods of extreme warmth in the Estuary and Gulf of St. Lawrence (Galbraith et al. 2022), with still unclear effects on the trophodynamics and community structure of these ecosystems. Over the same period, we observed a decrease in the amount of essential fatty acids in SLE beluga blubber, suggesting poorer body condition in more recent years (Bernier-Graveline et al. 2021). While some toxic substances such as PCBs and DDTs have declined in the environment and tissues of beluga following their ban (Lebeuf et al. 2014a), others such as polybrominated flame retardants (PBDEs) have increased exponentially in the environment and are at maxima in beluga tissues (De Wit 2002, Lebeuf et al. 2014a, 2014b, Simond et al. 2017). Shipping traffic has remained high in many parts of the SLE beluga habitat, with no indication of a decrease over time (Ménard et al. 2014). Activities directed toward beluga that might interfere with parturition or lactation have increased in sectors used particularly by females and calves, potentially interfering with critical behaviours (Ménard et al. 2014, Lair et al. 2016). Necropsy analyses of recovered carcasses showed an apparent increase in mortality of adult females associated with dystocia or postpartum complications at birth (Lair et al. 2016). At the same time, other factors appeared inconsistent with a declining population, in particular the fact that the incidence of cancers declined in animals born in the 1970s or later (Lair et al. 2016), likely increasing adult survival (Lesage 2021).

Since the last assessment in 2013 (DFO 2014), multiple aerial surveys have been conducted for beluga abundance estimation, and additional data has been acquired on health and demography, as well as on environmental factors and threats (e.g., reviewed in Lesage 2021; see also St-Pierre et al. 2023). A population viability analysis incorporating PCBs as a proxy for contaminant loads, noise effects on prey access, and prey abundance as potential threats to recovery has predicted that elevated sea surface temperatures in the summer months can affect calf survival negatively, whereas biomass of spring herring and demersal species, and sea ice extent and volume can affect it positively (Williams et al. 2021). Prey availability and other environmental factors were not good predictors of adult female mortality and fecundity, suggesting that such effects on survival or reproductive success would likely arise from extreme changes in adult female body condition. Williams et al. (2021) concluded that in order for the population to cope with the negative effects of climate warming, actions would need to be undertaken on all three stressors for the population to increase. It also became clear from this analysis that the recovery targets established at a growth rate of 2% per year, and a population

size of 7,000 (i.e., 70% of historical size) by year 2100 were unlikely to be met, even under the most optimistic scenarios (Williams et al. 2021).

In this study, we aim to assess the current status and trends of the SLE beluga population, estimating the risk of quasi-extinction under different scenarios and identifying new recovery targets for this endangered population using the best available information. We updated the previous model (Mosnier et al. 2015) in multiple ways, for instance: we extended the time series incorporated in the previous model to 2022, and included population size estimates obtained from both visual and photographic aerial surveys based on recent analyses (St-Pierre et al. 2023); we incorporated several new data sources, including age-at-death from carcasses; the process model is now more finely structured by age and includes density-dependence, is extended to include males and not just females, includes multiple causes of death, and allows for different scenarios to be examined for their effect on recovery and risk of quasi-extinction. We therefore expected to gain new insights into demographic processes and factors affecting recovery of the SLE beluga population.

METHODS

DATA SOURCES

The demography and dynamics of the SLE beluga population has been monitored since the 1980s through three main programs. First, systematic aerial photographic and visual surveys covering the entire summer habitat of SLE beluga were carried out on a regular basis since 1988 to monitor abundance (reviewed in St-Pierre et al. 2023). Length measurements of animals in the photographs obtained from these surveys have been used to monitor stage composition of the population: animals ≤ 0.5 body length of adjacently swimming animals were considered as newborn calves or yearlings (Gosselin et al. 2014; St-Pierre et al. 2023). Second, a program using a consistent methodology to monitor the number, age- and sex-composition of stranded beluga carcasses has been maintained since 1983 (Lesage et al. 2014, Lair et al. 2015, Lesage 2021). Full necropsies of nearly all relatively fresh individuals recovered through this program also allowed for a systematic and thorough examination of pathologies and diagnosis of cause of death (Lair et al. 2016). Finally, skiff surveys conducted each year since 1989 for beluga photo-identification provided annual indices of the proportion of calves and juveniles in the SLE beluga population (Michaud 2014).

Aerial survey data

Photographic strip-transect surveys provided abundance estimates and age composition every 3 to 5 years between 1988 and 2009, with a 10 yr gap between 2009 and the most recent survey in 2019 (St-Pierre et al. 2023). The 1988 survey was rejected due to multiple problems with the survey design and results (Gosselin et al. 2014), leaving eight abundance estimates available for the current analysis (St-Pierre et al. 2023). For age composition, we tallied the number of newborn calves and yearlings (age 0-1) observed in the photos for comparison with the number of older animals. Newborns and yearlings are smaller and darker in colour and thus clearly distinguishable on photographs, although this colouration may also cause some degree of negative detection bias. Conversely, newborns and yearlings likely spend a higher proportion of their time near the surface than adults, which could cause a positive availability bias. At present there is no way to determine the relative balance between these competing biases, or the associated uncertainty, thus for model fitting we treated the raw counts of newborns and yearlings relative to older animals and as an uncorrected binomial sample.

Visual line-transect surveys were initiated in 2001 and conducted on a regular basis (every 1-3 years), often with multiple replicate surveys per year (St-Pierre et al. 2023). This dataset comprised of 51 surveys were flown in 13 survey years over the period 2001-2022 (St-Pierre et al. 2023). Discrepancies in abundance estimates between the photographic and visual surveys (see St-Pierre et al. 2023) forced their consideration as two independent sources of data for model fitting, with the relative weighting of each (in terms of contribution to model likelihood) determined by the associated variance estimates.

Carcass data

A total of 606 beluga were reported dead over the period 1983-2022, including 283 that were fully necropsied (Appendix I, Lair et al. 2016, Lesage 2021, S. Lair, unpublished data). Age was estimated as the number of growth layer groups (GLG) in the teeth dentine (see Lesage et al. 2014), and was available for 544 whales. There were 61 other carcasses with undetermined age: for 30 of these, categorical age classes (adult, juvenile or newborn calves) were assigned based on other metrics including body length (< 3 m: juvenile; > 3.5 m adult female; > 3.8 m adult male; < 1.80 m newborn; Lesage et al. 2014), colour (white/off-white: adult), lack of teeth (old adults) or reproductive tracts (spermatogenesis activity and testis size for males; presence of *corpora* in ovaries for females). We found no apparent bias in age class composition between these two groups, so for model fitting we restricted analysis to the sampled animals with GLG estimates.

Primary cause of death can generally be determined in the majority (~75%) of dead animals receiving full necropsies (Lair et al. 2016). Dystocia/postpartum complications as primary causes of mortality were entered in the model as the number of such cases relative to the number of sexually mature female carcasses examined each year (Lair et al. 2016, Lair unpublished data). In cases where a dead female had a calf *in utero*, only the female was considered a case and we assumed the calf would not be represented in the stranded carcass data set. Females with postpartum complications but no calf *in utero* were considered to have released an unviable calf, which we assumed could potentially be represented in the stranded carcass data set (subject to carcass detection probability).

A final source of information derived from the carcass data was the empirical relationship between colour (grey vs. white or off-white) and age. We fit a simple logistic regression model with linear and quadratic terms to the data set of colour (grey = 1, white or off-white = 0) vs. age. The model provided excellent fit to the data (R^2 >0.95), and the estimated functional relationship allowed us to probabilistically infer the proportion of individuals of a given age that would be grey in colour. We used this function to relate visual estimates of the proportion of grey individuals in various data sets (see below) to the model-estimated age structure.

Skiff survey data

A program with various objectives but mainly photo-identification of SLE beluga has been conducted on a yearly basis since 1989 following a consistent survey protocol explicitly described elsewhere (Michaud 2014). Briefly, these surveys covered the central portion of the beluga summer habitat between early-June and mid-October, alternating sectors to sample all segments of the population and the variety of habitats that beluga use during summer. Once a herd was encountered, data on herd composition and behaviour was acquired over the first 15 min of the encounter while remaining 300-500 m away from the herd, then every 30 min until end of the encounter, usually 2 to 4 hours later. Individuals within a herd were categorized as either newborn calves (< 1 yr-old), bleuvet (1-2 yr-old), juvenile (grey) or adults (white or off-white). An annual index of the proportion of newborn calves and grey animals (categories bleuvet and juvenile together) was obtained for each year between 1989 and 2021 following the

methodology described in Michaud (2014). Only the proportion of grey individuals was used in the model (Appendix 2), because the low proportion of calves (1—4%) obtained by Michaud (2014) suggests a systematic underestimation of their occurrence likely due to their small size, dark colour, and proximity to females.

Other data sources

The model also incorporates data from three other sources. We estimated the stage structure of SLE beluga in 1938-1939 from the sex, length, colour, and sexual maturity of a hunted sample of 161 SLE beluga (Vladykov 1944). We used the number of grey individuals relative to the total number of hunted animals (excluding 0-age calves, which were considered potentially biased) as a binomial sample of the age distribution of the living population.

We used annual reported harvest data for the period 1866—1979 to help infer historical dynamics and provide context for more recent demographic trends. Data up to until 1960 were extracted directly from Reeves and Mitchell (1984, Table VII) and incorporated an average struck and loss rate of 0.2. Data for the period 1960-1979 (i.e., until harvests were officially banned) were more difficult to determine with precision. Laurin (1982) and Pippard and Malcolm (1978) both reported a minimum of 20 beluga being shot each year after 1960 and through the 1970's, with a small number of animals (21 over 7 years) being taken in the 1960s through a weir fishery (see Reeves and Mitchell 1984). We added to these numbers five whales each year to account for the minimal struck and loss reported by Laurin (1982).

Finally, we examined long-term (start date: 1969 to 1990) indices of five environmental factors for their potential relationship with newborn calf mortality based on findings from a previous study (Williams et al. 2021). Indices included ice duration (in days) in the SLE, ice volume (seasonal maximum) and average water temperature at 200 m in the Gulf of St. Lawrence (Galbraith et al. 2022); mean capelin biomass in the northern Gulf of St. Lawrence (standard sampled biomass; Duplisea et al. 2020); and spring spawner herring biomass in the southern Gulf of St. Lawrence (Rolland et al. 2022). All the above variables were centered and scaled to unit variance prior to model fitting.

MODEL OVERVIEW

We used a stage-structured, integrated population model to analyze demographic trends within the SLE beluga population. While we were interested in the drivers of beluga population dynamics over recent decades (the 1980s through the present), we extended our study period to encompass a much longer time period (1865-2022) in order to gain insights into historical potential abundance, and to ensure our model was initialized with a realistic age/sex structure (the long lifespan of belugas means that the age structure of the death assemblage reflects demographic processes over the previous half century). Our process model incorporated both sex and age structure, with a mixture of single-year and multi-year age classes providing an analytically tractable number of stages for this long-lived mammal, while at the same time allowing for a realistic treatment of age-based trends in abundance and survival. We evaluated the effects of multiple sources of mortality on population dynamics, including age and sex-specific hazards, density-dependent factors, environmental risk factors, direct human harvests (over the early part of the study period), and environmental stochasticity. We used Bayesian hierarchical methods to fit the process model to multiple data sets: photo-based and visual aerial survey data on abundance and stage structure, age/sex-at-death data from stranded carcasses, necropsy data on cause-of-death, stage composition data from skiff surveys and harvested animals, and historical harvest records.

To help in keeping track of the large number of processes, parameters, and variables included in the model, we provide summary tables of all possible demographic transitions (Table 1) and parameter symbols and definitions (Table 2).

PROCESS MODEL

We used a discrete process model with 1-year time step and assumed a post-breeding survey occurring in late summer (mid-Aug to early September), after most births have occurred, such that calves-of-the-year (aged 0yr) represented the first age class in the model. We considered individuals of age < 8yr to be juveniles and age ≥ 8yr as adults (Robeck et al. 2005, Suydam 2009, Inyakina et al. 2022). We evaluated a range of possible age classification structures for the model, with a goal of defining stage boundaries that ensured age-based differences in survival and fecundity would primarily occur between rather than within stages (Caswell 2001). Based on graphical comparisons of goodness of fit statistics for carcass age structure under different structures (see model fitting section below), we found that sufficient resolution in age-varying vital rates was achieved by single year stage durations for ages 0-3yr, followed by 4-year stage durations for ages 4-15 yr, and 8-year stage durations for ages >15yr. A loop diagram (Figure 1) illustrates the full suite of possible demographic transitions between the 13 resulting age classes (denoted by index *a*), which we further divided into two sexes and three adult female reproductive classes for a total of 37 stages (denoted by index *i*). Our use of multiple reproductive classes (following Mosnier et al. 2015) allowed us to estimate mortality risks specific to each stage, and accounts for the extended gestation period (12-16 months; Brodie 1971, Robeck et al. 2005) and calf dependency period (12-24 months; Matthews and Ferguson 2015), whereby females can be assigned to 1 of 3 classes based on their reproductive status at the time of the survey: available to become pregnant (*av*), pregnant with calf (*pr*), or accompanied by a newborn calf (*wc*). Transitions between age classes and reproductive status were determined by three vital rates: survival (S), growth (G), and reproduction (R), with the latter comprised of two separate processes: 1) the probability (P) of an available female at year t becoming pregnant at year t+1; and 2) the probability of a pregnant female at year t producing a newborn calf at year t+1 (determined by the newborn survival rate, S_n). A complete list of the demographic transitions defined by these vital rates is provided in Table 1.

To examine the patterns and potential causes of variation in beluga vital rates, we computed survival in terms of instantaneous hazards: this approach provides a useful mathematical framework with which to examine multiple “competing” causes of death, as well as age and sex-dependent mortality factors and the environmental variables that mediate their effects (Fine and Gray 1999, Gelfand et al. 2000). Each hazard (Λ) represents the instantaneous mortality rate from a particular cause of death, and the annual survival rate (S) can thus be calculated as the exponent of the negative sum of instantaneous hazard rates from all causes of death. We analyzed sources of variation in hazards in log-form, as this allows predictive variables to be expressed as simple additive linear functions. The predictors of log hazards for individuals of stage i at time t can be conceptually categorized as either fixed effects (e.g., age, sex, environmental variables) or random effects (unexplained sources of variation).

We defined two primary types of competing hazards: natural or environmental sources of mortality (baseline hazards, Λ_B), and direct human harvest mortality (Λ_H). We also defined a third hazard, dystocia/postpartum mortality (Λ_Z), a major cause of death for adult reproductive females (Lair et al. 2016; S. Lair, unpublished data). While dystocia/postpartum mortality could also be considered a component of baseline mortality, we decided to track it as a separate hazard because 1) it is limited to just one component of the population (adult females with status *pr*); 2) there is concern that it may have been increasing in recent years, potentially

affecting population recovery, and thus tracking it separately could help inform management recommendations; and 3) the existence of necropsy data on the relative frequency of dystocia/postpartum deaths over time provided an opportunity to measure its impacts as a distinct hazard (just as harvest records allowed us to measure the impacts of harvest mortality hazards).

In the case of baseline hazards, the key risk factors included age and sex-based factors, density dependent factors, environmental factors, and stochastic effects:

$$\log(\Lambda_{B,i,t}) = \zeta + \gamma_0 + \Delta_i \cdot \gamma_1 + \Omega_i \cdot \gamma_2 + \Gamma_i \cdot \gamma_3 + \Delta_i \cdot \left[\phi\left({}^{N_t}/_{1000}\right) + \sum_j \mathbf{X}_{j,t}\beta_j + \varepsilon_{D,t}\right] + \varepsilon_{A,t} \quad 1$$

The first parameter in equation 1, ζ, represents a minimum log hazard rate (a nuisance parameter which we set to an arbitrarily low value, ζ = -10, which corresponds to a survival rate of 0.9999), and all other parameters can thus be interpreted as log hazard ratios relative to this minimum. Parameter γ_0 determined baseline adult mortality in the absence of any other effects, γ_1 determined the effect of "early hazards" affecting younger animals (scaled by age-modifying vector Δ_i, which declines from a value of 1 for *a* = 1 to a value of 0 for *a* = *13*), and γ_2 determined the effect of "late hazards" affecting older animals (scaled by age-modifying vector Ω_i, which increases from a value of 0 for *a* = 1 to a value of 1 for *a* = *13*). Previous analyses (Mosnier et al. 2015) suggested that survival rates for males and females were identical for juveniles but differed for adults; accordingly, we included parameter γ_3 to represent the mean log hazard ratio for adult males relative to females, where γ_3 was multiplied by switch variable Γ_i in order to limit effects to adult males (Γ_i = 1 for adult males and 0 for all other stages). The magnitude of density-dependent hazards was determined by the product of parameter ϕ and the current population size (*N*, scaled by 1/1000 to simplify interpretation of parameter ϕ), while the effects of various environmental variables ($\mathbf{X}_{j,t}$, centered and scaled to unit variance and mean of 0) were determined by estimated parameters β_j (see section *Other data sources* for details). Earlier analyses (Williams et al. 2021) and mammalian life history theory (Fowler 1987, Holser et al. 2021) suggest that effects of density dependent hazards, environmental factors, and additional environmental stochasticity (determined by random effect ε_D) would be mostly limited to younger age classes (primarily calves and yearlings), and thus all these effects in Equation 1 were multiplied by age-modifying vector Δ_i. However, some sources of mortality (infectious disease, intoxication) are not restricted to younger animals, while yet other mortality factors such as cancer may affect mainly older animals (Lair et al. 2016); we therefore included an age-independent random effect term (ε_A) to account for variation in these additional hazards. Random effect terms ε_D and ε_A were assumed to be normally distributed with mean of 0 and standard deviations (SD) σ_D, and σ_A (respectively).

We note that our inclusion of age-specific hazard parameters γ_1 and γ_2 in Equation 1 is analogous to a Siler proportional hazards model (Breslow 1975); however, we built on the basic proportional hazards formulation to allow flexibility in the functional form of the age-modifying vectors. Specifically, age-based variation in the relative strength of early hazards was determined by the functional form of age modifying vector Δ_i:

$$\Delta_i = \frac{\hat{\Delta}_i - min(\hat{\Delta}_i)}{max(\hat{\Delta}_i) - min(\hat{\Delta}_i)}, \quad \hat{\Delta}_i = exp\left(\delta \cdot log\left(\frac{1}{\boldsymbol{v}[i]}\right)\right) \quad 2$$

while age-based variation in the strength of late hazards was determined by the functional form of Ω_i:

$$\Omega_i = \frac{\boldsymbol{v}[i]^{\omega+1}}{max(\boldsymbol{v}[i])^{\omega+1}} \quad 3$$

In Equations 2 and 3, **v** was a vector of the median age (in years) of each demographic stage *i*, and estimated parameters δ and ω determined the degree of non-linearity in the functional forms of Δ and Ω, respectively, thus allowing flexibility in the shape of the overall relationship between age and survival (Figure 2).

We modeled human harvest mortality as a separate hazard, Λ_H, calculated for each stage and year as:

$$\Lambda_{\mathrm{H},i,t} = exp\left(\zeta + \gamma_H + \varepsilon_{H,t}\right) \cdot \Theta_i \quad 4$$

where ζ represented the minimum log hazard rate (defined as for equation 1), γ_H represented the mean log hazard ratio associated with harvest mortality, and random effect term ε_H allowed for year to year differences in harvest effort (ε_H is normally distributed with mean = 0 and SD = σ_H). Harvest hazards were assumed to vary by age, which we achieved using age-modifying vector (Θ): we set $\Theta_i = 1$ for all adult stages and $0 < \Theta_i < 1$ for juvenile stages, based on evidence that harvesters tend to avoid the youngest age classes (Vladykov 1944, Reeves and Mitchell 1984). Different methods of harvest were associated with differing degrees of age bias (Reeves and Mitchell 1984), and in most cases there was no direct information on the age-distribution of the SLE beluga harvest, but based on anecdotal reports and the 1938-1939 hunted beluga sample (Vladykov 1944) we set $\Theta_i = 0.5$ for 0-age calves, $\Theta_i = 0.75$ for younger juveniles (ages 1 – 3), and $\Theta_i = 0.9$ for older juveniles (ages 4-7).

The third class of hazards tracked by our model was dystocia/postpartum mortality of adult reproductive females (we note that female mortality also implicitly involves mortality of a newborn calf or fœtus). There is evidence that poor body condition, deficiency in essential micronutrients or exposure to toxic substances affecting thyroidal activity are risk factors for dystocia/postpartum mortality in other species (reviewed in Lair et al. 2016). We thus assumed this mortality source would have both density dependent and density independent components, and we calculated dystocia/postpartum hazards as:

$$log\left(\Lambda_{Z,i,t}\right) = \zeta + \gamma_Z + \rho \cdot \phi\left(\frac{N_t}{1000}\right) + \varepsilon_{Z,t} \quad 5$$

where parameter γ_Z determined the baseline log hazard ratio for dystocia/postpartum mortality, parameter ϕ determined density-dependent increase in risks (as defined in Equation 1), parameter ρ is a rescaling parameter ($0<\rho<1$) that scales density dependent impacts on dystocia/postpartum hazards relative to the effect on baseline hazards, and random effect term ε_Z represents unexplained temporal variation in dystocia/postpartum mortality (ε_Z was normally distributed with mean = 0 and SD = σ_Z).

We combined the three types of hazards to calculate stage-specific annual survival rates as:

$$S_{i,t} = exp\left(-\left(\Lambda_{B,i.t} + \Lambda_{H,i.t} + \Upsilon_i \cdot \Lambda_{Z,i.t}\right)\right) \quad 6$$

In Equation 6, dystocia/postpartum hazards (Λ_Z) were multiplied by switch variable Υ_i in order to limit effects to pregnant females ($\Upsilon_i = 1$ for adult females of status *pr* and $\Upsilon_i = 0$ for all other stages).

Reproductive transitions in our model were divided into two components, pregnancy rates (*P*) and calf production rates. Females with status *av* at year *t* were assumed to transition to status *pr* at year *t*+1 with probability *P*, conditional upon their survival. We calculated pregnancy rates using a similar mathematical approach to survival rate calculations, although in this case the "hazard" corresponds to the instantaneous probability of not becoming pregnant. Thus, the age-specific annual pregnancy rate for "available" adult females was calculated as:

$$P_{i,t} = exp\left(-exp\left(\eta + \rho \cdot \left[\phi \cdot \left(\frac{N_t}{1000}\right) + \varepsilon_{D,t}\right]\right)\right) \cdot \varsigma_i \quad 7$$

where parameter η determined the expected mean probability of pregnancy at low population sizes, ϕ determined density-dependent reductions in pregnancy rates, parameter ρ is a rescaling parameter ($0<\rho<1$) that scales density dependent impacts on pregnancy rates relative to the effect on baseline hazards, and the random effect term ε_D determined the effects of environmental stochasticity (as in equation 1). The final term in Equation 7, ς_i, is an age-varying adjustment factor that accounted for the effects of reproductive senescence. Based on previously published data on reproductive senescence in belugas (Suydam 2009, Ellis et al. 2018), we set $\varsigma_i = 1$ for females < 40yr, $\varsigma_i = 0.8$ for ages 40-47, $\varsigma_i = 0.4$ for ages 48-55, and $\varsigma_i = 0.2$ for females aged ≥ 56, as these values resulted in age-specific pregnancy rates that closely approximated those reported by Ellis et al. (2018) and were also generally consistent with other published data on beluga reproductive rates for older animals (Brodie 1972, Burns and Seaman 1986, Heide-Jørgensen and Tielman 1994).

The second component of reproduction is calf production, defined as the probability that pregnant females in year *t* produce calves that survive to the time of the survey at *t*+1. We assumed that after the first few days postpartum (i.e., excluding dystocia or postpartum complications, where both the female and the fetus or newborn calf are assumed to die rapidly as described above), that virtually all pregnancies past that point resulted in viable newborn calves. Therefore, the calf production rate for pregnant females, conditional upon female survival, corresponds to newborn calf survival probability from birth to the time of the survey, a parameter we defined as S_n. Births start in late-June in the SLE, peak in July, and by the time of the survey (late August or early September) virtually all births have occurred (Michaud 2014). Newborns therefore have to survive from 0 – 3 months between their birth and the survey, at which point they are entered into the 0-age calf stage of the model. Based on an assumption that the rate of survival of newborns over the first few months is similar to or lower than the survival rate over the following 12 months, we calculated $S_{n,t}$ as equal to the survival rate of 0-age calves ($S_{1,t}$) raised to the power ¼ (which conservatively assumes a survival period of three months from birth to survey). Females of status *pr* at year *t* whose newborn calf survived to the survey at year *t*+1 transitioned to status *wc*, while females that lost their calf prior to the survey transitioned to status *av* but with a reduced probability of becoming pregnant right away (Figure 1).

The final vital rate required to calculate demographic transitions (Table 1) was *G*, defined as the probability that an individual advances to the next age class, conditional upon survival. For stages with 1-year stage durations ($i \leq 4$; Figure 1), G = 1; however, for stages that represent multi-year age classes ($i > 4$), G < 1. When the number of years that individuals spend in a stage is fixed, the exact value of G will depend on the stage duration (D_i = number of year classes within stage *i*), the survival rate for individuals within stage *i* ($S_{i,t}$), and the current population growth rate ($\lambda_t = N_t / N_{t-1}$). We calculated *G* using a standard formula for fixed stage duration growth rates (Caswell 2001):

$$G_{i,t} = \frac{\left[\left(\frac{S_{i,t}}{\lambda_t}\right)^{D_i} - \left(\frac{S_{i,t}}{\lambda_t}\right)^{D_i - 1}\right]}{\left[\left(\frac{S_{i,t}}{\lambda_t}\right)^{D_i} - 1\right]} \quad 8$$

We combined the stage-specific vital rates described in equations 1-8 to create a set of 17 composite equations (Table 1) that together define all possible demographic transitions in our process model (Figure 1). We used these composite equations to populate the cells of a projection matrix (**M**) with dimensions 37x37 (Figure S1). The abundance of beluga in each stage *i* at year *t* was compiled into a population vector of length 37 ($\mathbf{n}_t$), which when summed

gave the estimated total abundance for that year ($N_t = \sum \mathbf{n}_t$). We then used matrix multiplication (Caswell 2001) to calculate the expected abundance of beluga in each stage at year t+1 using the recursive equation:

$$\boldsymbol{n}_{t+1} = \boldsymbol{M}_t \times \boldsymbol{n}_t \quad (9)$$

We note that the parameterization of matrix $\mathbf{M}_t$ is unique for each year due to time-varying environmental variables, density-dependence, and random effects.

HISTORICAL VS. RECENT DYNAMICS

The process model described in the previous section is time-independent: that is, all parameters and demographic effects are assumed to apply equally across years (excluding time-varying environmental variables and stochastic variation in random effects). However, several major changes are known to have occurred over the time period of interest (1865 – 2022), requiring us to relax the assumption of time invariance. Following earlier analyses (Mosnier et al. 2015), we divided the study period into two phases: phase 1 (1865-1978) represents a historical period during which harvests occurred and for which we had limited data available for model fitting; phase 2 (1979-2022) spans the recent decades post-harvest for which we had more extensive data for fitting and thus greater ability to estimate variation in vital rates (the carcass age structure surveys actually began in 1983, but we selected a breakpoint 5 years earlier to allow equilibration of the youngest age classes by 1983). We assumed that the population was at or near its historical environmental carrying capacity at the beginning of phase 1 of the study period (1865) and was approximately an order of magnitude more abundant than the current population (Reeves and Mitchell 1984, Mosnier et al. 2015). The first recorded harvests began in 1866 and continued until 1979 when beluga hunting was banned, causing a dramatic decline in abundance (Reeves and Mitchell 1984, Hammill et al. 2007, Mosnier et al. 2015). After the cessation of harvests, the population was approximately stable (Hammill et al. 2007) and has showed no substantial recovery since (Mosnier et al. 2015). Such a pattern indicates that underlying mortality rates must have increased relative to pre-harvest levels: otherwise, under any reasonable assumptions of logistic population growth (such as those described by Hammill et al. 2007) the population should have at least tripled in the intervening 42 years. Increased mortality could reflect an increase in the strength of density-dependent hazards, the addition of density-independent risk factors, or both. We therefore made several adjustments to our process model to account for these changes.

First, we set harvest mortality hazards (Λ_H) equal to 0 for phase 2 of the study period (all years after 1979). We next modified our calculations of baseline and dystocia/postpartum hazards to allow the possibility of a directional increase in mortality over the study period, as explained below. The degree to which mortality increases were density-dependent or density-independent is uncertain: evidence of poor body condition and nutritional status of animals in recent decades (Simond et al. 2020, Bernier-Graveline et al. 2021) would suggest at least some increase in density-dependent effects, while other mortality factors such as those associated with contaminant exposure (Martineau et al. 1994, Lair et al. 2016) are likely to be density- and age-independent. We therefore specified two parameters for increased mortality, one for density-dependent effects (θ) and one for density independent effects (α), both of which were constrained to be ≥ 0. Parameter θ represented the log of the proportional increase in density dependent effects (as determined by parameter ϕ in Equation 1), while α represented the log hazard ratio associated with increased density independent effects.

A second area of uncertainty concerns the timing and rate of increase in mortality over the study period. Previous reports suggest potential increases in non-harvest mortality beginning in the early to mid-1900s caused by reduced fish stocks, habitat alteration, harassment, and pollution

(Reeves and Mitchell 1984), and increases in contaminant exposure date from at least the 1950s (Martineau et al. 1994). However, these reports are insufficient to quantify temporal variation in hazards over this period. One possible approach would be to limit the increased hazards to phase 2 only (i.e., implicitly fix $\theta = 0$ for phase 1); however, this is unlikely to be realistic given that cancer rates were already prevalent early in the 1980s. In addition, such a sudden change in mortality would be both biologically unrealistic and also problematic from a model fitting perspective. We therefore defined a simple, monotonically increasing function, χ_t, to determine variation in the relative magnitude of increased hazards over time. We assumed that $\chi_t = 0$ at the start of the study period ($t = 0$), and that it would increase as a sigmoidal function to reach an asymptote of 1 by $t = t_c$ (where t_c is the first year of phase 2 of the study period), since continued variation in mortality during phase 2 was already accounted for by other fixed and random effects in the model. We calculated χ_t as a logit function:

$$\chi_t = \begin{cases} logit^{-1}(6 - [1 + \xi] \cdot [t_c - t]^{0.5}) & for\ t < t_c \\ 1 & for\ t \geq t_c \end{cases} \quad 10$$

In Equation 10, the timing and rate of increase in χ is controlled by a single parameter, ξ, where $0 < \xi < 1$ and where values of $\xi \to 0$ producing a gradually increasing function beginning early in phase 1, and values of $\xi \to 1$ producing a sharply increasing function with an inflection point near the end of phase 1 (Figure 2). Data limitations precluded estimation of ξ during model fitting, so we instead evaluated several values of ξ between 0 and 1 to evaluate its impacts on other model parameters.

We next modified the equations for calculating baseline and dystocia/post partum hazards, as well as pregnancy rates, to account for temporal increases in density-dependent and density independent hazards:

$$log(\Lambda_{B,i,t}) = \zeta + \gamma_0 + \Delta_i\gamma_1 + \Omega_i\gamma_2 + \Gamma_i\gamma_3 + \Delta_i\left[exp(\chi_t\theta)\phi\left(\frac{N_t}{1000}\right) + \sum_j \boldsymbol{X}_{j,t}\beta_j + \varepsilon_{D,t}\right] + \chi_t\alpha + \varepsilon_{A,t} \quad 11$$

$$log(\Lambda_{Z,i,t}) = \zeta + \gamma_Z + \rho \cdot exp(\chi_t\theta)\phi\left(\frac{N_t}{1000}\right) + \chi_t\alpha + \varepsilon_{Z,t} \quad 12$$

$$P_{i,t} = exp\left(-exp\left(\eta + \rho\left[exp(\chi_t\theta)\phi\left(\frac{N_t}{1000}\right) + \varepsilon_{D,t}\right]\right)\right) \cdot \chi_i \quad 13$$

We note that baseline and dystocia/postpartum hazards rates are assumed to be affected by increases in both density-dependent and density-independent mortality (parameters θ and α, respectively), while pregnancy rates are assumed to be affected only by an increase in density dependent effects.

Finally, we set all random effects equal to 0 for phase 1 of the study period, given the lack of available data for estimating fine-scale variation in vital rates over these years. Similarly, given the lack of environmental covariate data coverage for this period, we also set $\beta_j = 0$ for phase 1. Because the random effects and centered/scaled environmental variables were all assumed to have mean = 0, these changes had no effect on parameter fitting for phase 2 of the study period, but they do mean that the process model was effectively deterministic for phase 1.

DATA MODEL

Fitting the process model to observed data required defining probabilistic relationships between each data set and the corresponding predictions generated by the process model. Raw data from the aerial surveys (photographic strip transect surveys and visual line transect surveys) were analyzed separately (see St-Pierre et al. 2023) to provide abundance point estimates and associated uncertainty measures (SE values). The uncertainty distributions associated with

survey estimates were lognormally distributed, thus we related the observed point estimates from photographic surveys ($ObsP_t$) and visual surveys ($ObsV_t$) to the model-estimated abundance values (N_t) using lognormal distributions:

$$ObsP_t \sim lognormal\left(\mu = log\left(\frac{N_t^2}{\sqrt{N_t^2+SE_{P,t}^2}}\right),\ \sigma = \sqrt{log\left(1+\frac{SE_{P,t}^2}{N_t^2}\right)}\right) \quad 14$$

$$ObsV_t \sim lognormal\left(\mu = log\left(\frac{N_t^2}{\sqrt{N_t^2+SE_{V,t}^2}}\right),\ \sigma = \sqrt{log\left(1+\frac{SE_{V,t}^2}{N_t^2}\right)}\right) \quad 15$$

The photographic surveys also provided uncorrected counts of calves and yearlings (Ncy_t) relative to total counts ($Ntotal_t$). We assumed these counts would be described by a binomial distribution with probabilities calculated from the model-estimated proportions of the population in the first two stages (i.e., ages 0 and 1):

$$Ncy_t \sim binomial\left(prob = \left(\frac{\boldsymbol{n}[1]_t+\boldsymbol{n}[2]_t}{\sum \boldsymbol{n}_t}\right),\ Ntotal_t\right) \quad 16$$

The carcass data set consisted of the number of stranded dead animals (with GLG age estimates), classified by age class and sex, for each year between 1983 – 2022. We compiled these data into annual vectors $\mathbf{c}_t$ = <$c_{g=1}$, $c_{g=2}$, … $c_{g=26}$ >, where subscript *g* indicates a unique combination of age class and sex (13 age classes for each sex; see Figure 1). We used the process model to derive equivalent vectors of the expected proportion of deaths occurring by age/sex class. Specifically, we took the elementwise product of the population vector at year *t*-1 ($\mathbf{n}_{t-1}$) and a vector of annual stage-specific mortality probabilities ($\mathbf{m}_t$ = <1-$S_{1,t}$, 1-$S_{2,t}$ … 1-$S_{37,t}$ >), which gave the expected number of dead animals by stage at year *t*. We combined the expected numbers of deaths for different female reproductive classes to obtain a vector of expected deaths by age class and sex ($\mathbf{d}_t$) that could be compared to the observed carcass counts ($\mathbf{c}_t$). We adjusted the first element of $\mathbf{d}_t$ (0-age calves) by adding the estimated number of newborn calves-of-the-year that did not survive until the survey (i.e., demographic transitions *k* and *l* in Table 1 and Figure 1), including those associated with female deaths from dystocia/postpartum hazards where the dead calf was released to the environment (see *Data Sources* section, above). We further adjusted $\mathbf{d}_t$ to reflect under-representation of dead calves in the data set, as newborn carcasses are much less likely to be recovered than older/larger animals (Mosnier et al. 2015, Lesage 2021): we multiplied the first element of $\mathbf{d}_t$ by ψ_1, a detection probability parameter that was estimated as part of model fitting. We assumed that the frequency distribution of observed carcass counts would be described by a multinomial distribution with probabilities determined by the age/sex-at-death distributions predicted by the process model:

$$\boldsymbol{c}_t \sim multinomial\left(prob = \frac{\boldsymbol{d}_t}{\sum \boldsymbol{d}_t}\right) \quad 17$$

In addition to age/sex-at-death distributions, data from a sub-set of carcasses provided information on cause of death. For each year we tabulated the number of necropsies of adult females for which dystocia/postpartum mortality was determined to be the primary cause of death ($AFDz_t$), relative to the total number of adult female necropsies conducted ($AFDtotal_t$). We assumed these data would be described by a binomial distribution with probabilities calculated from model-estimated proportions of adult female deaths attributable to dystocia/postpartum hazards:

$$AFDz_t \sim binomial\left(prob = \frac{\sum_{i=14:21} \boldsymbol{n}[i]_{t-1}\boldsymbol{m}[i]_t\left(\frac{\Lambda_{Z,i,t}}{\Lambda_{Z,i,t}+\Lambda_{B,i,t}}\right)}{\sum_{i=6:29} \boldsymbol{n}[i]_{t-1}\boldsymbol{m}[i]_t},\ AFDtotal_t\right) \quad 18$$

In Equation 18, the binomial probability was calculated as the ratio of deaths of pregnant females from dystocia/postpartum hazards to deaths of all adult females (the summation in the numerator is over values of index *i* corresponding to pregnant female stages, while the summation in the denominator is over values of index *i* corresponding to all adult female stages). For pregnant females we calculated the fraction of deaths from dystocia/postpartum hazards as the ratio of Λ_Z to $\Lambda_B + \Lambda_Z$, noting that harvest hazards (Λ_H) were effectively zero by the time the carcass surveys were initiated.

Data used from skiff surveys consisted of the mean annual proportions of grey individuals (excluding calves) in the population (Pgr_t), estimated as part of a previous analysis (Michaud 2014). These proportions corresponded to the number of grey individuals (excluding calves) divided by the total number of whales. We assumed these proportional data would be well described by a beta distribution with *a* and *b* parameters calculated from model-estimated proportions of grey individuals in the population at year *t*:

$$Pgr_t \sim beta\left(a = \left(\psi_2 \cdot \frac{\sum_{i\neq 1} \boldsymbol{n}[i]_t \cdot f_g[i]}{\sum_i \boldsymbol{n}[i]_t}\right) \cdot \nu,\ b = \left(1 - \psi_2 \cdot \frac{\sum_{i\neq 1} \boldsymbol{n}[i]_t \cdot f_g[i]}{\sum_i \boldsymbol{n}[i]_t}\right) \cdot \nu\right) \quad 19$$

where ν represents a precision parameter, estimated as part of model fitting, and $f_g[i]$ represents the probability of grey colour as a function of stage, derived from the empirical relationship between age and colour estimated from carcass data (see *Data Sources* section, above). The proportions of grey individuals estimated from skiff surveys tend to be biased slightly low (on average) relative to the inferred age structure based on photographic survey counts of 0-1 age juveniles, so we included an estimated adjustment parameter (ψ_2) to account for this bias.

Data on the number of grey individuals (*NGhv*) relative to total abundance (*NThv*) were also available from a sample of harvested animals in 1938-39 (Vladykov 1944). To avoid the effects of sampling bias we excluded 0-age calves from both these tallies. We assumed these data would be described by a binomial distribution with probabilities calculated from the model-estimated proportions of grey individuals in the population in 1939 (calculated as for the skiff-based surveys, previous paragraph):

$$NGhv \sim binomial\left(prob = \left(\frac{\sum_{i\neq 1} \boldsymbol{n}[i]_{t=1939} \cdot f_g[i]}{\sum_{i\neq 1} \boldsymbol{n}[i]_{t=1939}}\right),\ NThv\right) \quad 20$$

The number of reported or estimated harvests per year (H_t) were assumed to be described by a Poisson distribution with rate parameter corresponding to the mean number of harvest mortalities predicted by the model:

$$H_t = Poisson\left(\sum_i \boldsymbol{n}[i]_{t-1}\boldsymbol{m}[i]_t\left(\frac{\Lambda_{H,i,t}}{\Lambda_{H,i,t}+\Lambda_{B,i,t}+Y_i\Lambda_{Z,i,t}}\right)\right) \quad 21$$

Three additional data constants were included in model fitting to help ensure demographically reliable results. These effectively represent priors placed on certain emergent properties of the model, corresponding to explicitly stated assumptions (and associated uncertainties) that were consistent with published findings but for which there were no empirical data that could be used for fitting. The first of these was the mean annual rate of population growth at the start of the time series ($\lambda_{t=0}$). While not known with certainty, it is assumed that the pre-harvest population must have been at or near to the historical value of *K*, the environmental carrying capacity (Hammill et al. 2007). We therefore inferred that the mean annual growth rate at time 0, after accounting for density-dependent effects, must have been approximately 1. To ensure that this

was the case, for each set of parameter values and initial population size ($N_{t=0}$) evaluated during model fitting, we calculated the associated population projection matrix (solving equations 1 to 8 with harvest hazards and environmental/random effects forced to 0) and iteratively conducted matrix multiplication (Equation 9) for a sufficient number of time steps (200) to allow stabilization of the stage structure and expected growth rate ($\lambda_{exp,t=0}$). We assumed the "observed" growth rate ($\lambda_{t=0}$, fixed at 1.0) was drawn from a normal distribution with mean of $\lambda_{exp,t=0}$ and an arbitrarily small standard error:

$$\lambda_{t=0} \sim normal\left(\lambda_{exp,\,t=0},\ SE = 0.0001\right) \quad 22$$

By including Equation 22 as part of model fitting we constrained the joint posterior of all parameters such that the asymptotic value of *K* (the density at which $\lambda \rightarrow 1$) corresponded to the estimated pre-harvest abundance, while also ensuring appropriate stable stage structure at *t*=0.

The second constant was the maximum growth rate at low population density (λ_{max}), which we assumed would be close to the 4% maximum rate of growth reported for many cetacean populations (Wade 1998) including beluga (Lowry et al. 2019). For each set of parameter values evaluated during model fitting, and a "low" population size of N=100 animals, we calculated the associated population projection matrix (solving equations 1 to 8 with harvest hazards and environmental/random effects forced to 0) and iteratively conducted matrix multiplication (equation 9) for a sufficient number of time steps (200) to allow stabilization of the stage structure and expected growth rate ($\lambda_{exp,N100}$). We assumed the observed maximum growth rate (λ_{max} , fixed at 1.04) was drawn from a normal distribution with mean of $\lambda_{exp,N100}$ and an arbitrarily small standard error:

$$\lambda_{max} \sim normal\left(\lambda_{exp,\,N100},\ SE = 0.0025\right) \quad 23$$

We note that the standard error in Equation 23 was larger than for Equation 22, reflecting greater uncertainty about the expected growth rate at low population size. By including Equation 23 as part of model fitting we constrained the joint posterior of all parameters such that the expected growth rate at low population density (excluding effects of environmental variables, harvest, or other sources of increased mortality) was consistent with literature-based estimates of λ_{max}.

A third constant, based on expert opinion, was used to constrain the relative partitioning of increased mortality over the 20th century between density-dependent vs. density independent effects (parameters α and θ). There is at present no rigorous basis for ascertaining this ratio; however, based on review of reported patterns of mortality and risk factors in the literature (Martineau et al. 1994, Lebeuf et al. 2014a, Lair et al. 2016, Poirier et al. 2019, Lesage 2021), it appeared reasonable to assume a greater increase in density independent effects relative to density-dependent effects during this early period. We define R_{DiD} as the ratio of the increase in density independent log hazards (α) relative to the realized increment in density-dependent log hazards at some specified density (we arbitrarily selected the estimated abundance at the beginning of phase 2 of the study period, $N_{t=tc}$). We set an average value for this ratio of 1.5, and an associated standard error of 0.25, thus implying 95% confidence that the true value of R_{DiD} was between 1 and 2. We assumed gamma distributed error (appropriate for a ratio) with an inverse scale parameter set to produce the desired level of uncertainty:

$$R_{DiD} \sim gamma\left(\frac{\alpha}{exp(\theta)\cdot\phi\cdot\left(\frac{N_{t=tc}}{1000}\right)-\phi\cdot\left(\frac{N_{t=tc}}{1000}\right)} \cdot 8.57,\ inv.scale = 8.57\right) \quad 24$$

PRIOR MODEL

We used vague prior distributions for most model parameters, which we define as weakly informed based on biological feasibility but having no information specific to this analysis. We used Cauchy priors for unconstrained parameters and half-Cauchy priors for parameters constrained to be positive (such as variance parameters), with location parameters of 0 and scale parameters set at appropriate values given the range of biologically possible values. The Cauchy distribution has been suggested as an effective, uninformative prior because it has a taller peak than the Normal distribution, is leptokurtic ("fat tailed"), and has no defined mean, and thus provides wide potential bounds on parameter space, a tendency to shrink towards 0 for non-significant parameters, and minimized influence of the prior on the estimation of the posterior (Gelman et al. 2008). For calf detection probability parameters (ψ_1 and ψ_1), which were constrained to the 0-1 range, we used a flat *Beta* prior with parameters a = b = 1. In the case of initial population size ($N_{t=0}$) we used a weakly informative lognormal distribution with parameters μ = 9.3 and σ = 0.3, as this distribution encompassed a broad range of values consistent with all previously reported historical estimates, and with a mode close to 10,000 (the upper value proposed by Hammill et al. 2007).

In the case of two parameters, η (baseline pregnancy rates) and ρ (the scale of density dependent effects on dystocia hazards and pregnancy rates relative to effects on calf survival) we were unable to use vague priors, as the sets currently available for model fitting were insufficient to distinguish between reductions in pregnancy rates and reductions in neonatal survival, thus preventing model convergence. We therefore set informed priors on these based on expert opinion and on literature-reported values. For the baseline pregnancy rate parameter (η) we used a normal prior with mean = -1.7 and SE = 0.1, as this distribution resulted in a range of maximum pregnancy probabilities (0.80-0.85) and a prevalence of pregnant animals (30-40% of adult females) consistent with previously reported values (Vladykov 1944, Burns and Seaman 1986, Heide-Jørgensen and Teilmann 1994, Suydam 2009). For parameter ρ, we used a *Beta* prior with parameters a = b = 50, which resulted in a bell-shaped distribution centered at 0.5. A value of ρ = 0.5 for scaling density-dependent effects resulted in a reduction in pregnancy rates from 0.85 to 0.75 (or a reduction from 35% to 25% females pregnant) as density increased from near 0 to near *K*, generally consistent with the range of reproductive rates measured from populations of differing status (Kleinenberg et al. 1964, Suydam 2009, McGuire et al. 2020).

A complete list of prior distributions for all model parameters is provided in Table 2.

MODEL FITTING

The observed data variables constrained the possible values of unknown parameters in the process model, allowing us to estimate posterior distributions for these parameters using standard Markov Chain Monte Carlo (MCMC) methods. We used R (R.Core.Team 2022) and Stan software (Carpenter et al. 2017) to code and fit the model, saving 20,000 samples after a burn-in of 1,000 samples. We evaluated model convergence by graphical examination of trace plots from 20 independent chains and by ensuring that the Gelman-Rubin convergence diagnostic (R-hat) was <1.05 and the effective sample size (SS_{eff}) was >500 for all fitted model parameters. We plotted and visually compared prior and posterior distributions for all parameters to assess the degree to which posteriors were distinct from priors (Figure S2). We conducted graphical posterior predictive checking to evaluate model goodness of fit, ensuring that 1) out-of-sample predictive distributions of abundance were consistent with distributions of aerial survey data (both photo-based and visual surveys); 2) out-of-sample predictive distributions of stage composition were consistent with survey estimates of proportion grey and proportion calves/yearlings; and 3) out-of-sample predictive distributions of mortality age

structure were consistent with the carcass data set. We assessed the relative influence of different data sources on model predictions by conducting Leave-out-one cross validation analysis of the point-wise log likelihoods (Vehtari et al. 2017). Specifically, we used Pareto smoothed importance sampling to estimate the Pareto-*k* statistic for each observation, which can be used as a measure of the observation's influence on the posterior distribution of the model.

We repeated model fitting for three different values of the parameter ξ, which determines the timing and rate of increase in mortality during the 20th century: $\xi = 0.1$, $\xi = 0.5$ and $\xi = 0.9$. We present graphical summaries of estimated population trends associated with each value of ξ, and report on any associated differences in parameter estimates. However, based on the lack of significant differences for most parameters between alternative values of ξ, we used the fitted model with $\xi = 0.5$ to generate all remaining tables and plots.

We evaluated the potential effects of 5 different environmental variables on survival (see *Data Sources* section for more details). We first fit a model with all 5 variables, and then re-fit the model after sequentially removing non-significant variables (defined as variables for which the 80% quantiles of the posterior distribution of the associated β parameter overlapped 0) in reverse order of significance. The final model retained only those environmental variables having significant effects on hazard rates. We note that the limited time series available restricted us to considering simple linear relationships between log hazard rates and environmental variables (see equation 11), which we recognize is likely to be a simplification of more complex non-linear relationships between environmental drivers and mortality.

We report summary statistics for the posterior distributions of estimated parameters (including mean, SD, and 95% credible intervals, or CI), and also for key derived parameters including estimated abundance in 2022 (Table 3). We graphically examined model-predicted dynamics over the study period including trends in abundance, harvest mortality, pregnancy and survival rates, female deaths from dystocia/postpartum hazards, age-specific variation in survival, and stage composition of the living population and death assemblage.

Based on the model estimated abundance estimate for 2022 and associated uncertainty, we calculated the Potential Biological Removal (PBR) following standard procedures for cetaceans (Wade 1998). We then used the model to estimate functional carrying capacity (*K*) under current conditions, which we distinguish from the historical K (i.e., pre-harvest abundance, estimated as part of model fitting). To estimate current *K*, we retained the increased density-dependent effects (θ) at their estimated values, but set parameter α (increased density-independent hazards) to 0, as we assumed that α represented the combined effects of emergent mortality factors subject to management and mitigation. We also fixed stochastic fluctuations (ε) at 0 (i.e., their mean values over phase 2 of the study period), but in the case of environmental variables (e.g., Gulf Temperature at 200 m) we used the mean value for the period 2000-2022, to account for non-reversable shifts in climate-driven variables. We iteratively drew all parameters from their joint posterior distributions to parameterize the matrix, then sequentially varied *N* to find the abundance at which the dominant eigenvalue of the parameterized matrix = 1. We repeated this 10,000 times in order to accurately characterize uncertainty around the estimate of *K*, which we report as the median value and the 95% CI. Based on the point estimate of *K*, and the precautionary assumption that maximum net productivity level (MNPL) would occur at approximately 60% of *K* (which we validated by numerical simulations using the model), we calculated two abundance thresholds for management: a Precautionary Reference level (PRL), also referred to as the Upper Stock Limit, and a Limit Reference Level (LRL), signifying the level below which significant harm can occur (DFO 2013, Hammill et al. 2017). We set PRL to 80% of

MNPL, or 48% of estimated *K*, and we set LRL to 40% of MNPL, or 24% of estimated *K* (Hammill et al. 2017).

SIMULATING DYNAMICS FOR FUTURE SCENARIOS

We generated projections of future population dynamics under various scenarios by running Monte Carlo simulations of the process model, parameterized by drawing from the joint posteriors of all parameters and with environmental covariates and random effects drawn randomly from appropriate sampling distributions. We assumed that more recent conditions would be most reflective of future conditions, and thus we used the observed distributions of environmental covariates and random effects for the 2010-2022 period as the basis for future projections (unless otherwise stated). We conducted simulations under various scenarios to evaluate model sensitivities and management implications. Specifically, we evaluated climate change scenarios with differing levels of increased water temperatures (we specify % increases in mean water temperature after 100 years, assuming a continuous rate of increase from present values) and proportional increases or reductions in mean hazard rates (Λ_B or Λ_Z). A complete list of the scenarios evaluated is provided in Table 4.

For each scenario, we iterated 100-year population projections for 10,000 iterations, in order to quantify the effects of parameter uncertainty and sampling variance. We presented the results of simulations in several ways: 1) we summarized the average minimum abundance over the projection period (min_N), the mean abundance at the end of the projection period, and the 95% CI for abundance at the end of the projection period; 2) we compared the expected final population size to the baseline scenario (current conditions with no management actions or directional change in environmental variables); 3) we summarized the proportion of iterated simulations under each scenario for which the final estimated abundance was greater than each of 4 reference thresholds: MNPL, PRL, LRL, and a quasi-extinction threshold (QE) which we defined for the purposes of this analysis as a population with 50 or fewer adult females; 4) we summarized the proportion of iterated simulations under each scenario where the mean instantaneous growth rate (*r*) over a single generation time (28 years) was greater than 1% or lower than -1%.

RESULTS

RETROSPECTIVE ANALYSES

Fitting the model to the multiple independent data sets provided excellent convergence, as indicated by R-hat <1.05 and SS_{eff} > 500 for all parameters (Table 3). Posterior distributions for model parameters were highly distinct from prior distributions (Figure S2), indicating sufficient information across data sets to minimize the influence of priors (for parameters η and ρ the available data sets did not contain sufficient information to update the priors). Graphical posterior predictive checks indicated good model fit, with observed data distributions corresponding closely to distributions of out-of-sample projected estimates (Figure S3), and posterior distributions for all estimated parameters were biologically feasible and generally consistent with previously published analyses (Hammill et al. 2007, Lesage et al. 2014, Mosnier et al. 2015, Williams et al. 2021). An analysis of the relative influence of the various data sources on model posteriors indicated relatively high influence of data on carcass age structure, cause of death, and photo-based estimates of abundance and age composition, and relatively low influence of data from visual surveys (Figure S4).

Results from fitting three versions of the model with alternative values of ξ (0.1, 0.5 and 0.9) showed slightly differing trends during phase 1 of the study period, but identical trends during

phase 2 (Figure 3). The only base parameter that changed substantially between the three model fits was the estimate of pre-harvest abundance (N_0), which varied inversely with ξ. The parameter determining baseline strength of density dependence (ϕ) also decreased slightly for smaller values of ξ and larger values of N_0, however this was offset by corresponding increases in θ such that the cumulative density-dependent hazards in phase 2 of the study period remained constant between the three model fits, as did all other parameters. For all three model fits the average hazard rates in phase 2 of the study were significantly higher than at the beginning of phase 1, with the combined estimates of θ and α (Table 3) producing an overall increase in baseline hazards of 17% (CI_{95} = 2% – 56%) at the beginning of phase 2, although the realized hazard increase depended on current abundance and the degree to which the additional hazards were density-dependent. The estimate of pre-harvest abundance averaged across the three model fits was 13,558. Combining the posterior distributions across the three model fits resulted in a 95% credible interval for pre-harvest abundance (i.e., historical *K*) of 12,428 – 17,432. The remaining results are reported for the model fit with ξ = 0.5, although we note these results are almost identical to results from models with alternative values of ξ (except for the differences mentioned above).

Hazard rates were higher (relative to adults of 10-20 years age) for very young animals (primarily calves and yearlings) and for older animals, producing an “inverted-U” age specific survival schedule typical for large mammals (Figure 4). Density-dependent effects on hazard rates were associated with a reduction in 0-age calf survival rates from 61% for a population growing at r_{max}, to 31% for a population at *K* (Figure 4). Environmental variables also affected calf survival, although of the 5 different environmental covariates evaluated (see *Data Sources* section), only Gulf average temperature at 200m showed strongly significant effects on baseline hazards (Figure S5). An increase in mean annual temperature from 4.6 degrees (the long-term average) to 5.2 degrees (the average after 2010) was associated with a 40% increase in the hazard rate for 0-age calves. There was also a consistent but non-significant negative relationship between Gulf ice volume and hazard rate, which could be interpreted as a tendency towards higher calf survival on years with higher ice volume (Figure S5).

In addition to the variation in survival attributable to the fixed effects included in the model, there was a substantial degree of unexplained variation in hazard rates, which we generically refer to as stochasticity (while recognizing that this actually reflects the impacts of factors not included in the model). Interestingly, patterns of stochasticity often differed between density-dependent hazards (which primarily affect calves and pregnant females) and the density-independent hazards that affected all ages (Figure 5). For example, density-dependent hazards were generally higher than average between 2010 and 2020, while density-independent hazards were generally lower than average over the same decade. Both density-dependent and density independent random effects showed increased volatility between the late 1990s and early 2000s (Figure 5), consistent with findings from a previous model (Mosnier et al. 2015).

The process model integrated multiple hazards, reflecting both fixed and random effects, to estimate temporal variation in survival rates for different classes of the population (Figure 6). As previously reported (Mosnier et al. 2015), calves showed the greatest magnitude of variation in survival, followed by yearlings. In some cases, the estimated trends were consistent across age-sex classes: for example, all age/sex classes experienced a downwards spike in survival in the early 2000s (Figure 6), although this period of lower survival was most severe and prolonged for calves. However, in the decade since 2010, survival trends appear to have diverged somewhat among age/sex classes. Survival rates over this period were mostly higher than average for older age classes, although there was a downward trend over the last 3-5 years (2018-2022), particularly for pregnant females that experience dystocia/postpartum hazards in addition to baseline hazards. In contrast, for calves there was a steady decline in

survival since 2010, with the survival rate over the last few years approaching the lowest values observed since 1980 (Figure 6). Although pregnancy rates for “available” females (*av*) do not appear to have changed substantially (Figure 7), the lower survival of calves combined with higher levels of mortality for pregnant females (Figure 6) resulted in a decline in the proportion of adult females with calves since 2010 (Figure 8), as well as an increase in the proportion of adult female deaths from dystocia/postpartum hazards (Figure 9).

The above-described trends in survival and calf production have resulted in shifts in the age/sex structure over time, for both the living population and the death assemblage. The estimated % calves and yearlings in the population tended to track calf survival rates fairly closely, with a high degree of volatility in the late 1990s and early 2000s, and a declining trend since 2010 (Figure 10A). The % grey category, which encompassed a wider range of ages (mostly juveniles, although including some younger adults) and thus was less responsive to survival changes for a single cohort, showed an increasing trend from 1980 – 2003, followed by a declining trend between 2003 and 2010. After 2010 the % greys stabilized at approximately 30% of the population, although there is suggestion of a decline starting in the last 3 years (Figure 10B). We note that the temporal pattern of % greys roughly tracks the trends in % calves/yearlings, but with a 2-5 year lag, as we would expect demographically.

The frequency distribution of dead animals provided another window into demographic processes, although we caution that distributions of living and dying animals are both related yet divergent because they are produced by the opposite demographic process (survival vs. death). Broadly speaking, the age/sex structure of the death assemblage has shifted “leftwards” since the early 1980s, from a distribution dominated by the oldest age classes to a distribution dominated by calves (as well as more younger adult age classes; Figure 11). The demographic bulge of older dying animals in the 1980s (Figure 11A) was indicative of a population that had declined from a more abundant state in previous decades, consistent with our model predictions (Figures S4). The preponderance of older juveniles and younger adults in the 2001-2010 period (Figure 11C) was indicative of elevated mortality across all age classes in the early 2000s (Figure 6). The higher representation of calves since 2011 (Figure 11D) likely reflected a decline in calf survival relative to other age classes over this period (Figure 6). The model-predicted trends in the age structure of both the living population and the death assemblage (Figures 10 and 11) were generally consistent with observed data trends in the three relevant data sets (% calves/yearlings from photo surveys, % greys from skiff surveys, and the age/sex distribution of stranded carcasses), after correcting for detection biases against calves (determined by parameters ψ_1 and ψ_2; Table 3). One exception was that our model estimates of % calves/yearlings were slightly lower than observed values between 1990-2000; however, this was not surprising given that the model was constrained by inconsistent trends in age structure between the three data sets over this period.

The ultimate outcome of all demographic processes is variation in abundance over time. Model-estimated trends from 1980–2007 (Figure 12) were fairly consistent with the pattern of trends estimated by an earlier model (Mosnier et al. 2015), although we note that absolute abundance values in the current model were higher by approximately five hundred animals than the earlier model estimates due to an update in the aerial survey data used by both models (following a comprehensive re-analysis; see St-Pierre et al. 2023). Both models suggest a pattern of overall stability through 1999, followed by a sharp increase, then decrease, then stability in abundance by 2007. However, after 2007 the inferred trends diverge: the earlier model predicted a declining trend through 2012 (although with extremely wide CI), while the current model suggested an increasing trend through approximately 2018. This increasing trend stabilized by 2018, and there has been no net growth (or possibly a slight decline) between 2018 and 2022 (Figure 12). The increasing trend from 2010–2018 estimated by the current model was likely driven by

higher adult survival over this period (Figure 6), while the stabilization/decline at the end of the time series likely reflected the continuing decline in calf survival combined with an uptick in age-independent mortality over the last few years (Figure 5). We note that the abundance trends estimated by our model appear consistent with the combined time series of photo and visual survey estimates, with model estimates effectively interpolating between the two data sets but adhering more closely to the photo surveys (Figure 12). This is expected given that the visual survey data had higher associated uncertainty estimates and thus less influence on estimated parameters (Figure S4). The estimated abundance for the final year of the time series (2022) was 1,850 (CI_{95} = 1,528 – 2,180).

PROSPECTIVE ANALYSES: MANAGEMENT THRESHOLDS AND FUTURE SCENARIOS

Based on an estimated N_{min} value of 1,711 (the 20th percentile if the posterior distribution for estimated abundance in 2022), we calculated PBR as:

$$PBR = 0.5 \cdot r_{max} \cdot N_{min} \cdot F_R = 0.5 \cdot 0.04 \cdot 1{,}711 \cdot 0.1 = 3.4 \quad (25)$$

We used the model results to estimate the functional carrying capacity (*K*) under current conditions. The point estimate for *K* was 6,706, with CI_{95} = 4,309 – 10,435. This is substantially lower than the estimate of pre-harvest abundance (13,558, CI_{95} = 12,428 – 17,432), corresponding to the historical *K*. Based on the point estimate of current *K* we can infer values for other reference thresholds: MNPL = 4,024, PRL = 3,219, and LRL = 1,609. We used these thresholds to evaluate the status of the population as-of the most recent estimate, and its expected future status assuming continuation of recent (2010-2022) environmental conditions and patterns of stochasticity. The point estimate of abundance for 2022 falls below the PRL and above the LRL, although the lower limit of the CI_{95} falls below the LRL. Projecting the population forward 100 years suggests an 87% probability that the future population will be below MNPL (if current conditions persist) as well as an 78% probability it will fall below PRL, a 41% probability it will fall below LRL, and a 0.06% probability it will fall below QE. There was a 16% probability of the baseline scenario having a mean instantaneous growth rate of <-1% over the next 28 years (Table 5).

We repeated the above assessment for 6 different future projection scenarios (as defined in Table 4), to evaluate how worsening conditions and/or the mitigating effects of management actions might impact projected status of the population (Table 5, Figure S6). Because of the strong relationship between Gulf temperature and baseline hazards, we found that even a 10% additional increase in average Gulf temperatures over the next century (an increase of one-half degree C) could lead to a 26% reduction in projected abundance relative to the baseline scenario, with associated increases in the probabilities of falling below management thresholds (Figure S6 A). For reference, average Gulf temperatures over the period 2010-2022 have already increased by three quarters of a degree C relative to the average for 1970-2009. A 20% increase in Gulf temperatures (an increase of one degree C) would be expected to have even more dire consequences (a 44% reduction in projected abundance) and would increase quasi-extinction probability to 1.4% (Figure S6 B). Conversely, if conservation efforts were able to reduce density-independent hazards (such as those associated with pollution impacts, toxic algal blooms or disease outbreaks) by 25%, this could increase projected abundance by 34% relative to the baseline scenario and reduce the probability of being below PRL to 23% (Figure S6 C). Similar though less dramatic improvements could be achieved by reducing dystocia/postpartum mortality (Table 5).

DISCUSSION

The integrated model presented here builds upon the insights and methods of previous quantitative analyses of the SLE beluga population (e.g., Kingsley 1998, Hammill et al. 2007, Lesage et al. 2014, Michaud 2014, Mosnier et al. 2015, Lesage 2021, Williams et al. 2021). We relied heavily on those previous analyses to inform our model structure, assumptions, and parameterization. By integrating multiple data sets using Bayesian hierarchical modeling, we were able to increase the resolution of population structure in our process model, allowing for greater insights into how specific threats affect demographic processes and components of the population. In particular, by combining historical harvest records, abundance estimates from multiple survey types, cause of death and age-at-death data from the carcass record, and age structure data from multiple survey platforms, we were better able to infer temporal trends in stage-specific mortality, including effects of density-dependent and density-independent factors and environmental variables. Diverse sources of information helped constrain model parameters and accommodate specific biases inherent to various types of data, such as the detection bias associated with observing small calves (both visually and in the carcass record). The use of multiple data types to gain greater insights into demographic processes is of course the defining feature of integrated population models (Besbeas et al. 2005, Abadi et al. 2010, Rhodes et al. 2011, Zipkin and Saunders 2018). While this feature has clear benefits, in some cases it can produce results that may challenge previous inferences based on individual data sets. This point is illustrated by the apparent model under-estimate of the proportion of calves/yearlings prior to 2000, as inferred from photo-based survey data (Figure 10A). The relatively minor discrepancy between model estimates and photo-based estimates between 1990-1999 reflects the models "compromise" between higher values implied by the photo survey data and lower values inferred from contemporaneous carcass age distributions and skiff survey data on percent greys in the population (Figure 11, Figure 10B); however, the resulting inferences about age structure raise questions about an earlier assumption that the proportion of juveniles in the population experienced a sustained downwards shift after 1999 (Michaud 2014, Mosnier et al. 2015). This example demonstrates both the benefits and challenges inherent in the use of integrated models for conservation.

Our current model is similar in structure to an earlier Bayesian model that used some of the same data sources (Mosnier et al. 2015). A cursory comparison of the trends predicted by the two models suggest substantial inconsistencies (e.g., compare Figure 12 from the current report to Figure 4 from Mosnier et al. 2015). However, closer examination of results shows that many of the key inferences are remarkably consistent between the two models. Most importantly, the absolute differences in abundance are entirely the result of the change in the magnitude of aerial survey estimates (based on data re-analysis), and do not reflect any intrinsic differences between model dynamics or projections. Moreover, the estimated trends in calf survival, pregnancy, and overall abundance were highly consistent between the two models through about 2007 (i.e., for all but the last 5 years of inference for the earlier model). The discrepancy in trends after 2007 is not at all surprising given the extended time series of survey data and the additional data sets (particularly carcass age structure data) that were available for fitting the current model but not the earlier one.

Another similarity between the earlier model (Mosnier et al. 2015) and the current analysis is the use of the long time series of harvest records to inform hind-casting of trends to a historic period where other data are limited. Understanding this historic period is important both because the past dynamics set the stage for current dynamics, and also because it can provide insight into population potential under more "pristine" conditions (prior to the advent of modern pollutants, climate change and fisheries collapses). As with previous analyses (Reeves and Mitchell 1984, Hammill et al. 2007, Mosnier et al. 2015), our model results indicate that the magnitude of

harvests over many decades, combined with basic beluga life history, reproduction and survivorship schedules, are consistent with a much higher historical abundance and a dramatic decline over the late 19th and early 20th centuries (Figure S4). However, our model approach built on the previous analyses to explicitly incorporate and estimate density-dependent effects on calf survival and pregnancy rates, as well as the directional shifts in density-dependent and density independent hazards that must have occurred to explain the discrepancy between historic abundance and current trends. Making these phenomena explicit within the model (rather than just implicit assumptions, as was the case in the previous analyses), served to highlight the sensitivity of hind-cast estimates of abundance to uncertainties about the nature of variation in survival over the 20th century. As a result, our projections of historical abundance have a higher degree of uncertainty than previous estimates, which we believe is a realistic representation of the true uncertainty about past dynamics. Moreover, the magnitude of our historical mean abundance estimate (13,558 individuals) is higher than past estimates, reflecting both the updated analysis of aerial survey data (which shifted all abundance estimates upwards) and our more detailed and demographically rigorous treatment of age/sex differences in mortality and density-dependent effects. Given this high degree of uncertainty and new insights into past dynamics, we caution against continued use of previous estimates of historical *K* as recovery targets or management benchmarks. Nor do we recommend switching to our current estimate of historical abundance. Instead, we suggest alternative approaches that are more relevant to current dynamics and that recognize that the effective carrying capacity for SLE beluga in the current environment has fundamentally changed from historical levels, as discussed below.

In addition to new insights about historical dynamics, our model results provide an updated picture of recent trends in survival and abundance. The previously reported increase in the volatility of survival rates (particularly calf survival) starting around 1999 (Mosnier et al. 2015) was also well supported by our model (see Figure 6). However, a new finding from our current analysis is that trends in calf survival rates and the survival rates of older animals began to diverge after 2010. Our results show that older juveniles and adults experienced an increase in survival rates starting around 2010 (Figure 6), reflecting a “stochastic” decrease in density-independent hazards (Figure 5). While this shift was incorporated as a random effect in our model, it is reasonable to hypothesize that it reflects an observed reduction in gastrointestinal cancers in SLE beluga occurring at the same time and attributed to reduced exposure to environmental contaminants such as PAH and PCBs (Lair et al. 2016, Poirier et al. 2019). Regardless, increased survival of older animals appears to have contributed to an increasing trend in abundance between 2010 and 2018, contrary to previous inferences of population decline over that period. At the same time, calf survival rates showed the opposite pattern to older animals, with reduced survival (Figure 6) and increased density-dependent hazards (Figure 5) occurring after 2010, leading to a dramatic increase in the number of calves appearing in the carcass records (Figure 11). Pregnant females also experienced higher mortality during this period (Figure 6), as dystocia/peripartum hazards did not decline in parallel with baseline hazards, resulting in an increase in their representation in the carcass record as well (Figure 9). The continued decline in the survival of calves and pregnant females, combined with a more recent uptick in baseline hazards after 2018, appears to have reversed the increasing trend in abundance over the last few years of the time series (Figure 12).

The Integrated Population Model presented here provides novel insights into key demographic processes for the SLE beluga, but there are also some important limitations and remaining challenges. Our process model currently combines multiple sources of mortality in to a single “baseline hazards” term; ideally these various mortality factors could be partitioned into separate hazards terms. Our model also does not explicitly allow for sudden catastrophic pulses of mortality, such as those associated with unusual mortality events (Lair et al. 2016, Lesage

2021). The high degree of uncertainty in many of the estimated parameters (and thus, by extension, in model projections) is a limitation that reduces the model's utility for making precise inferences about status and trends. One clear source of this uncertainty is the substantial discrepancy between the two aerial survey data sets in terms of estimated abundance. The Bayesian MCMC algorithm automatically weights data contributions to overall likelihood based on variance (see Figure S4), thus helping to avoid spurious data points from exerting undue leverage on results; nonetheless, the large discrepancies are major contributors to overall model uncertainty and should be resolved if at all possible. Given the relatively small number of surveys, the model is also potentially sensitive to single surveys with lower variance estimates: for example, the 2019 visual and photo-based estimates may be exerting a fairly strong influence on estimated trends over the last decade.

There are two other major contributors to uncertainty in our model results and predictions, each of which could potentially be addressed in differing ways:

1. Uncertainty about the relative contributions of density-dependent vs. density-independent factors to increased mortality. The data used for model fitting in the current analyses could not resolve this question, and thus we relied on an assumed range of values to set a prior. Yet the different demographic implications of density-dependent vs. density independent mortality are substantial (Ohlberger et al. 2014), and this is perhaps the primary contributor to uncertainty in future projections. Also unclear is the degree to which Allee effects – factors causing a positive correlation between population density and individual fitness, and which may become important at low abundance for some social species (Angulo et al. 2018) – or inbreeding depression (Patenaude et al. 1994) have contributed to the failure of SLE beluga to recover, although we note that both of these factors would manifest demographically as either reduced survival or reduced fecundity at lower populations sizes, and thus are implicitly accounted for in our model. We believe that much of this uncertainty could be resolved in future analyses by incorporating more information on causes of death (i.e., from necropsies) and how they vary over time and between demographic groups. Incorporation of multiple causes of death into model structure as competing hazards would be straight forward, using the same approach we used in the current model for dystocia/postpartum hazards, and in many cases it would be clear from the data or expert opinion the degree to which specific mortality hazards were density-dependent (e.g., Tinker et al. 2021).
2. Uncertainty about the actual mechanisms or external factors driving the variation in hazard rates. Our model evaluated several environmental variables as potential predictors of mortality (of which Gulf Temperature at 200 m was strongly significant), and also explicitly tracked dystocia/postpartum hazards. However, with the exception of those two factors (and harvest deaths historically), all other underlying factors responsible for fluctuations in mortality over the last two decades were not explicitly included and thus were effectively combined within the random effect terms. This was an appropriate solution given limited data availability, but it is not ideal for understanding process or evaluating specific management actions, and ultimately contributes to uncertainty about future population trends. A much better solution (though difficult) would be to identify and include in the model the relevant data for factors really driving mortality trends. This might include adding empirical data on causes of death (see above), as well as additional environmental covariates (e.g., various pollutant levels, more finely resolved prey data, etc.). As an example, the cessation in 1976 of PAH emissions and ban on PCBs in 1979 may be the causal factor for the observed reduction in gastrointestinal cancers in SLE beluga (Lair et al. 2016, Poirier et al. 2019) that resulted in reduced hazards for adults after 2010 (Figure 6), but at present this remains a hypothesis only, as the relevant variables were not explicitly

included in the model. In the case of the significant relationship found between Gulf mean temperature and calf mortality, our model currently assumes a simple linear relationship between temperature and log hazard rate. We recognize that the mechanistic underpinnings of this temperature effect are probably mediated by prey dynamics, and thus likely to be highly non-linear and complex, but future work will be needed to elucidate these mechanisms.

Even without having addressed the main sources of uncertainty discussed above, the results from our model can help inform management decisions and recovery targets. Past recovery targets for SLE beluga included achieving a 2% annual growth rate, an interim target of 1000 mature individuals, and achieving a long-term population size of 7070 individuals, which was considered to be 70% of the estimated "pristine" value of *K* (DFO 2012). As stated above, we do not recommend continued use of earlier estimates of pristine *K* as a recovery target, both because our current analyses suggest that this value underestimates both the magnitude and uncertainty around historical abundance, and (more importantly) because pre-harvest abundance provides an unrealistic and no-longer-relevant recovery target (Williams et al. 2021). We use our model to estimate a functional, "current *K*" that represents the potential equilibrium abundance that could be achieved within the environment that SLE beluga now occupy. This current *K* estimate (6,706 individuals) is slightly lower than the previously targeted long-term population size of 7,070. We caution that the estimate of current *K* presented here is sensitive to our assumptions about the relative degree of density-dependence of emerging mortality factors, and future work to better understand these processes could result in more robust estimates of *K*. However, while the prospect of basing recovery targets on a current *K* estimate (as opposed to a historical K estimate) may prompt understandable resistance to the risk of "shifting baselines", we point out the historical *K* estimate encompasses even more untested assumptions and uncertainties than the current *K* estimate, and thus in many respects represents an even more arbitrary basis for management.

Based on the updated current *K* estimate, we provide corresponding estimated values of MNPL, PRL and LRL (Table 5). We suggest that maintaining population abundance above the revised LRL threshold with some level of confidence (e.g., 80% certainty) would provide a reasonable minimum management target. Other target recovery criteria might include some minimum probability that future projections do not significantly decline (e.g., 90% probability of exceeding a mean growth rate of -1% over a single generation time). The model-estimated abundance for 2022 was still well below the estimated value of current *K*. Based on the range of variation in environmental conditions and unexplained hazards observed since 2010, there is a substantial probability that the population will remain below MNPL (87%) or PRL (78%) over the next 100 years if current conditions persist (Table 5). Additional simulations could be used to explore the range of likely outcomes of management actions aimed at mitigating specific hazards, or accounting for the emergence of new hazards (e.g., emerging pollutants or climate driven changes in productivity), like the examples in Table 4 (and see Table 5, Figure S6).

ACKNOWLEDGEMENTS

We thank M. Moisan for the analysis of skiff survey data, and Y. Morin, P. Rivard and S. Aucoin for age determination of carcasses. We are also grateful to the staff of the Réseau québécois d'urgences pour les mammifères marins (RQUMM), C. Guimont and R. Plante for the collection and transport of beluga carcasses, and the veterinarians and veterinary students involved in beluga necropsies including S. Lair, D. Martineau, S. DeGuise, C. Girard, I. Mikaelian, A. Dallaire, and S. Larrat. Over the years, the beluga carcass monitoring program has been supported through contributions from the St. Lawrence Action Plan (Canada - Quebec Agreement) and Parks Canada, Canadian Cooperative Wildlife Health Center (Faculté de

Médecine Vétérinaire, Université de Montréal), Institut National d'Écotoxicologie du Saint-Laurent (INESL), Les Industries Filmar (2005) Inc., World Wildlife Fund, and Alcan. This study was funded by the Species at Risk and Marine Conservation Target programs of Fisheries and Oceans Canada.

REFERENCES CITED

Abadi, F., Gimenez, O., Arlettaz, R., and Schaub, M. 2010. An assessment of integrated population models: bias, accuracy, and violation of the assumption of independence. Ecology 91:7–14.

Angulo, E., Luque, G. M., Gregory, S. D., Wenzel, J. W., Bessa-Gomes, C., Berec, L., and Courchamp, F. 2018. Allee effects in social species. J. Anim. Ecol. 87:47–58.

Beauchesne, D., Daigle, R. M., Vissault, S., Gravel, D., Bastien, A., Bélanger, S., Bernatchez, P., Blais, M., Bourdages, H., and Chion, C. 2020. Characterizing exposure to and sharing knowledge of drivers of environmental change in the St. Lawrence system in Canada. Front. Mar. Sci. 7:383.

Béland, P., DeGuise, S., Girard, C., Lagace, A., Martineau, D., Michaud, R., Muir, D. C., Norstrom, R. J., Pelletier, E., and Ray, S. 1993. Toxic compounds and health and reproductive effects in St. Lawrence beluga whales. J. Great Lakes Res. 19:766–775.

Bernier-Graveline, A., Lesage, V., Cabrol, J., Lair, S., Michaud, R., Rosabal, M., and Verreault, J. 2021. Lipid metabolites as indicators of body condition in highly contaminant-exposed belugas from the endangered St. Lawrence Estuary population (Canada). Environ. Res. 192:110272.

Besbeas, P., Freeman, S. N., and Morgan, B. J. 2005. The potential of integrated population modelling. Aust. New Zeal. J. Stat. 47:35–48.

Breslow, N. E. 1975. Analysis of survival data under the proportional hazards model. Int. Stat. Rev. 45–57.

Brodie, P. F. 1971. A reconsideration of aspects of growth, reproduction, and behavior of the white whale (*Delphinapterus leucas*), with reference to the Cumberland Sound, Baffin Island, population. J. Fish. Res. Board Can. 28:1309–1318.

Brodie, P. F. 1972. Significance of accessory corpora lutea in odontocetes with reference to *Delphinapterus leucas*. J. Mammal. 53:614–616.

Burns, J. J., and Seaman, G. A. 1986. Investigations of belukha whales in coastal waters of western and northern Alaska. II. Biology and ecology. US Department of Commerce, NOAA, OCSEAP Final Report 56:221–357.

Cairns, D.K., Chaput, G., Poirier, L.A., Avery, T.S., Castonguay, M., Mathers, A., Casselman, J.M., Bradford, R.G., Pratt, T., Verreault, G., Clarke, K., Veinott, G., and Bernatchez, L. 2014. Recovery Potential Assessment for the American Eel (Anguilla rostrata) for eastern Canada: life history, distribution, reported landings, status indicators, and demographic parameters. DFO Can. Sci. Advis. Sec. Res. Doc. 2013/134. xiv + 157 p.

Carpenter, B., Gelman, A., Hoffman, M. D., Lee, D., Goodrich, B., Betancourt, M., Brubaker, M., Guo, J., Li, P., and Riddell, A. 2017. Stan: A Probabilistic Programming Language. J. stat. Softw. 76:32.

Caswell, H. 2001. Matrix population models: construction, analysis, and interpretation. 2nd ed. Sinauer Associates, Sunderland, MA.

Chion, C., Bonnell, T. R., Lagrois, D., Michaud, R., Lesage, V., Dupuch, A., McQuinn, I. H., and Turgeon, S. 2021. Agent-based modelling reveals a disproportionate exposure of females and calves to a local increase in shipping and associated noise in an endangered beluga population. Mar. Pollut. Bull. 173:112977.

De Guise, S., Lagace, A., and Béland, P. 1994. Tumors in St. Lawrence beluga whales (*Delphinapterus leucas*). Vet. Pathol. 31:444–449.

De Wit, C. A. 2002. An overview of brominated flame retardants in the environment. Chemosphere 46:583–624.

DFO. 2012. Recovery Strategy for the beluga whale (*Delphinapterus leucas*) St. Lawrence Estuary population in Canada. Species at Risk Act Recovery Strategy Series. Fisheries and Oceans Canada, Ottawa. x + 88 p.

DFO. 2013. Proceedings of the National Workshop for Technical Expertise in Stock Assessment (TESA): Maximum Sustainable Yield (MSY) Reference Points and the Precautionary Approach when Productivity Varies; December 13-15, 2011. DFO Can. Sci. Advis. Sec. Proceed. Ser. 2012/055.

DFO. 2014. Status of beluga (*Delphinapterus leucas*) in the St. Lawrence River estuary. DFO Can. Sci. Advis. Sec. Sci. Advis. Rep. 2013/076.

Duplisea, D. E., Merette, D., Roux, M. J., Benoît, H., Blais, M., Galbraith, P., and Plourde, S. 2020. gslea: the Gulf of St Lawrence ecosystem approach data matrix R-package. R package version 0.1.

Ellis, S., Franks, D. W., Nattrass, S., Currie, T. E., Cant, M. A., Giles, D., Balcomb, K. C., and Croft, D. P. 2018. Analyses of ovarian activity reveal repeated evolution of post-reproductive lifespans in toothed whales. Sci. Rep. 8:12833.

Erbe, C., Dunlop, R., and Dolman, S. 2018. Effects of noise on marine mammals. Effects of anthropogenic noise on animals: 277–309.

Fine, J. P., and Gray, R. J. 1999. A proportional hazards model for the subdistribution of a competing risk. J. Am. Stat. Assoc. 94:496–509.

Fowler, C. W. 1987. A review of density dependence in populations of large mammals. Pages 401–441 Current mammalogy. Springer.

Galbraith, P. S., Chassé, J., Dumas, J., Shaw, J.-L., Caverhill, C., Lefaivre, D., and Lafleur, C. 2022. Physical oceanographic conditions in the Gulf of St. Lawrence during 2021. DFO Can. Sci. Advis. Sec. Res. Doc. 2022/034. iv + 83 p.

Gelfand, A. E., Ghosh, S. K., Christiansen, C., Soumerai, S. B., and McLaughlin, T. J. 2000. Proportional hazards models: a latent competing risk approach. J. Royal Statist. Soc. Ser. C (Applied Statistics) 49:385–397.

Gelman, A., Jakulin, A., Pittau, M. G., and Su, Y.-S. 2008. A weakly informative default prior distribution for logistic and other regression models. Annals Appl. Stat. 2:1360–1383.

Gervaise, C., Simard, Y., Roy, N., Kinda, B., and Menard, N. 2012. Shipping noise in whale habitat: Characteristics, sources, budget, and impact on belugas in Saguenay–St. Lawrence Marine Park hub. J. Acoust. Soc. Am. 132:76–89.

Gosselin, J-F., Hammill, M.O. and Mosnier, A. 2014. Summer abundance indices of St. Lawrence Estuary beluga (*Delphinapterus leucas*) from a photographic survey in 2009 and 28 line transect surveys from 2001 to 2009. DFO Can. Sci. Advis. Sec. Res. Doc. 2014/021. iv + 51 p.

Hammill, M., and Sauvé, C. 2017. Growth and condition in harp seals: evidence of density-dependent and density-independent influences. ICES J. Mar. Sci. 74:1395–1407.

Hammill, M. O., Measures, L. N., Gosselin, J.-F., and Lesage, V. 2007. Lack of recovery in St. Lawrence Estuary beluga. DFO Can. Sci. Advis. Sec. Res. Doc. 2007/026.

Hammill, M.O., Stenson, G.B., and Doniol-Valcroze, T. 2017. A management framework for Nunavik beluga. DFO Can. Sci. Advis. Sec. Res. Doc. 2017/060. v + 34 p.

Harington, C. R. 2008. The evolution of Arctic marine mammals. Ecol. Appl. 18:S23–S40.

Heide-Jørgensen, M. P., and Teilmann, J. 1994. Growth, reproduction. age structure and feeding habits of white whales (*Delphinapterus leucas*) in West Greenland Waters. Comm. Greenland Biosci. 39:195–212.

Holser, R. R., Crocker, D. E., Robinson, P. W., Condit, R., and Costa, D. P. 2021. Density-dependent effects on reproductive output in a capital breeding carnivore, the northern elephant seal (*Mirounga angustirostris*). Proc. R. Soc. B 288:20211258.

Inyakina, N. V., Musidray, A. A., Nikitkina, E. V., Mukhachev, E. V., Politov, V. P., and Shiryaev, G. V. 2022. Dependence of the Testosterone Concentration in the Blood of Male Beluga Whales *Delphinapterus leucas* on the Age and Season. Biol. Bull. 49:101–106.

Kingsley, M. C. 1998. Population index estimates for the St. Lawrence belugas, 1973–1995. Mar. Mamm. Sci. 14:508–529.

Kleinenberg, S. E., Yablokov, A. V., Bel'kovich, B. M., and Tarasevich, M. N. 1964. Beluga (*Delphinapterus leucas*): investigation of the species. Akad. Nauk SSSR, Moscow. Translated from Russian. Israel Program for Sci. Transl., Jerusalem, 1969. 376 p.

Lair, S., Gentes, M-L. and Measures, L.N. 2015. Documentation de l'évolution du protocole d'examen des carcasses de béluga de l'estuaire du Saint-Laurent de 1983 à 2012. Rapp. tech. can. sci. halieut. aquat. 3143 : viii + 65 p.

Lair, S., Measures, L. N., and Martineau, D. 2016. Pathologic findings and trends in mortality in the beluga (Delphinapterus leucas) population of the St Lawrence Estuary, Quebec, Canada, from 1983 to 2012. Vet. Pathol. 53:22–36.

Laurin, J. 1982. Étude écologique et éthologique de la population de bélugas (*Delphinapterus leucas*) du fjord du Saguenay, Québec. Thèse de maîtrise, Université de Montréal (Qc). 145 p

Lebeuf, M. 2009. La contamination du béluga de l'estuaire du Saint-Laurent par les polluants organiques persistants en revue. Rev. Sci. Eau 22:199–233.

Lebeuf, M., Measures, L., Noël, M., Raach, M., and Trottier, S. 2014a. A twenty-one year temporal trend of persistent organic pollutants in St. Lawrence Estuary beluga, Canada. Sci. Total Environ. 485:377–386.

Lebeuf, M., Raach, M., Measures, L., Ménard, N., and Hammill, M. 2014b. Temporal trends of PBDEs in adult and newborn beluga (*Delphinapterus leucas*) from the St. Lawrence Estuary. DFO Can. Sci. Advis. Sec. Res. Doc. 2013/120. v + 11 p.

Lesage, V. 2021. The challenges of a small population exposed to multiple anthropogenic stressors and a changing climate: The St. Lawrence Estuary beluga. Polar Res. 40.

Lesage, V., Measures, L., Mosnier, A., Lair, S., Michaud, R. and Béland, P. 2014. Mortality patterns in St. Lawrence Estuary beluga (*Delphinapterus leucas*), inferred from the carcass recovery data, 1983-2012. DFO Can. Sci. Advis. Sec. Res. Doc. 2013/118. iv + 23 p.

Lesage, V., S. Lair, S. Turgeon, and P. Béland. 2020. Diet of St. Lawrence Estuary Beluga (*Delphinapterus leucas*) in a changing ecosystem. Can. Field-Nat. 134:21–35.

Lowry, L. F., Citta, J. J., O'corry-Crowe, G., Quakenbush, L. T., Frost, K. J., Suydam, R., Hobbs, R. C., and Gray, T. 2019. Distribution, abundance, harvest, and status of Western Alaska beluga whale, *Delphinapterus leucas*, stocks. Mar. Fish. Rev. 81:54–71.

Martineau, D., Béland, P., Desjardins, C., and Lagacé, A. 1987. Levels of organochlorine chemicals in tissues of beluga whales (*Delphinapterus leucas*) from the St. Lawrence Estuary, Quebec, Canada. Arch. Environ. Contam. Toxicol. 16:137–147.

Martineau, D., De Guise, S., Fournier, M., Shugart, L., Girard, C., Lagacé, A., and Béland, P. 1994. Pathology and toxicology of beluga whales from the St. Lawrence Estuary, Quebec, Canada. Past, present and future. Sci Total Environ. 154:201–215.

Matthews, C. J., and Ferguson, S. H. 2015. Weaning age variation in beluga whales (*Delphinapterus leucas*). J. Mamm. 96:425–437.

McGuire, T. L., Stephens, A. D., McClung, J. R., Garner, C. D., Shelden, K. E. W., Boor, G. K. H., and Wright, B. 2020. Reproductive natural history of endangered Cook Inlet Beluga whales: insights from a long-term photo-identification study. Polar Biol. 43:1851–1871.

McQuinn, I. H., Lesage, V., Carrier, D., Larrivée, G., Samson, Y., Chartrand, S., Michaud, R., and Theriault, J. 2011. A threatened beluga (Delphinapterus leucas) population in the traffic lane: Vessel-generated noise characteristics of the Saguenay-St. Lawrence Marine Park, Canada. J. Acoust. Soc. Am. 130:3661–3673.

Ménard, N., R. Michaud, C. Chion and S. Turgeon. 2014. Documentation of Maritime Traffic and Navigational Interactions with St. Lawrence Estuary Beluga (*Delphinaterus leucas)* in Calving Areas Between 2003 and 2012. DFO Can. Sci. Advis. Sec. Res. Doc. 2014/003. v + 24 p.

Michaud, R. 2014. St. Lawrence Estuary beluga (*Delphinapterus leucas*) population parameters based photo-identification surveys, 1989-2012. DFO Can. Sci. Advis. Sec. Res. Doc. 2013/130. iv + 27 p.

Mosnier, A., T. Doniol-Valcroze, J.-F. Gosselin, V. Lesage, L. N. Measures, and M. O. Hammill. 2015. Insights into processes of population decline using an integrated population model: the case of the St. Lawrence Estuary beluga (Delphinapterus leucas). Ecol. Model. 314:15–31.

Norman, S. A., Dreiss, L. M., Niederman, T. E., and Nalven, K. B. 2022. A Systematic Review Demonstrates How Surrogate Populations Help Inform Conservation and Management of an Endangered Species—The Case of Cook Inlet, Alaska Belugas. Front. Mar. Sci. 242.

Ohlberger, J., Rogers, L. A., and Stenseth, N. C. 2014. Stochasticity and determinism: how density-independent and density-dependent processes affect population variability. PLoS One 9:e98940.

Patenaude, N. J., Quinn, J. S., Beland, P., Kingsley, M., and White, B. N. 1994. Genetic variation of the St. Lawrence beluga whale population assessed by DNA fingerprinting. Mol. Ecol. 3:375–381.

Pippard, L. 1985. Status of the St. Lawrence River population of Beluga, *Delphinapterus leucas*. Can. Field-Nat. Ottawa ON 99:438–450.

Pippard, L., and Malcolm, H.1978. White whales (*Delphinapterus leucas*). Observations on their distribution, population and critical habitats in the St. Lawrence and Saguenay rivers. Unpublished report prepared for Department of Indian and Northern Affairs. Page 161 pp. Parks Canada, Ottawa, Ontario.

Poirier, M. C., Lair, S., Michaud, R., Hernández-Ramon, E. E., Divi, K. V., Dwyer, J. E., Ester, C. D., Si, N. N., Ali, M., and Loseto, L. L. 2019. Intestinal polycyclic aromatic hydrocarbon-DNA adducts in a population of beluga whales with high levels of gastrointestinal cancers. Environ. Mol. Mutagen. 60:29–41.

R.Core.Team. 2022. R: A language and environment for statistical computing. R Foundation for Statistical Computing, Vienna, Austria.

Reeves, R. R., and Mitchell, E. 1984. Catch history and initial population of white whales(*Delphinapterus leucas*) in the river and Gulf of St. Lawrence, eastern Canada. Nat. Can. 111:63–121.

Rhodes, J. R., Ng, C. F., de Villiers, D. L., Preece, H. J., McAlpine, C. A., and Possingham, H. P. 2011. Using integrated population modelling to quantify the implications of multiple threatening processes for a rapidly declining population. Biol. Conserv. 144:1081–1088.

Richardson, W. J., Greene, C. R. Jr, Malme, C. I., and Thomson, D. H. 2013. Marine mammals and noise. Academic press.

Robeck, T. R., Monfort, S. L., Calle, P. P., Dunn, J. L., Jensen, E., Boehm, J. R., Young, S., and Clark, S. T. 2005. Reproduction, growth and development in captive beluga (*Delphinapterus leucas*). Zoo Biol. 24:29–49.

Rolland, N., Turcotte, F., McDermid, J.L., DeJong, R.A., and Landry, L. 2022. Assessment of the NAFO Division 4TVn southern Gulf of St. Lawrence Atlantic Herring (*Clupea harengus*) in 2020-2021. DFO Can. Sci. Advis. Sec. Res. Doc. 2022/068. xii + 142 p.

Savenkoff, C., Castonguay, M., Chabot, D., Hammill, M. O., Bourdages, H., and Morissette, L. 2007. Changes in the northern Gulf of St. Lawrence ecosystem estimated by inverse modelling: evidence of a fishery-induced regime shift? Estuar. Coast. Shelf Sci. 73:711–724.

Sergeant, D. E., and Hoek, W.1988. An update of the status of white whales *Delphinapterus leucas* in the Saint Lawrence Estuary, Canada. Biol. Conserv. 45:287–302.

Simard, Y., Lepage, R., and Gervaise, C. 2010. Anthropogenic sound exposure of marine mammals from seaways: Estimates for Lower St. Lawrence Seaway, eastern Canada. Appl. Acoust. 71:1093–1098.

Simard, Y., Roy, N., Giard, S., and Yayla, M. 2014. Canadian year-round shipping traffic atlas for 2013: Volume 1, East Coast marine waters. Can. Tech. Rep. Fish. Aquat. Sci 3091:327.

Simond, A. E., Houde, M., Lesage, V., and Verreault, J. 2017. Temporal trends of PBDEs and emerging flame retardants in belugas from the St. Lawrence Estuary (Canada) and comparisons with minke whales and Canadian Arctic belugas. Environ. Res. 156:494–504.

Simond, A. E., Houde, M., Lesage, V., Michaud, R., and Verreault, J. 2020. Metabolomic profiles of the endangered St. Lawrence Estuary beluga population and associations with organohalogen contaminants. Sci. Total Environ. 717:137204.

Southall, B. L., Nowacek, D. P., Bowles, A. E., Senigaglia, V., Bejder, L., and Tyack, P. L. 2021. Marine mammal noise exposure criteria: assessing the severity of marine mammal behavioral responses to human noise. Aquat. Mamm. 47:421–464.

Starr, M., Lair, S., Michaud, S., Scarratt, M., Quilliam, M., Lefaivre, D., Robert, M., Wotherspoon, A., Michaud, R., and Ménard, N. 2017. Multispecies mass mortality of marine fauna linked to a toxic dinoflagellate bloom. PloS one 12:e0176299.

St-Pierre, A.P., Lesage, V, Mosnier, A., Tinker, M.T., Gosselin, J.-F. 2023. Summer abundance estimates for St. Lawrence Estuary beluga (*Delphinapterus leucas*) from 52 visual line transect surveys and 11 photographic surveys conducted from 1990 to 2022. DFO Can. Sci. Advis. Sec. Res. Doc. 2023/048. v + 81 p.

Suydam, R. S. 2009. Age, growth, reproduction, and movements of beluga whales (*Delphinapterus leucas*) from the eastern Chukchi Sea. University of Washington.

Tinker, M. T., Carswell, L. P., Tomoleoni, J. A., Hatfield, B. B., Harris, M. D., Miller, M. A., Moriarty, M. E., Johnson, C. K., Young, C., Henkel, L., Staedler, M. M., Miles, A. K., and Yee, J. L. 2021. An Integrated Population Model for Southern Sea Otters. U.S. Geological Survey Open-File Report 2021–1076, 50 p., https://doi.org/10.3133/ofr20211076. Reston, VA.

Vehtari, A., Gelman, A., and Gabry, J. 2017. Practical Bayesian model evaluation using leave-one-out cross-validation and WAIC. Stat. Comput. 27:1413–1432.

Vergara, V., Wood, J., Lesage, V., Ames, A., Mikus, M.-A., and Michaud, R. 2021. Can you hear me? Impacts of underwater noise on communication space of adult, sub-adult and calf contact calls of endangered St. Lawrence belugas (*Delphinapterus leucas*). Polar Res. 40.

Vladykov, V. 1944. Etudes sur les mammiferes aquatiques: III. Chasse, biologie et valeur economique du Marsouin Blanc ou Beluga (*Delphinapterus leucas*) du fleuve et du golfe Saint Laurent. Institut de zoologie, Universite de Montreal.

Wade, P. R. 1998. Calculating limits to the allowable human-caused mortality of cetaceans and pinnipeds. Mar. Mamm. Sci. 14:1–37.

Wagemann, R., Stewart, R. E. A., Beland, P., and Desjardins, C. 1990. Heavy metals and selenium in tissues of beluga whales, *Delphinapterus leucas*, from the Canadian Arctic and the St. Lawrence Estuary. Can. Bull. Fish. Aquat. Sci./Bull. Can. Sci. Halieut. Aquat. 1990.

Williams, R., Lacy, R. C., Ashe, E., Hall, A., Plourde, S., McQuinn, I. H., and Lesage, V. 2021. Climate change complicates efforts to ensure survival and recovery of St. Lawrence Estuary beluga. Mar. Pollut. Bull. 173:113096.

Worm, B., and Myers, R. A. 2003. Meta-analysis of cod–shrimp interactions reveals top-down control in oceanic food webs. Ecology 84:162–173.

Zipkin, E. F., and Saunders, S. P. 2018. Synthesizing multiple data types for biological conservation using integrated population models. Biol. Conserv. 217:240–250.

TABLES

Table 1. Demographic transitions for St Lawrence beluga model. The ID codes (column 1) correspond to the annotations associated with transition arrows shown in the loop diagram (Figure 1) and cell contents of the projection matrix (Figure 2). Adult females are divided into 3 classes corresponding to reproductive status: available for reproduction (AF_{av}), pregnant (AF_{pr}) and with dependent calf (AF_{wc}). In the equations, "S" represents the probability of survival, "G" represents the probability of "growing" (advancing to the next age class), conditional upon survival, "P" represents the probability of becoming pregnant for females of status AF_{av}, "S_n" represents the probability that newborn calves-of-the-year survive to the fall survey, and the index "i" identifies the age/sex/status class, or stage, corresponding to the row or column number of the population projection matrix (Figure S1) and can be cross referenced to the loop diagram (Figure 1).

ID	Description	Equation
a	Survival/growth, juveniles (juv.) aged 0-3yr	S_i, *i* = 1, 2, 3, 4
b	Survival/persistence (same stage), juvenile aged 4-7yr	$S_i \cdot (1 - G_i)$, *i* = 5
c	Survival/growth (to adult male), juvenile aged 4-7yr	$0.5 \cdot S_i \cdot G_i$, *i* = 5
d	Survival/persistence (same stage), adult males	$S_i \cdot (1 - G_i)$, *i* = 30, 31, … 37
e	Survival/growth (to next stage), adult males	$S_i \cdot G_i$, *i* = 30, 31, … 37
f	Survival/growth (to adult female), juvenile aged 4-7yr	$0.5 \cdot S_i \cdot G_i$, *i* = 5
g	Survival/persistence, no pregnancy, AF_{av}	$S_i \cdot (1 - G_i) \cdot (1 - P_i)$, *i* = 6, 7, … 13
h	Survival/growth, no pregnancy, AF_{av}	$S_i \cdot G_i \cdot (1 - P_i)$, *i* = 6, 7, … 13
i	Survival/persistence, become pregnant, AF_{av}	$S_i \cdot (1 - G_i) \cdot Pr_i$, *i* = 6, 7, … 13
j	Survival/growth, become pregnant, AF_{av}	$S_i \cdot G_i \cdot P_i$, *i* = 6, 7, … 13
k	Survival/persistence, newborn calf dies, AF_{pr}	$S_i \cdot (1 - G_i) \cdot (1 - S_n)$, *i* = 14, 15, … 21
l	Survival/growth, newborn calf dies, AF_{pr}	$S_i \cdot G_i \cdot (1 - S_n)$, *i* = 14, 15, … 21
m	Survival/persistence, newborn calf survives, AF_{pr}	$S_i \cdot (1 - G_i) \cdot S_n$, *i* = 14, 15, … 21
n	Survival/growth, newborn calf survives, AF_{pr}	$S_i \cdot G_i \cdot S_n$, *i* = 14, 15, … 21
o	Survival/persistence, female with calf (AF_{wc})	$S_i \cdot (1 - G_i)$, *i* = 22, 23, … 29
p	Survival/growth, female with calf (AF_{wc})	$S_i \cdot G_i$, *i* = 22, 23, … 29
q	Reproduction, pregnant female produces calf (age 0)	$S_i \cdot S_n$, *i* = 14, 15, … 21

Table 2. Summary and descriptions of the parameters included in the model.

Symbol	Name	Prior	Description
γ_0	gamma_0	Half-Cauchy(0, 1)	Baseline log hazards: determines adult survival in ideal conditions
γ_1	gamma_1	Half-Cauchy(0, 1)	Log hazard ratio, early hazards (primarily affecting calves/juveniles)
γ_2	gamma_2	Half-Cauchy(0, 1)	Log hazard ratio, late hazards (primarily affecting older animals)
γ_3	gamma_3	Cauchy(0, .5)	Log hazard ratio, males relative to females
γ_Z	gamma_Z	Cauchy(0, 1)	Log-hazard ratio for Dystocia/postpartum mortality, pregnant females
γ_H	gamma_H	Cauchy(0, 1)	Log-hazard ratio for Harvest mortality (for adult animals: reduced for juveniles)
δ	delta	Half-Cauchy(0, .1)	Parameter determining shape of age-based adjustment function for early hazards (Δ)
ω	omega	Half-Cauchy(0, .1)	Parameter determining shape of age-based adjustment function for late hazards (Ω)
ϕ	phi	Half-Cauchy(0, .1)	Effect of density-dependence (pre-harvest conditions)
β_j	Beta_j	Cauchy(0, 1)	Effect of environmental variable j on mortality of calves/juveniles
σ_D	sigma_D	Half-Cauchy(0, .5)	Standard error, environmental stochasticity affecting calves/juveniles
σ_A	sigma_A	Half-Cauchy(0, .5)	Standard error, stochasticity in hazards affecting all ages
σ_F	sigma_F	Half-Cauchy(0, .5)	Standard error, stochasticity in dystocia/postpartum hazards
σ_H	sigma_H	Half-Cauchy(0, .5)	Standard error, annual variation in harvest hazards
θ	theta	Half-Cauchy(0, .5)	Log of proportional increase in density-dependent mortality effects
α	alpha	Half-Cauchy(0, .5)	Density-independent component of increased mortality
η	eta	Normal(-1.7, 0.1)	Parameter determining baseline probability an available female becomes pregnant
ρ	rho	Beta(50, 50)	Parameter determining proportional strength of density-dependent effects on pregnancy and dystocia hazards relative to effects on calf mortality
ψ_1	psi_1	Beta(1, 1)	Bias adjustment parameter, proportion of calves detected in carcass record
ψ_2	psi_2	Beta(1, 1)	Bias adjustment parameter, proportion of grey individuals on skiff surveys
ν	nu	Half-Cauchy(0, 5)	Precision parameter, beta-distributed proportion grey animals on skiff surveys
$N_{t=0}$	N_initial	Lognormal(9.3, .3)	Abundance at the beginning of the study period (1865)
$N_{t=T}$	N_final	*NA (derived)*	Abundance at the end of the study period (2022)

Table 3. Summary of model fitting results: posterior distribution and model fitting statistics for base parameters and select derived parameters.

Parameter	Mean	SD	2.75% Q	5% Q	50% Q	95% Q	97.5% Q	SS_{eff}	R-hat
γ_0	3.2270	0.7078	1.7711	2.0013	3.2470	4.3642	4.5754	950.58	1.0164
γ_1	6.0743	0.7223	4.6785	4.9114	6.0572	7.3097	7.5488	960.23	1.0159
γ_2	4.8303	0.7778	3.4892	3.6581	4.7763	6.2352	6.5152	967.32	1.0187
γ_3	0.0643	0.0986	-0.1085	-0.0810	0.0529	0.2424	0.2865	3888.17	1.0029
γ_Z	5.4792	0.2940	4.8480	4.9727	5.4975	5.9321	6.0033	1904.27	1.0083
γ_H	6.0378	0.0695	5.9002	5.9217	6.0380	6.1532	6.1740	1659.13	1.0132
δ	0.2731	0.1365	0.0602	0.0838	0.2560	0.5192	0.5913	1040.34	1.0162
ω	0.1657	0.2083	0.0038	0.0078	0.0933	0.5893	0.7792	1821.00	1.0091
ϕ	0.0686	0.0066	0.0564	0.0581	0.0684	0.0800	0.0824	3649.03	1.0041
β_I	0.3421	0.1633	0.0340	0.0796	0.3378	0.6159	0.6724	2517.37	1.0058
σ_D	0.4688	0.1847	0.2129	0.2246	0.4421	0.8096	0.8827	1510.12	1.0124
σ_A	1.0239	0.1821	0.6893	0.7418	1.0144	1.3413	1.4193	1558.76	1.0105
σ_F	0.1908	0.1972	0.0337	0.0375	0.1220	0.6034	0.7938	2758.54	1.0056
σ_H	1.5275	0.1172	1.3172	1.3485	1.5202	1.7332	1.7761	5467.80	1.0039
θ	0.2344	0.2205	0.0204	0.0276	0.1570	0.7090	0.8477	1897.79	1.0060
α	0.0489	0.0576	0.0032	0.0045	0.0282	0.1654	0.2165	1956.15	1.0063
η	-1.6971	0.0503	-1.7957	-1.7804	-1.6964	-1.6150	-1.5989	5650.10	1.0009
ρ	0.5010	0.0501	0.4031	0.4173	0.5016	0.5818	0.5957	4941.40	1.0010
ψ_1	0.0814	0.0168	0.0512	0.0558	0.0801	0.1107	0.1181	1862.63	1.0080
ψ_2	0.9195	0.0423	0.8336	0.8469	0.9207	0.9867	0.9933	2002.87	1.0051
ν	75.40	24.45	37.56	41.73	72.10	119.96	132.05	3193.08	1.0035
$N_{t=0}$	13287	504.5	12395	12525	13252	14166	14326	4386.08	1.0035
$N_{t=T}$	1850	166	1528	1582	1850	2127	2180	6565.03	1.0010

Table 4. Description of Scenarios evaluated using forward projections of the best-fit model, with modifications to parameters as described. All model projections were run for 100 years and replicated 10000 times to capture parameter uncertainty and sampling variance.

Scenario	Description	Explanation
Scenario 0	Base model	Project model with no management action or expected change in conditions: parameters drawn from estimated joint posterior distribution, and environmental variables and random effects drawn from observed distributions over most recent 12 years (2010-2022)
Scenario 1	10% incr. Temp.	Same as base, but Gulf water temperature increases by 10% over 100 years (i.e., one half degree Celsius higher than 2010-2022 values)
Scenario 2	20% incr. Temp.	Same as base, but Gulf water temperature increases by 20% over 100 years (i.e., one degree Celsius higher than 2010-2022 values)
Scenario 3	25% reduced Base Hz.	Same as base, but reduce baseline hazards (Λ_B) by 25%
Scenario 4	25% increased Base Hz.	Same as base, but increase baseline hazards (Λ_B) by 25%
Scenario 5	25% reduced DyPP Hz.	Same as base, but reduce dystocia/postpartum hazards (α) by 25%
Scenario 6	25% increased DyPP Hz.	Same as base, but increase dystocia/postpartum hazards (α) by 25%

Table 5. Summary of results from future simulations generated using Integrated Population Model for St. Lawrence Estuary beluga. Model projections were run for 100 years and replicated 10000 times to capture parameter uncertainty and sampling variance (refer to Table 4 for details of each simulation). The distributions of simulation results were then compared to target thresholds, including 60% K (MNPL) = 4,024, PRL = 3,219, LRL = 1,609, and QE = 50 adult females. The probability that the mean instantaneous rate of growth (r) over a single generation (28 years) was expected to be greater than 1% or less than -1% is also shown.

Scenario	Description	Mean N	CI95_lo	CI95_hi	Min_N	% Change vs Base	Prob. >60%K	Prob. >PRL	Prob. >LRL	Prob. <QE	Prob. r > 1%	Prob. r < -1%
Historical K	Pre-harvest est. K	13,558	12,428	17,432	-	-	-	-	-	-	-	-
Current K	Model est. K	6,706	4,309	10,435	-	-	-	-	-	-	-	-
Scenario 0	Base model	2,285	338	6,289	1,235	-	0.1308	0.2230	0.5944	0.0006	0.181%	0.2592
Scenario 1	10% incr. Temp.	1,687	155	5,503	1,043	-26.2	0.0710	0.1264	0.3918	0.0030	0.069%	0.2312
Scenario 2	20% incr. Temp.	1,272	67	4,949	842	-44.3	0.0476	0.0830	0.2660	0.0144	-0.044%	0.2056
Scenario 3	25% redc. Base Hz.	5,335	1,352	11,721	1,674	133.5	0.6418	0.7728	0.9582	0.0000	1.419%	0.6798
Scenario 4	25% incr. Base Hz.	945	84	3,148	686	-58.6	0.0098	0.0224	0.1600	0.0098	-0.926%	0.0602
Scenario 5	25% redc. DyPP Hz.	2,484	376	6,738	1,280	8.7	0.1618	0.2570	0.6450	0.0000	0.279%	0.286
Scenario 6	25% incr. DyPP Hz.	2,099	306	5,861	1,191	-8.1	0.1022	0.1864	0.5380	0.0004	0.087%	0.2304

FIGURES

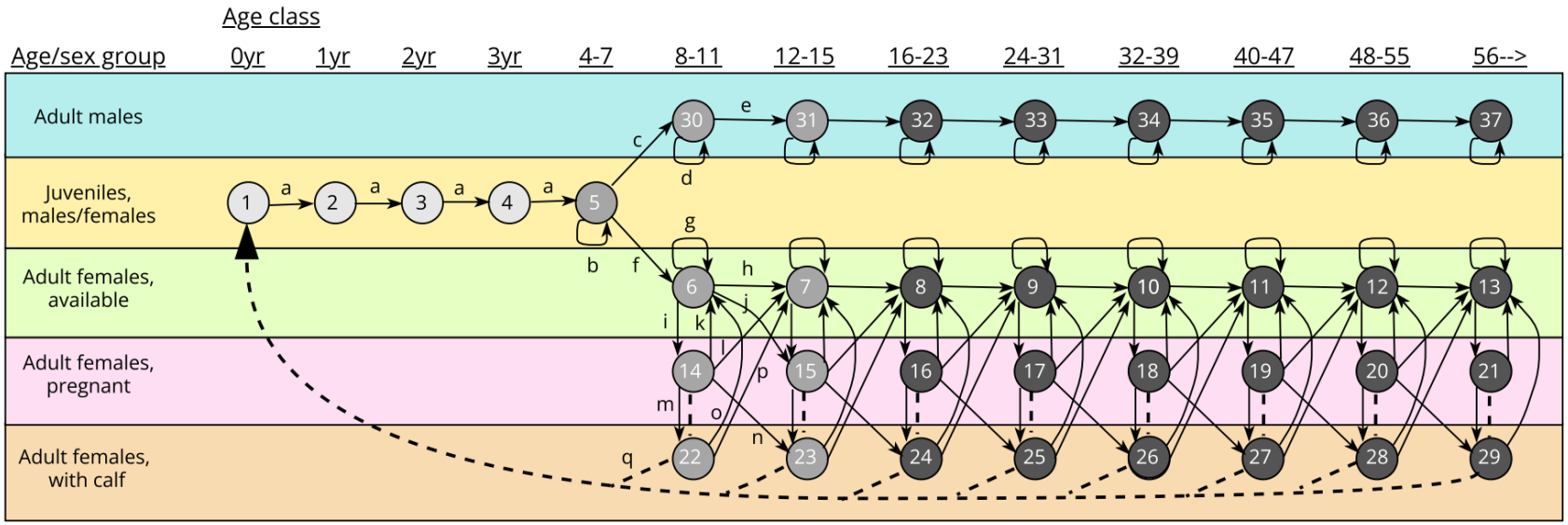

Figure 1. Loop diagram showing demographic transitions for a population model of St. Lawrence Estuary beluga. Demographic stages are represented by circles (annotated by sequential stage numbers), where each stage is defined by a unique combination of age, sex, and reproductive status. We note that age classes are of variable duration, with the shading of circles indicating stage duration: light grey = 1yr, medium grey = 4 yr and dark grey = 8yr stage durations. Stages are arranged in columns (corresponding to age class) and rows (corresponding to age/sex groupings), with connecting arrows representing all possible transitions between stages. Solid arrows represent survival/growth transitions while dashed arrows represent reproductive contributions to the 0yr age class (=newborn calves). The lower-case letter annotations associated with arrows identify the type of transition and can be cross-referenced to the definitions in Table 2 (in the case of identical transitions repeated across age classes, only the first instance is labelled).

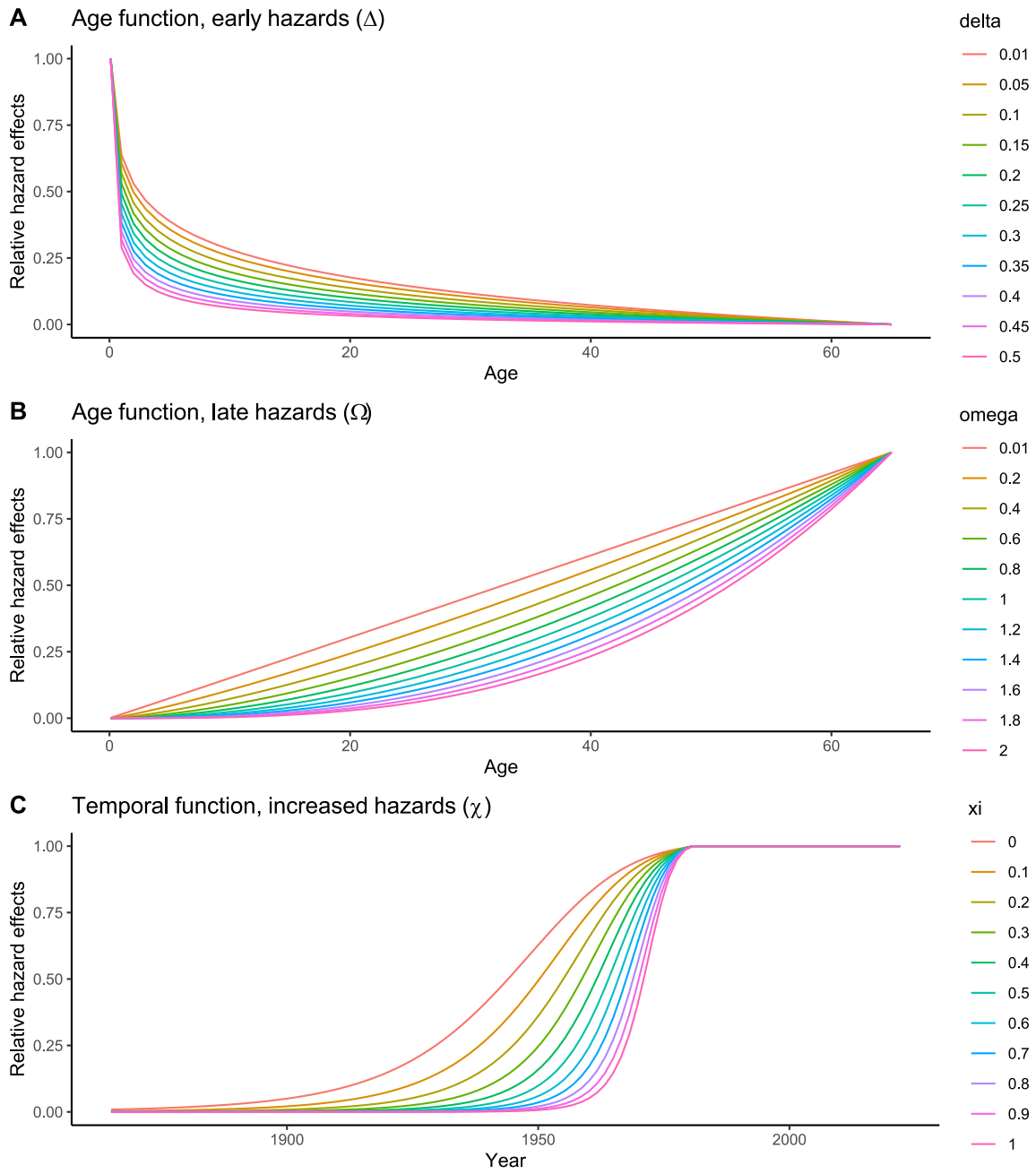

Figure 2. Parameter modifying functions that mediate the strength of specific hazards (based on age or time) used in an Integrated Population Model for St. Lawrence Estuary Beluga.

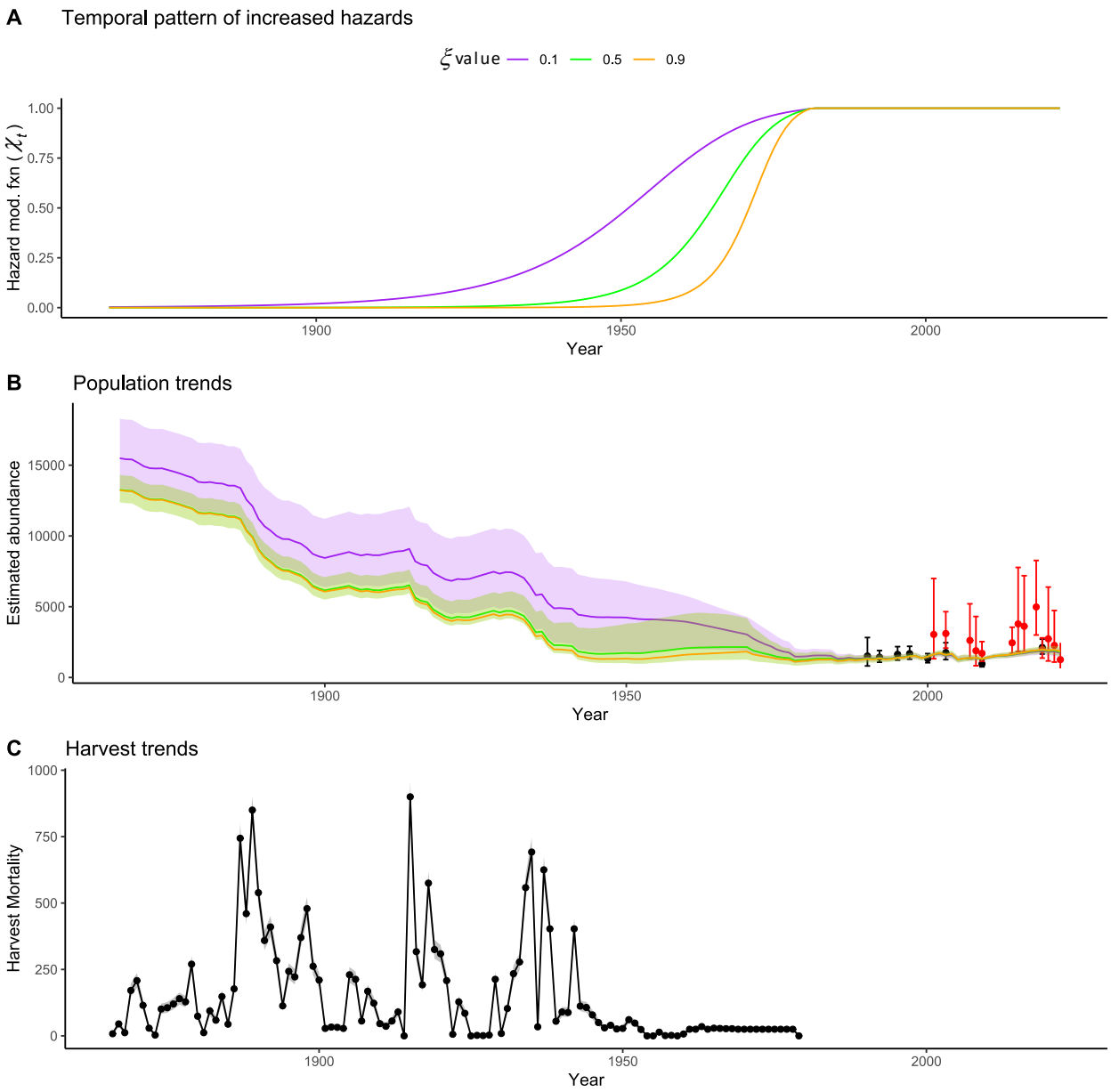

Figure 3. Estimated historical trends in the St Lawrence Beluga population generated from an integrated population model. Panel A shows 3 possible relationships between increased hazards and time (temporal function χ) associated with alternative values of ξ. Panel B shows estimated abundance values associated with alternative χ functions (dark lines = mean estimate, shaded ribbons = CI95), as well as associated observed estimates from photo surveys (black points) and visual surveys (red points). Panel C shows harvest mortality as estimated from the model (line = mean and shaded ribbon = CI95) and reported data (points).

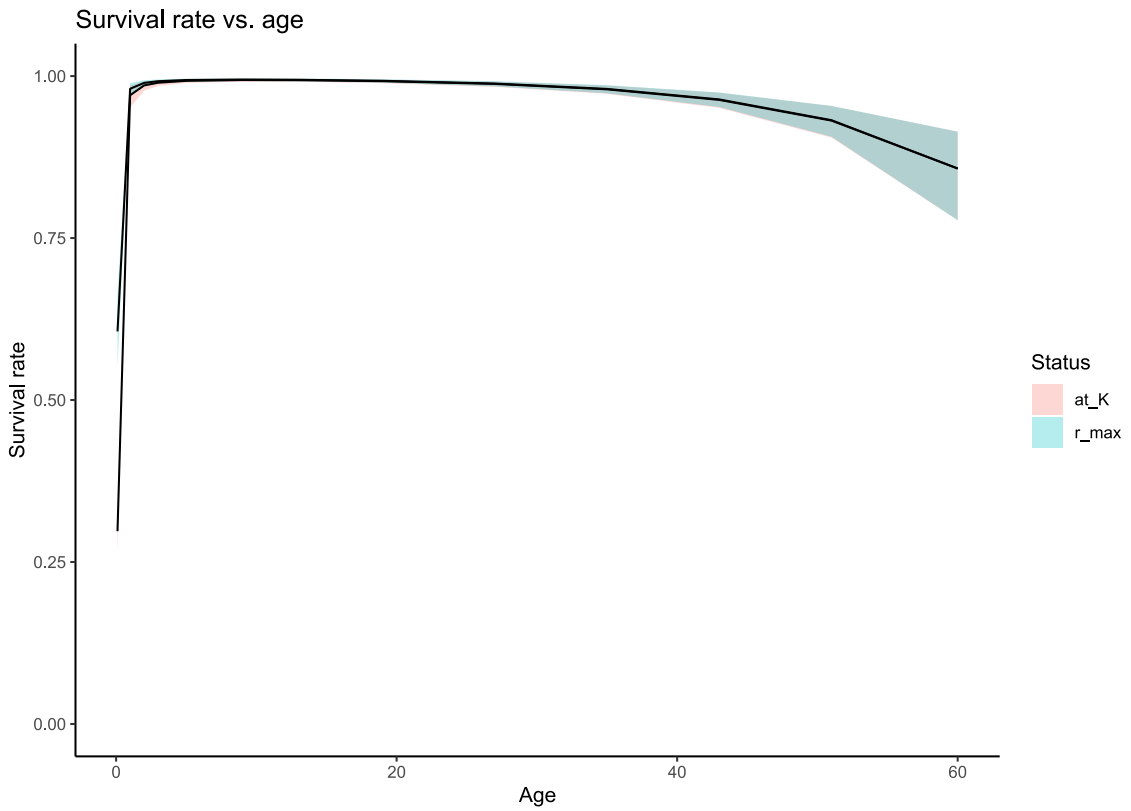

Figure 4. Plot of estimated annual survival rate as a function of age for St. Lawrence Estuary beluga. Survival rates are density-dependent and so are plotted for two different relative densities: 1) high density, at carrying capcity (K), and 2) at low density, when the populaiton is growing at the maximum growth rate (r_{max}). Mean survival under both conditions is plotted as a solid line, and 95% uncertainty bands (the credible intervals) are plotted as shaded bands.

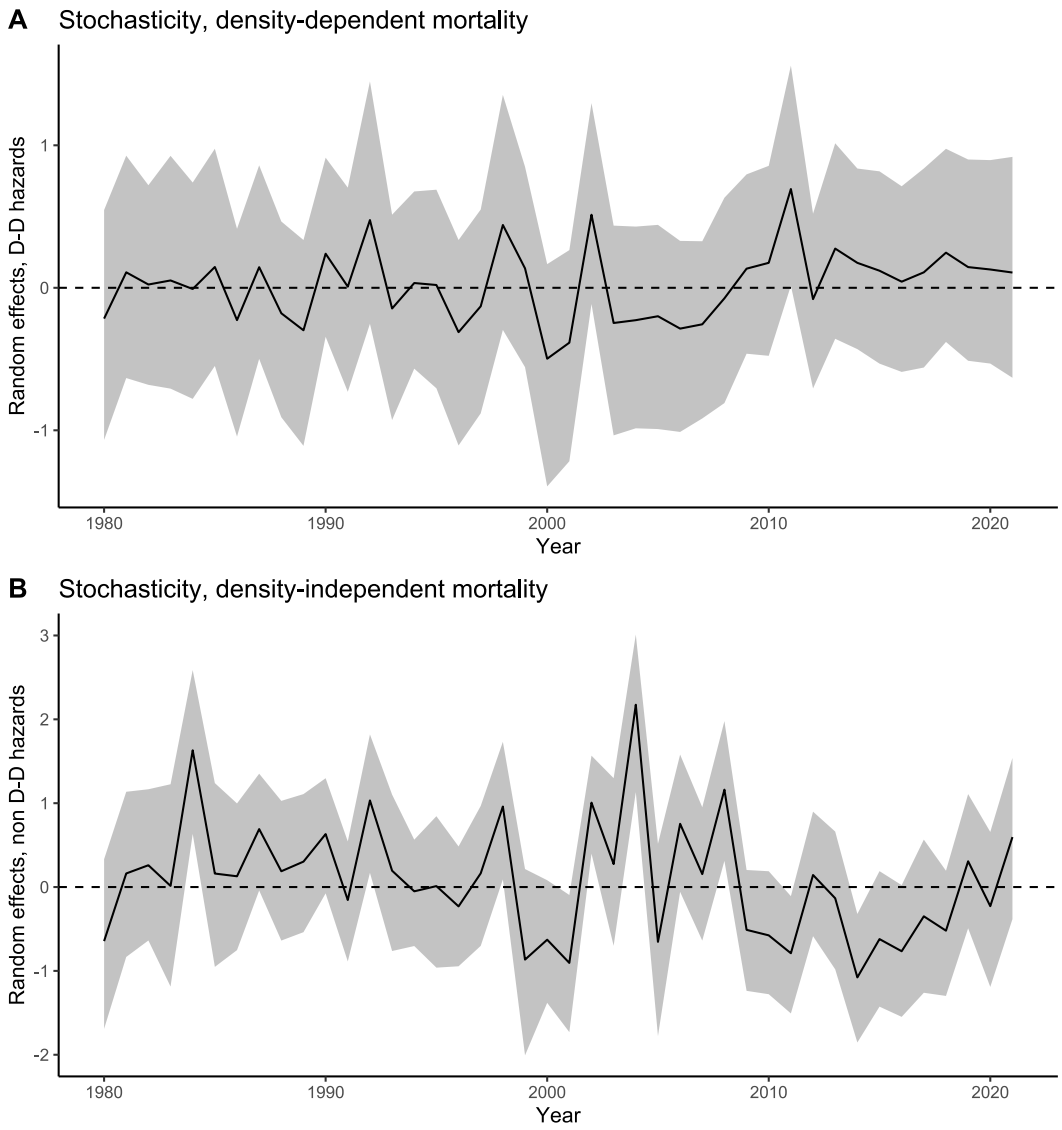

Figure 5. Plots of the random effect terms for densty dependent base hazards (panel A) and density independent base hazards (panel B) over phase 2 of the study period, from an Integrated Model of St Lawrence beluga. The solid lines show the mean estmated value and the shaded bands show the 95% CI. The dashed horizontal line shows the mean value of 0: when the average is above this value there is higher than average unexplained mortality.

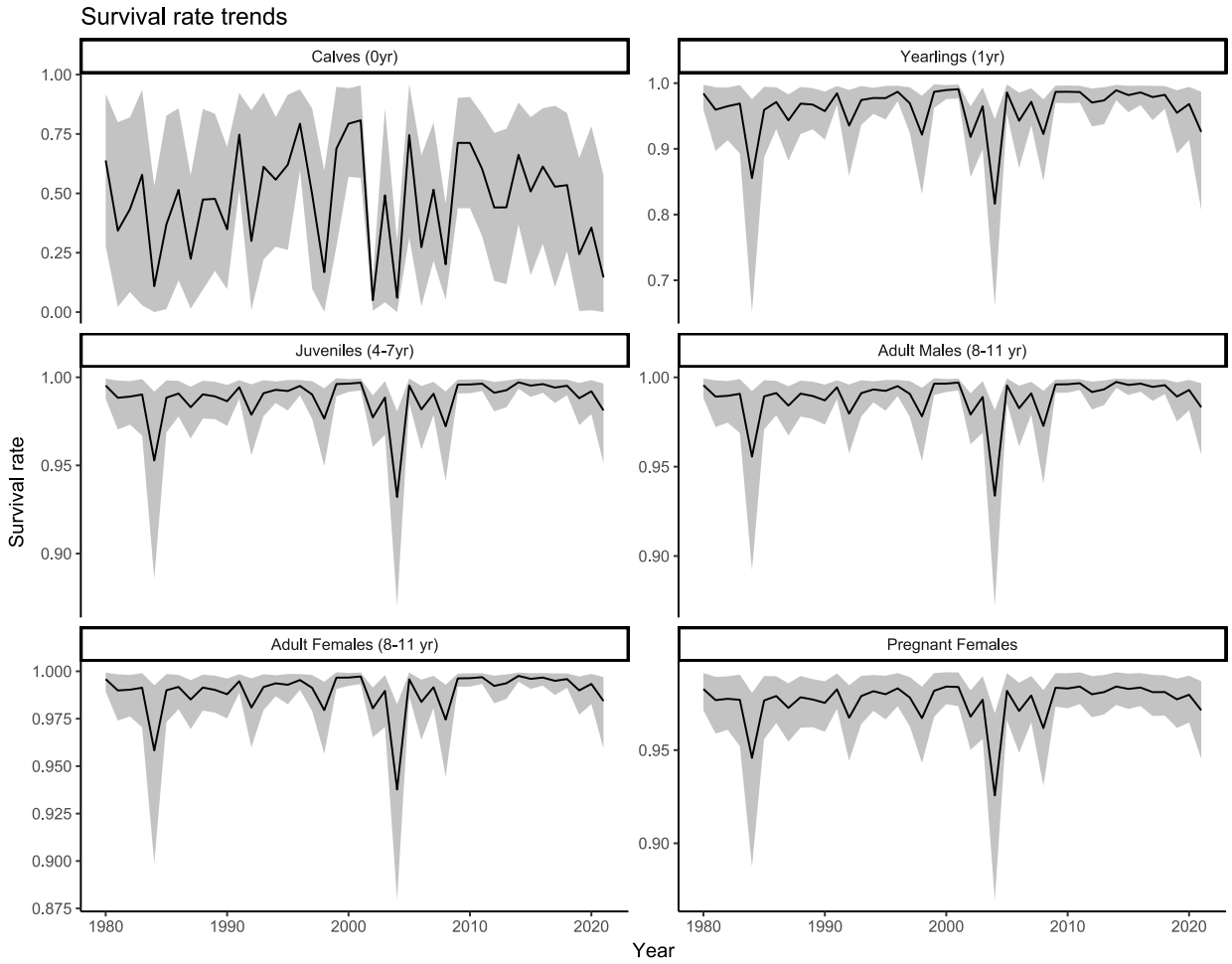

Figure 6. Plots of temporal variation in the estmated annual survival rates for 6 age/sex classes, from an Integrated Model of St Lawrence beluga. The solid lines show the mean estmated value and the shaded bands show the 95% CI.

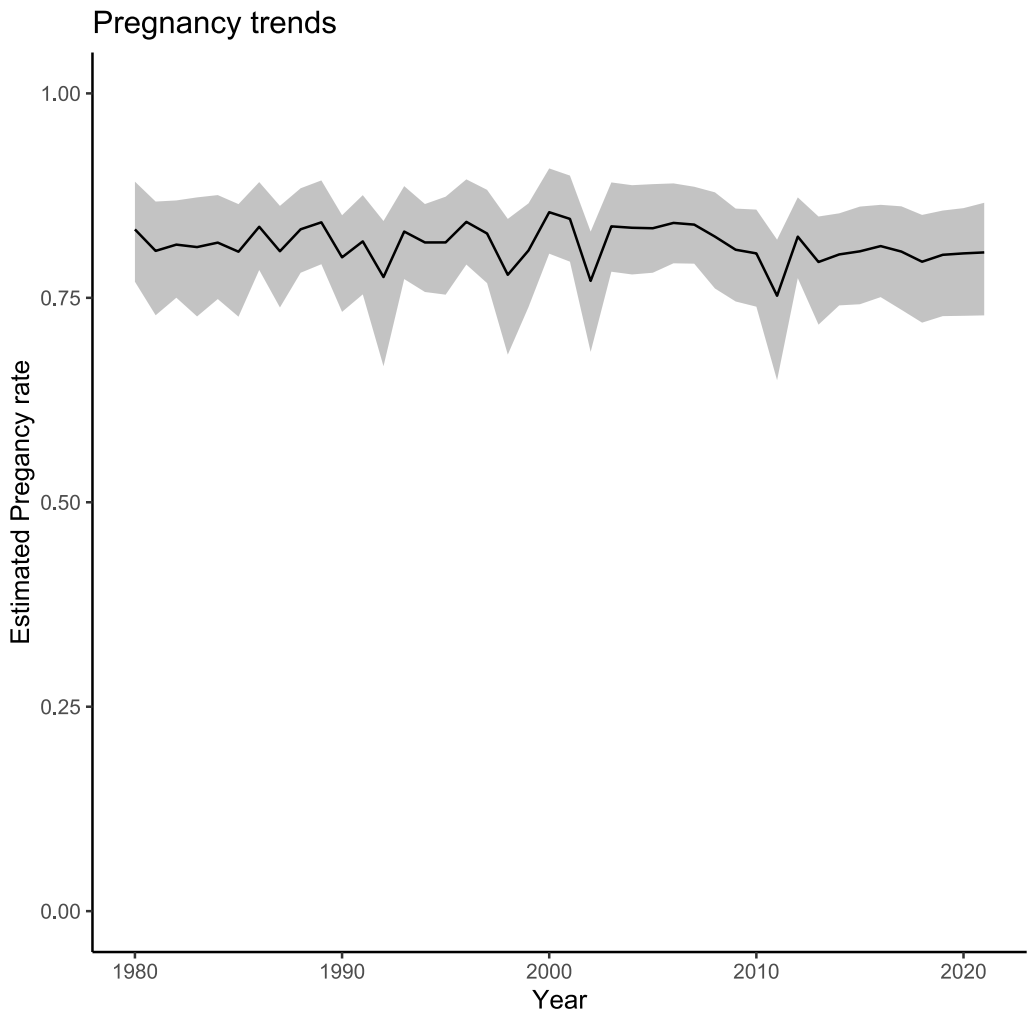

Figure 7. Plot of temporal variation in the estmated pregnancy rate for available adult females, from an Integrated Model of St Lawrence beluga. The solid line shows the mean estmated value and the shaded band shows the 95% CI.

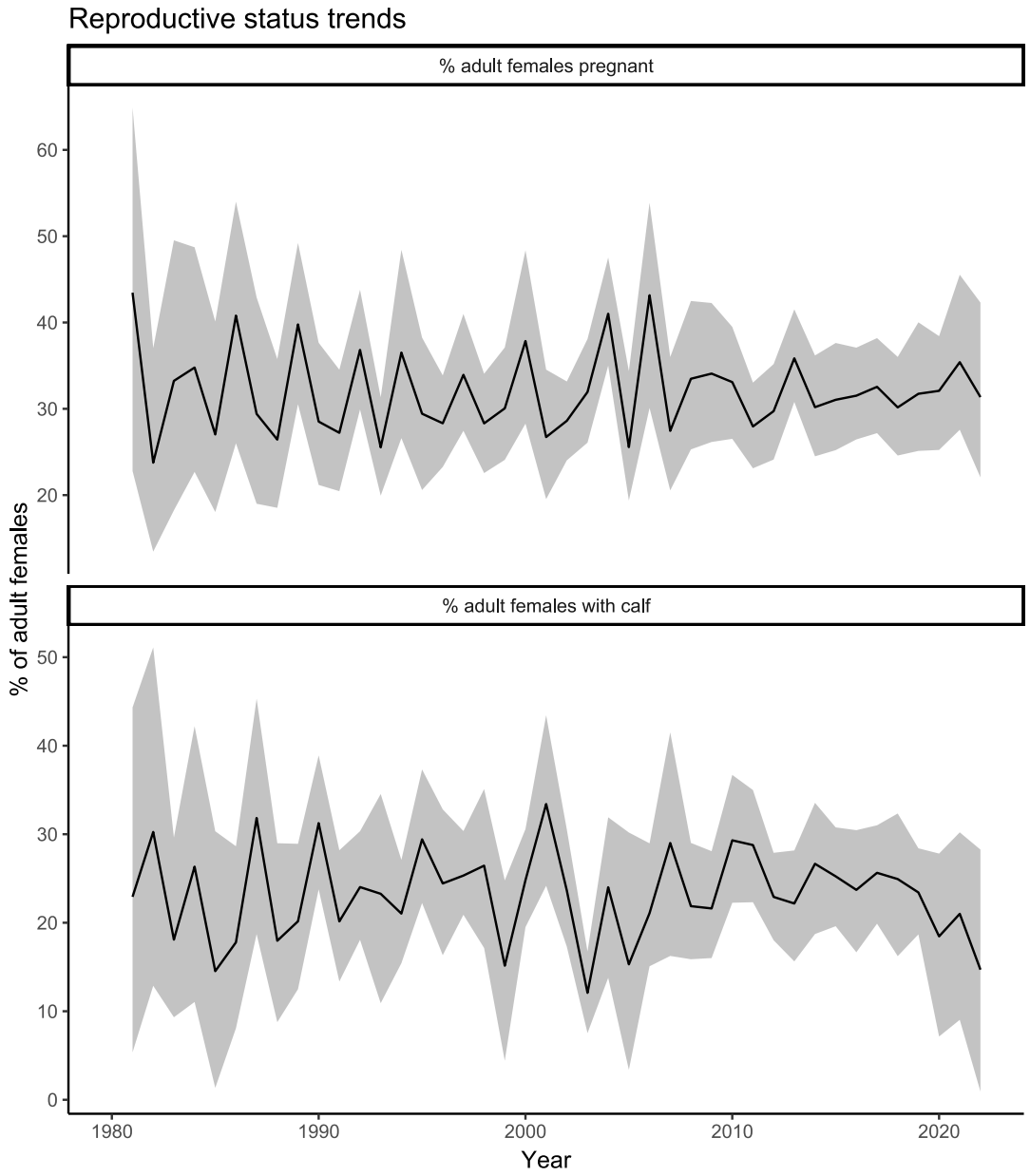

Figure 8. Plots of temporal variation in the estmated proportion of adult females in each of 2 reproductive states, from an Integrated Model of St Lawrence beluga. Panel A shows the prportion of adult females that are pregnat each year, and Panel B shows the Proportion of females accompanied by a dependent calf. The solid lines show the mean estmated value and the shaded bands show the 95% CI.

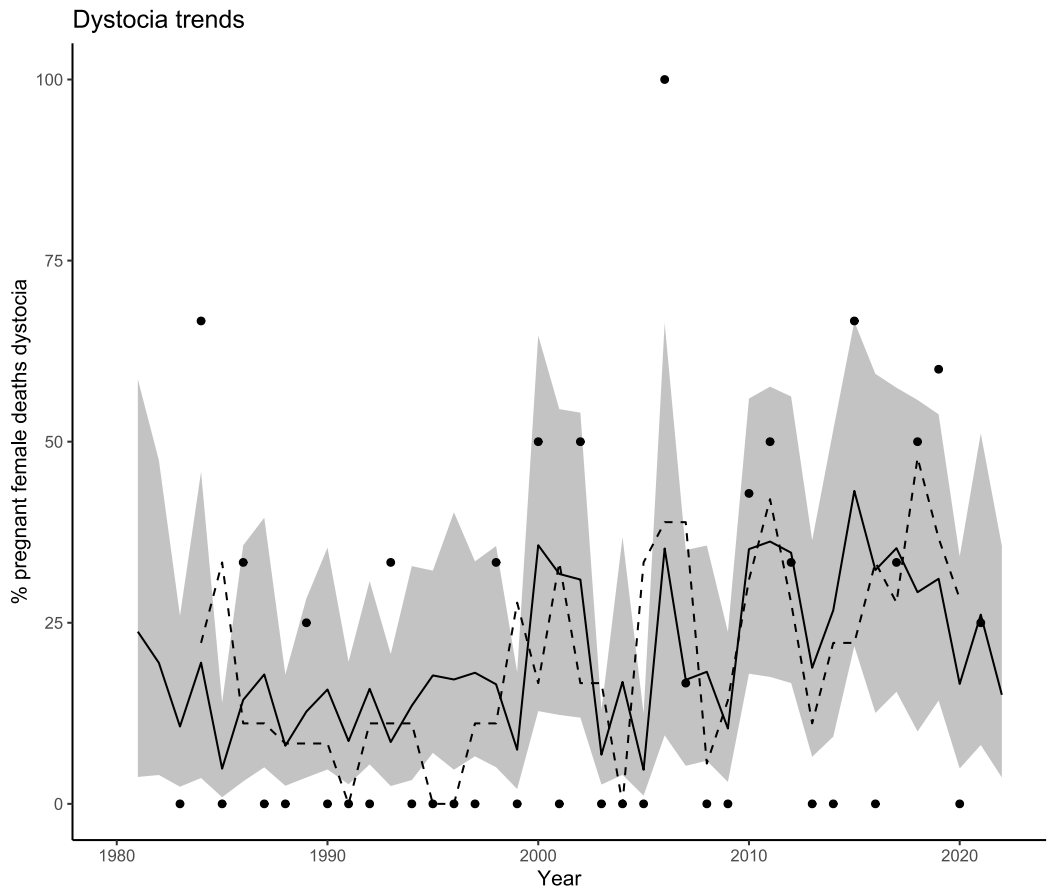

Figure 9. Plot of temporal variation in the estmated proportion of adult female deaths attributable to dystocia/postpartum hazards, from an Integrated Model of St Lawrence beluga. The solid line shows the mean estmated value each year and the shaded band shows the 95% CI as estimated by the model. The solid points represent observed data: the binomial proportions calculated from the ratio of the number of necropsied females with dystocia/postpartum as primary cause of death vs. the total number of adult females necropsied (these data were used for model fitting). The dashed line shows a simple 3-year running average smoother fit to the observed data, for comparison with rhe model estimated values.

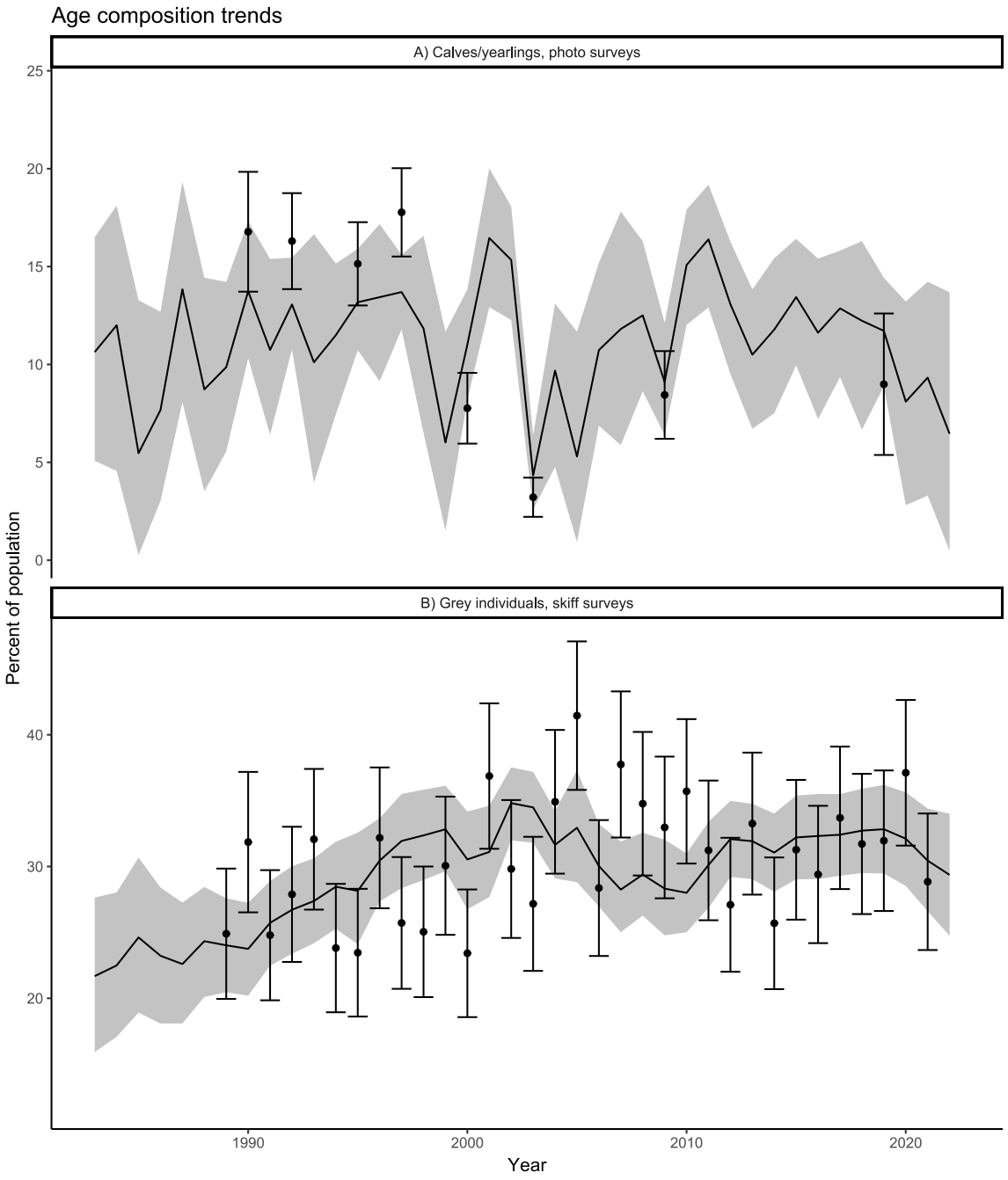

Figure 10. Plots of temporal variation in the estmated percentage of the living populaiton composed of calves and yearlings (Panel A) and of grey-colored individuals (Panel B). For the estimates of % grey individuals, 0-age calves were excluded from the analysis. In each plot the solid lines show the mean estmated value and the shaded bands show the 95% CI. The points and error bars show the observed data correspondig to each estimated statistic: the percent of counts from the photo-based aerial suveys comprisd of calves and yearlings (Panel A) and the percent of grey individuals observed during skiff surveys (Panel B).

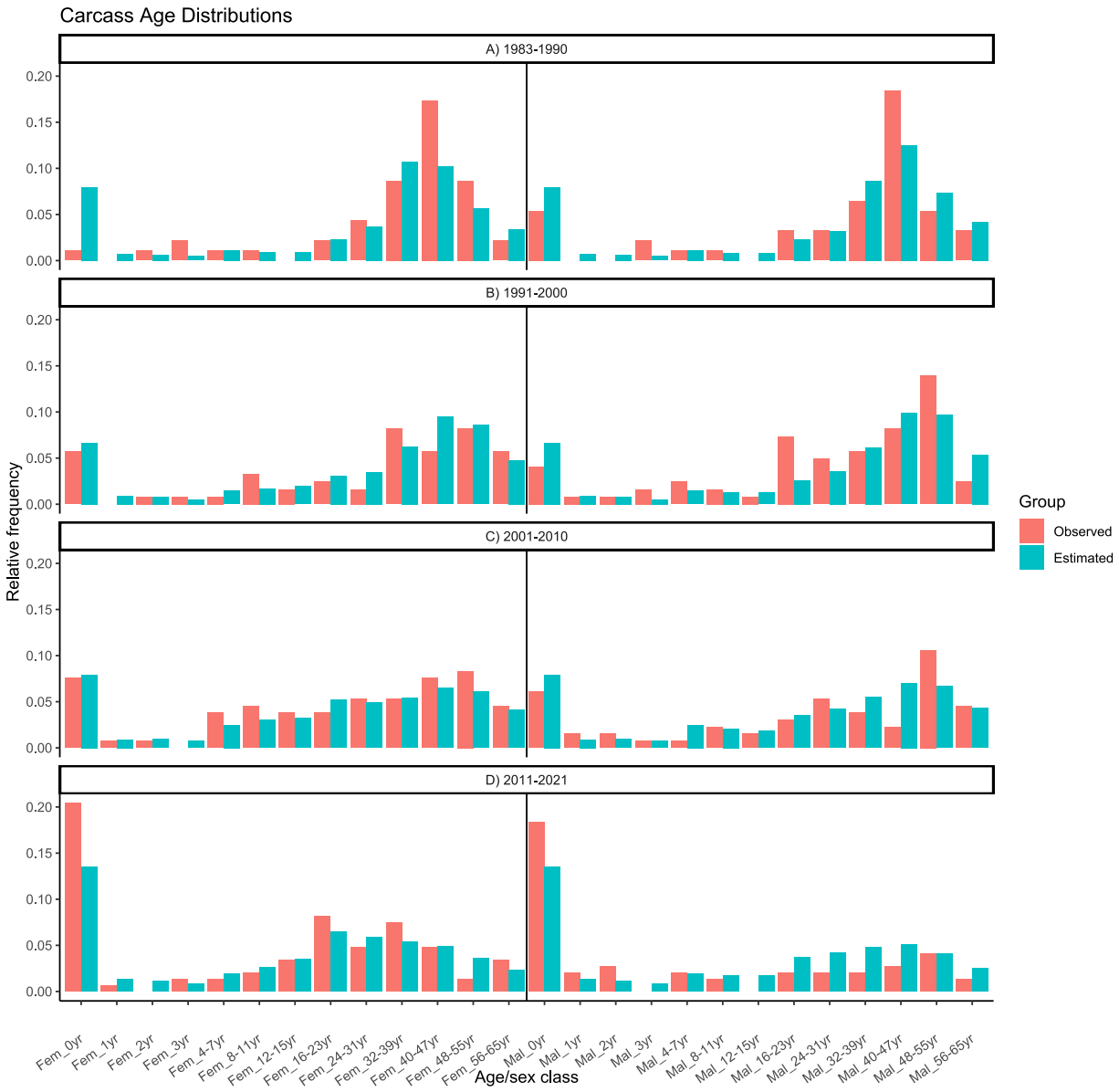

Figure 11. Bar plot showing the age/sex distributin of dead stranded animals for four different temporal periods. Age/sex classes are ordered along the horizontal axis by age (females on left and males on right), and the vertical axis shows the relative frequency of dead individuals within each class. The red bars show observed data (i.e. from counts of dead belugas collected each year, grouped by age/sex class) and the blue-green bars show estimated age/sex distribution of animals dying each year.

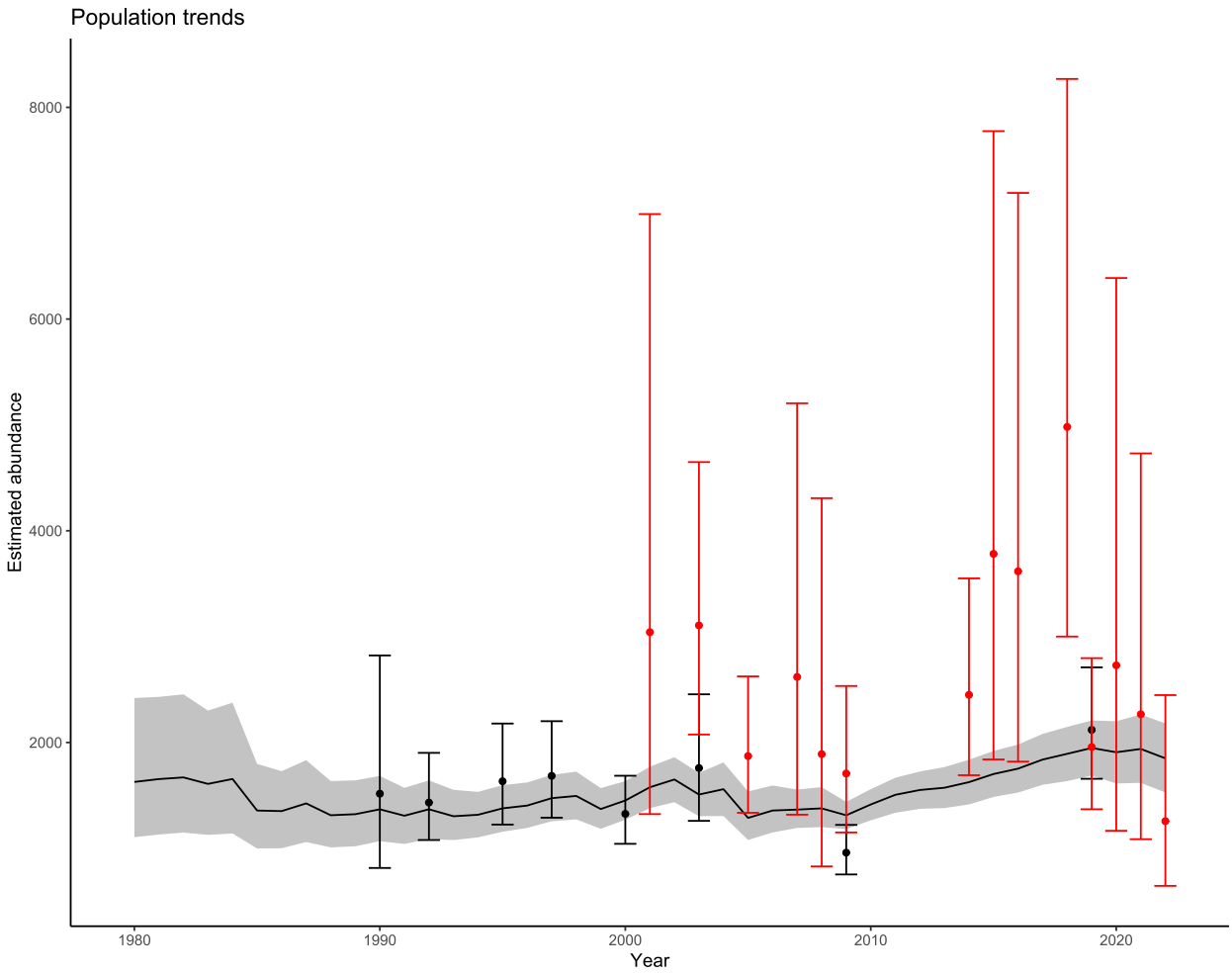

Figure 12. Plot of model estimated trends in abundance from an Integrated Population Model fit to the St. Lawrence Estuary beluga population. The solid line shows the mean abundance estimated by the model for each year, while the shaded band shows the uncertainty (95% CI) around that estimate. The points represent survey-based estimates of abundance from aerial photo-based surveys (black points) and aerial visual surveys (red points), and the associated error bars represent the 95% confidence intervals around each point estimate, calculated from the total variance asssociated wth each survey.

APPENDIX 1. STRANDED CARCASS DATA USED FOR FITTING THE INTEGRATED POPULATION MODEL

Table S 1. Counts of female carcases grouped by year and age category.

Year	0yr	1yr	2yr	3yr	4-7yr	8-12yr	13-15yr	16-23yr	24-31yr	32-39yr	40-47yr	48-55yr	>56yr
1983	0	0	0	0	0	0	0	0	0	0	0	1	1
1984	0	0	0	1	0	0	0	0	0	2	2	0	0
1985	0	0	0	0	0	0	0	1	0	0	1	1	0
1986	0	0	0	1	0	0	0	0	1	1	1	0	0
1987	0	0	0	0	1	0	0	1	0	3	0	0	0
1989	0	0	1	0	0	0	0	0	0	1	7	4	0
1990	0	0	0	0	0	0	0	0	3	1	2	2	0
1993	0	0	0	0	0	1	1	0	0	0	1	3	1
1994	0	0	0	0	0	0	1	1	1	0	0	1	0
1997	0	0	1	0	0	0	0	0	0	1	1	0	3
1998	0	0	0	0	1	0	0	1	0	0	1	0	2
2001	0	0	0	0	0	0	2	0	0	0	0	1	1
2002	0	0	0	0	0	2	0	0	1	0	0	0	1
2005	0	0	0	0	1	0	0	0	0	1	0	2	0
2006	0	0	0	0	2	1	1	1	0	1	1	0	0
2009	0	0	0	0	0	1	1	1	0	0	0	1	0
1988	1	0	0	0	0	1	0	0	0	0	3	0	1
1991	1	0	0	0	0	0	0	0	0	2	1	1	0
1992	1	0	0	0	0	0	0	0	0	0	1	1	0
1995	1	0	0	1	0	0	0	0	0	0	2	2	0
1996	1	0	0	0	0	1	0	0	0	3	0	0	1
2000	1	0	0	0	0	2	0	1	0	3	0	1	0
2003	1	0	0	0	0	0	0	0	0	0	2	0	1
2004	1	0	0	0	0	1	1	0	2	0	1	2	2
2007	1	0	0	0	0	0	0	1	1	2	1	2	0
2013	1	1	0	1	1	0	0	0	2	0	2	0	0
2018	1	0	0	0	0	0	0	1	0	1	3	0	0
2019	1	0	0	0	1	0	0	2	0	1	0	1	0
2022	1	0	0	0	0	0	0	0	0	1	2	1	0
1999	2	0	0	0	0	0	0	0	1	1	0	1	0
2010	2	1	1	0	1	0	0	1	2	0	4	1	0
2011	2	0	0	0	0	0	1	0	1	1	1	0	2
2014	2	0	0	0	0	1	0	0	0	2	0	0	0
2015	2	0	0	0	0	0	0	2	0	2	0	0	0
2017	2	0	0	0	0	1	1	1	0	0	1	1	0
2021	2	0	0	0	0	1	0	2	1	1	0	0	1
2008	5	0	0	0	1	1	0	1	1	3	1	2	1
2016	5	0	0	1	0	0	2	2	0	2	0	0	0
2020	5	0	0	0	0	0	0	0	2	1	0	0	2
2012	7	0	0	0	0	0	1	2	1	0	0	0	0

Table S 2. Counts of male carcases grouped by year and age category.

Year	0yr	1yr	2yr	3yr	4-7yr	8-12yr	13-15yr	16-23yr	24-31yr	32-39yr	40-47yr	48-55yr	>56yr
1983	2	0	0	0	0	0	0	1	0	1	0	0	1
1984	0	0	0	2	0	0	0	0	1	1	0	2	0
1985	0	0	0	0	0	1	0	0	0	1	6	0	0
1986	1	0	0	0	0	0	0	1	0	0	3	0	0
1987	0	0	0	0	0	0	0	0	1	1	1	1	0
1989	1	0	0	0	1	0	0	0	0	1	1	2	0
1990	1	0	0	0	0	0	0	1	1	0	3	0	1
1993	0	0	0	0	0	0	0	0	0	1	3	0	1
1994	2	0	0	0	0	1	0	1	1	0	1	2	0
1997	0	0	0	1	1	0	0	0	2	0	0	3	0
1998	0	0	0	0	1	1	0	2	0	1	3	0	1
2001	0	0	0	0	0	0	0	3	0	0	0	3	2
2002	1	1	0	1	0	0	0	0	0	0	2	2	0
2005	0	0	0	0	0	0	0	1	0	0	1	1	0
2006	1	0	0	0	0	0	1	1	0	1	0	3	0
2009	0	0	1	0	0	0	0	0	1	1	1	2	0
1988	1	0	0	0	0	0	0	0	2	3	2	1	0
1991	0	0	0	0	1	0	0	1	0	1	0	0	0
1992	0	0	0	0	1	0	0	0	0	0	0	2	1
1995	1	0	0	0	0	0	0	2	1	0	1	2	2
1996	1	0	1	0	0	0	0	0	1	1	0	1	0
2000	0	0	1	1	0	0	1	0	1	1	0	3	1
2003	0	0	0	0	0	0	0	0	1	3	0	1	1
2004	0	0	0	0	0	1	0	0	0	0	0	2	0
2007	1	1	0	0	0	0	0	1	1	0	0	1	1
2013	1	0	0	0	0	2	1	1	1	0	2	0	0
2018	1	1	0	0	0	0	0	0	1	0	0	1	0
2019	3	0	0	0	0	0	0	0	0	0	0	1	0
2022	2	1	1	0	0	0	0	0	0	0	0	0	0
1999	5	1	0	0	0	0	0	1	0	0	1	1	0
2010	3	1	0	0	0	1	0	1	0	0	1	1	1
2011	3	0	0	0	0	0	0	0	0	0	0	1	0
2014	5	0	0	0	1	0	0	0	0	1	1	0	0
2015	1	0	0	0	0	0	0	0	0	1	0	0	0
2017	3	0	1	0	0	0	0	0	2	1	0	0	0
2021	2	0	0	0	1	1	0	0	1	0	0	0	0
2008	1	0	1	0	0	0	0	0	0	0	0	1	0
2016	0	0	0	0	0	0	0	1	0	0	0	1	1
2020	2	0	1	0	1	0	0	0	0	0	1	1	0
2012	2	0	0	0	0	0	0	0	2	1	0	0	0

APPENDIX 2. DATA ON PROPORTION OF GREY INDIVIDUALS FROM SKIFF SURVEYS

Table S 3. Estimates based on multiple skiff surveys per year of the mean proportion of grey individuals in the population, and the associated standard error.

Year	Proportion grey	Proportion grey SE
1989	0.2489822	0.02888375
1990	0.3185342	0.03164528
1991	0.2478776	0.0293515
1992	0.2788954	0.04699021
1993	0.3207036	0.03573639
1994	0.2381289	0.02754265
1995	0.2346102	0.02969697
1996	0.3217839	0.03864932
1997	0.2571971	0.03280613
1998	0.2504622	0.02878592
1999	0.3006393	0.03919418
2000	0.2341548	0.03057708
2001	0.3686939	0.05544695
2002	0.2981512	0.04298003
2003	0.2716939	0.03593495
2004	0.3491584	0.03784508
2005	0.4145559	0.0442584
2006	0.2836973	0.03726471
2007	0.3774896	0.0555679
2008	0.3477057	0.06313177
2009	0.329694	0.04028457
2010	0.3571105	0.04307053
2011	0.3122695	0.03623413
2012	0.2709951	0.04772748
2013	0.3325997	0.048287
2014	0.2569434	0.02641769
2015	0.3127364	0.04631133
2016	0.2940015	0.04397167
2017	0.3369856	0.0367393
2018	0.3171821	0.03413617
2019	0.3196218	0.04549226
2020	0.3711851	0.04082216
2021	0.2884716	0.03516331

APPENDIX 3. SUPPLEMENTARY FIGURES

(next pages)

To Stage \ From stage...	1	2	3	4	5	6	7	8	9	10	11	12	13	14	15	16	17	18	19	20	21	22	23	24	25	26	27	28	29	30	31	32	33	34	35	36	37
1	0	0	0	0	0	0	0	0	0	0	0	0	0	q	q	q	q	q	q	q	q	0	0	0	0	0	0	0	0	0	0	0	0	0	0	0	0
2	a	0	0	0	0	0	0	0	0	0	0	0	0	0	0	0	0	0	0	0	0	0	0	0	0	0	0	0	0	0	0	0	0	0	0	0	0
3	0	a	0	0	0	0	0	0	0	0	0	0	0	0	0	0	0	0	0	0	0	0	0	0	0	0	0	0	0	0	0	0	0	0	0	0	0
4	0	0	a	0	0	0	0	0	0	0	0	0	0	0	0	0	0	0	0	0	0	0	0	0	0	0	0	0	0	0	0	0	0	0	0	0	0
5	0	0	0	a	b	0	0	0	0	0	0	0	0	0	0	0	0	0	0	0	0	0	0	0	0	0	0	0	0	0	0	0	0	0	0	0	0
6	0	0	0	0	f	g	0	0	0	0	0	0	0	k	0	0	0	0	0	0	0	o	0	0	0	0	0	0	0	0	0	0	0	0	0	0	0
7	0	0	0	0	0	h	g	0	0	0	0	0	0	l	k	0	0	0	0	0	0	p	o	0	0	0	0	0	0	0	0	0	0	0	0	0	0
8	0	0	0	0	0	0	h	g	0	0	0	0	0	0	l	k	0	0	0	0	0	0	p	o	0	0	0	0	0	0	0	0	0	0	0	0	0
9	0	0	0	0	0	0	0	h	g	0	0	0	0	0	0	l	k	0	0	0	0	0	0	p	o	0	0	0	0	0	0	0	0	0	0	0	0
10	0	0	0	0	0	0	0	0	h	g	0	0	0	0	0	0	l	k	0	0	0	0	0	0	p	o	0	0	0	0	0	0	0	0	0	0	0
11	0	0	0	0	0	0	0	0	0	h	g	0	0	0	0	0	0	l	k	0	0	0	0	0	0	p	o	0	0	0	0	0	0	0	0	0	0
12	0	0	0	0	0	0	0	0	0	0	h	g	0	0	0	0	0	0	l	k	0	0	0	0	0	0	p	o	0	0	0	0	0	0	0	0	0
13	0	0	0	0	0	0	0	0	0	0	0	h	g	0	0	0	0	0	0	l	k	0	0	0	0	0	0	p	o	0	0	0	0	0	0	0	0
14	0	0	0	0	0	i	0	0	0	0	0	0	0	0	0	0	0	0	0	0	0	0	0	0	0	0	0	0	0	0	0	0	0	0	0	0	0
15	0	0	0	0	0	j	i	0	0	0	0	0	0	0	0	0	0	0	0	0	0	0	0	0	0	0	0	0	0	0	0	0	0	0	0	0	0
16	0	0	0	0	0	0	j	i	0	0	0	0	0	0	0	0	0	0	0	0	0	0	0	0	0	0	0	0	0	0	0	0	0	0	0	0	0
17	0	0	0	0	0	0	0	j	i	0	0	0	0	0	0	0	0	0	0	0	0	0	0	0	0	0	0	0	0	0	0	0	0	0	0	0	0
18	0	0	0	0	0	0	0	0	j	i	0	0	0	0	0	0	0	0	0	0	0	0	0	0	0	0	0	0	0	0	0	0	0	0	0	0	0
19	0	0	0	0	0	0	0	0	0	j	i	0	0	0	0	0	0	0	0	0	0	0	0	0	0	0	0	0	0	0	0	0	0	0	0	0	0
20	0	0	0	0	0	0	0	0	0	0	j	i	0	0	0	0	0	0	0	0	0	0	0	0	0	0	0	0	0	0	0	0	0	0	0	0	0
21	0	0	0	0	0	0	0	0	0	0	0	j	i	0	0	0	0	0	0	0	0	0	0	0	0	0	0	0	0	0	0	0	0	0	0	0	0
22	0	0	0	0	0	0	0	0	0	0	0	0	0	m	0	0	0	0	0	0	0	0	0	0	0	0	0	0	0	0	0	0	0	0	0	0	0
23	0	0	0	0	0	0	0	0	0	0	0	0	0	n	m	0	0	0	0	0	0	0	0	0	0	0	0	0	0	0	0	0	0	0	0	0	0
24	0	0	0	0	0	0	0	0	0	0	0	0	0	0	n	m	0	0	0	0	0	0	0	0	0	0	0	0	0	0	0	0	0	0	0	0	0
25	0	0	0	0	0	0	0	0	0	0	0	0	0	0	0	n	m	0	0	0	0	0	0	0	0	0	0	0	0	0	0	0	0	0	0	0	0
26	0	0	0	0	0	0	0	0	0	0	0	0	0	0	0	0	n	m	0	0	0	0	0	0	0	0	0	0	0	0	0	0	0	0	0	0	0
27	0	0	0	0	0	0	0	0	0	0	0	0	0	0	0	0	0	n	m	0	0	0	0	0	0	0	0	0	0	0	0	0	0	0	0	0	0
28	0	0	0	0	0	0	0	0	0	0	0	0	0	0	0	0	0	0	n	m	0	0	0	0	0	0	0	0	0	0	0	0	0	0	0	0	0
29	0	0	0	0	0	0	0	0	0	0	0	0	0	0	0	0	0	0	0	n	m	0	0	0	0	0	0	0	0	0	0	0	0	0	0	0	0
30	0	0	0	0	c	0	0	0	0	0	0	0	0	0	0	0	0	0	0	0	0	0	0	0	0	0	0	0	0	d	0	0	0	0	0	0	0
31	0	0	0	0	0	0	0	0	0	0	0	0	0	0	0	0	0	0	0	0	0	0	0	0	0	0	0	0	0	e	d	0	0	0	0	0	0
32	0	0	0	0	0	0	0	0	0	0	0	0	0	0	0	0	0	0	0	0	0	0	0	0	0	0	0	0	0	0	e	d	0	0	0	0	0
33	0	0	0	0	0	0	0	0	0	0	0	0	0	0	0	0	0	0	0	0	0	0	0	0	0	0	0	0	0	0	0	e	d	0	0	0	0
34	0	0	0	0	0	0	0	0	0	0	0	0	0	0	0	0	0	0	0	0	0	0	0	0	0	0	0	0	0	0	0	0	e	d	0	0	0
35	0	0	0	0	0	0	0	0	0	0	0	0	0	0	0	0	0	0	0	0	0	0	0	0	0	0	0	0	0	0	0	0	0	e	d	0	0
36	0	0	0	0	0	0	0	0	0	0	0	0	0	0	0	0	0	0	0	0	0	0	0	0	0	0	0	0	0	0	0	0	0	0	e	d	0
37	0	0	0	0	0	0	0	0	0	0	0	0	0	0	0	0	0	0	0	0	0	0	0	0	0	0	0	0	0	0	0	0	0	0	0	e	d

Figure S 1. Stage-based projection matrix for St Lawrence Estuary beluga model. Each cell represents the probability of transition from the stage in column i to the stage in row j. Letters symbols represent the equations that describe those probabilities in terms of vital rates and can be cross referenced to the values in Table 1.

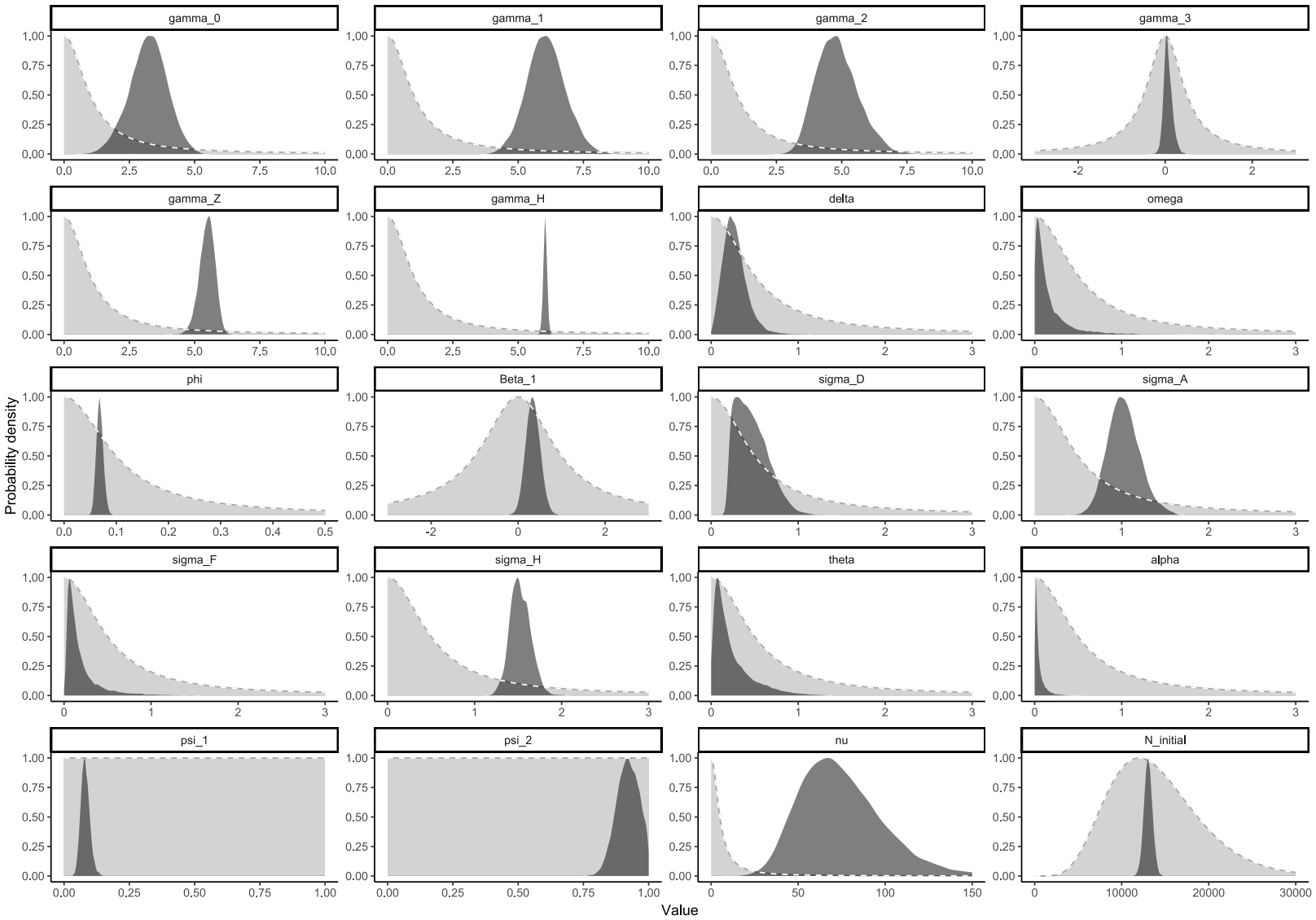

Figure S 2. Comparison of prior distributions (light grey) to posterior distributions (dark grey) for the base parameters of an integrated population model of St Lawrence Beluga

Figure S3 A)

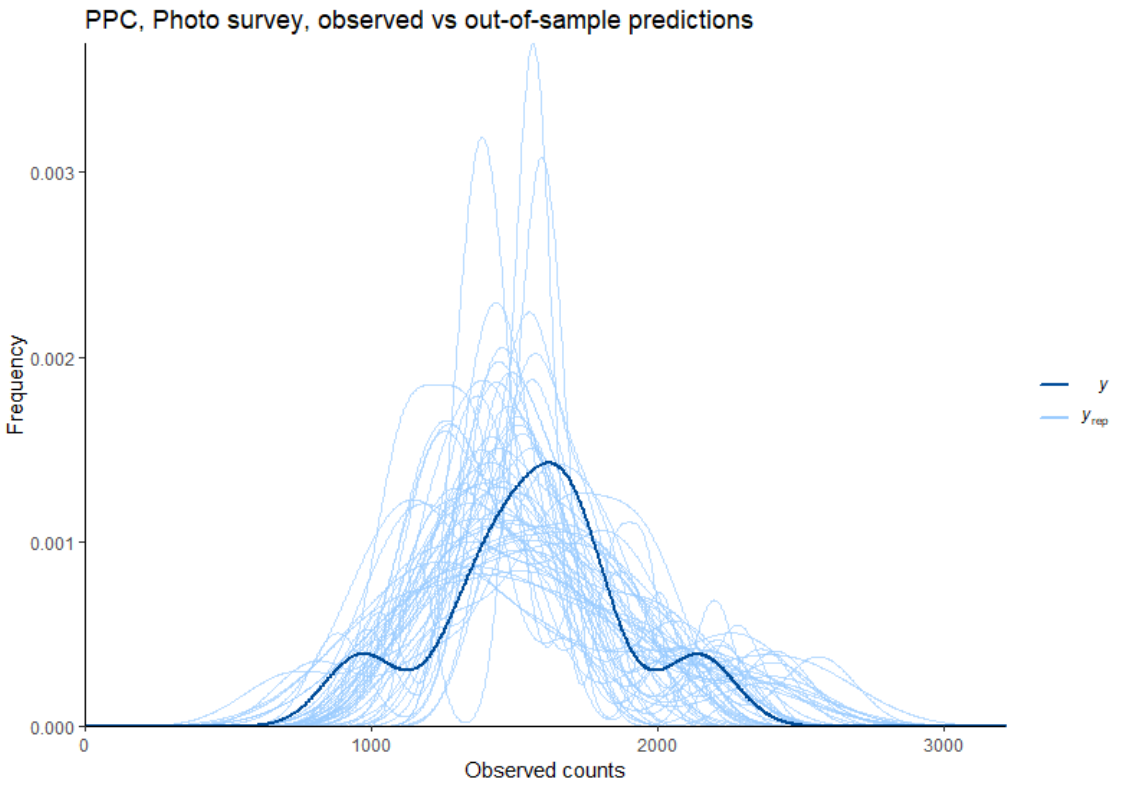

Figure S3 B)

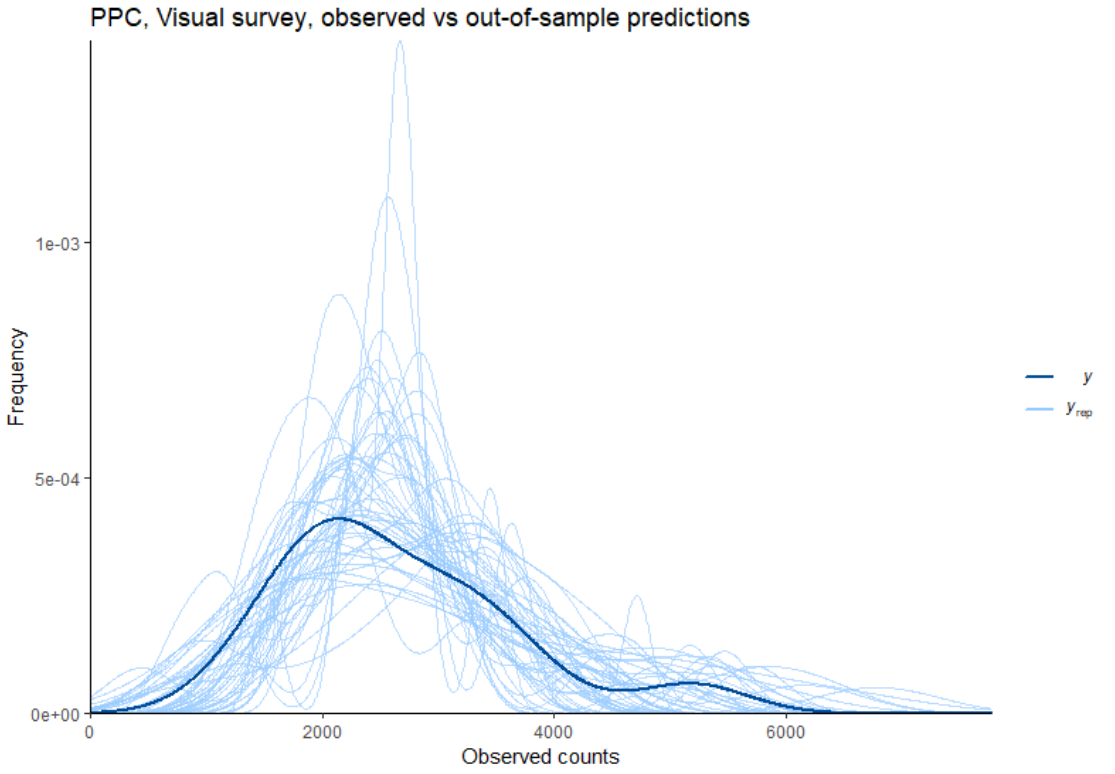

Figure S3 C)

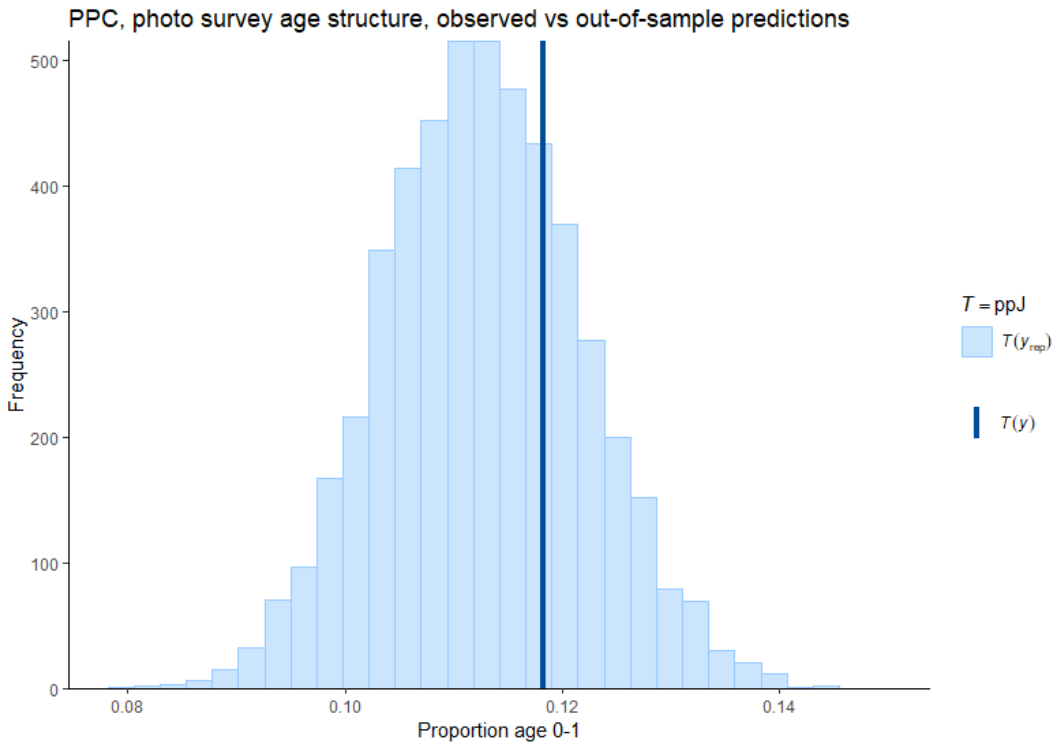

Figure S3 D)

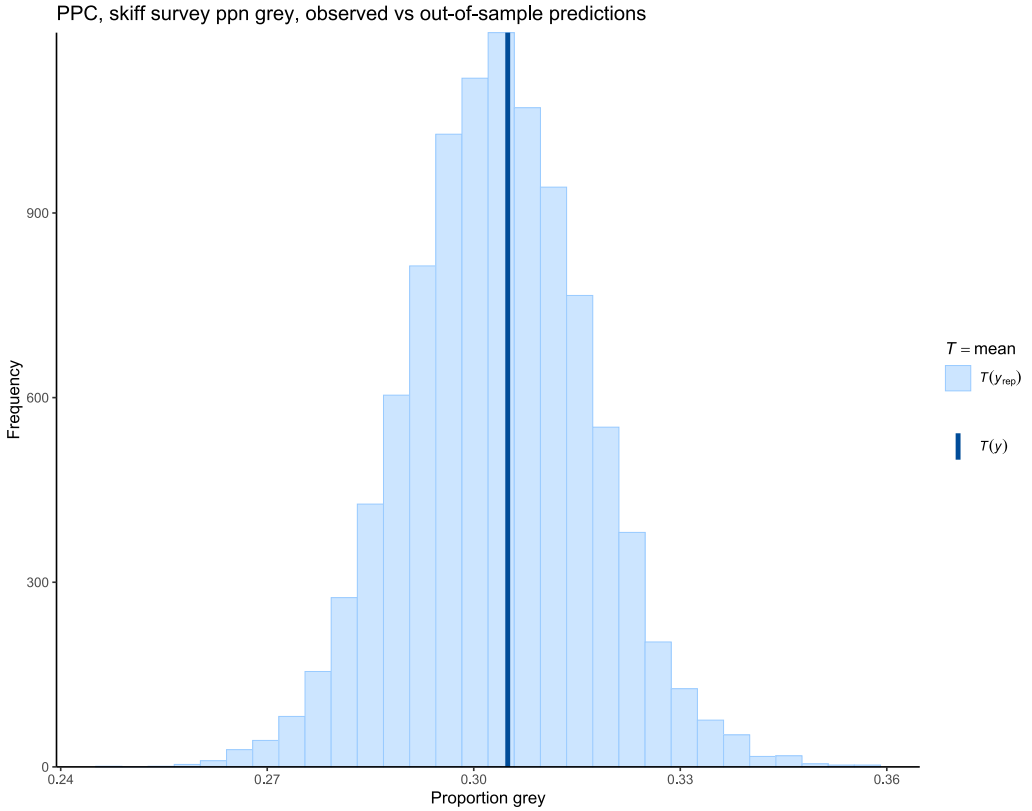

Figure S3 E)

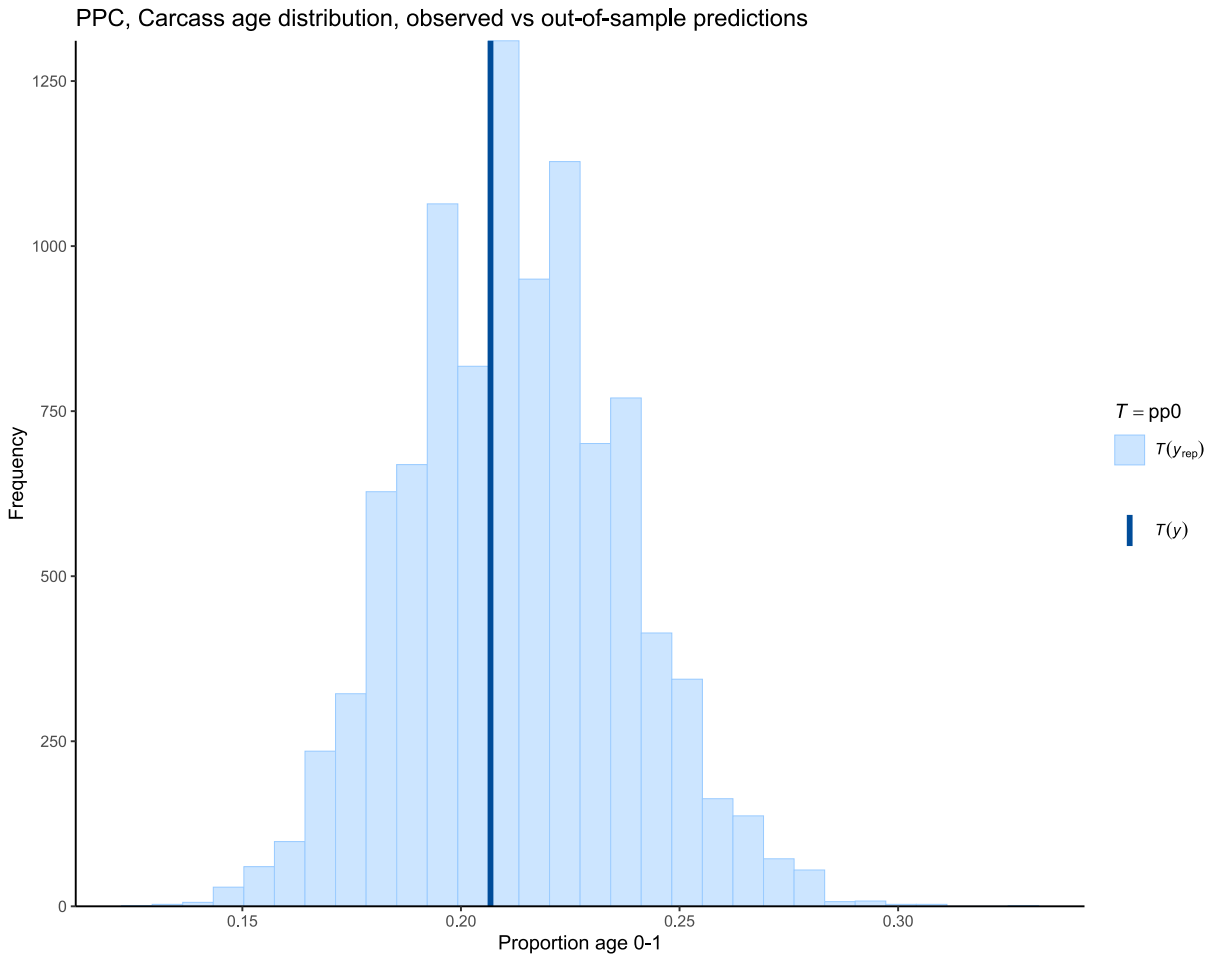

Figure S 3. Posterior predictive plots for an integrated population model of St Lawrence Estuary Beluga. Panels A – E show comparisons of the distributions of observed data (dark blue lines) vs out-of-sample predicted values (light blue lines or bars) generated by the model.

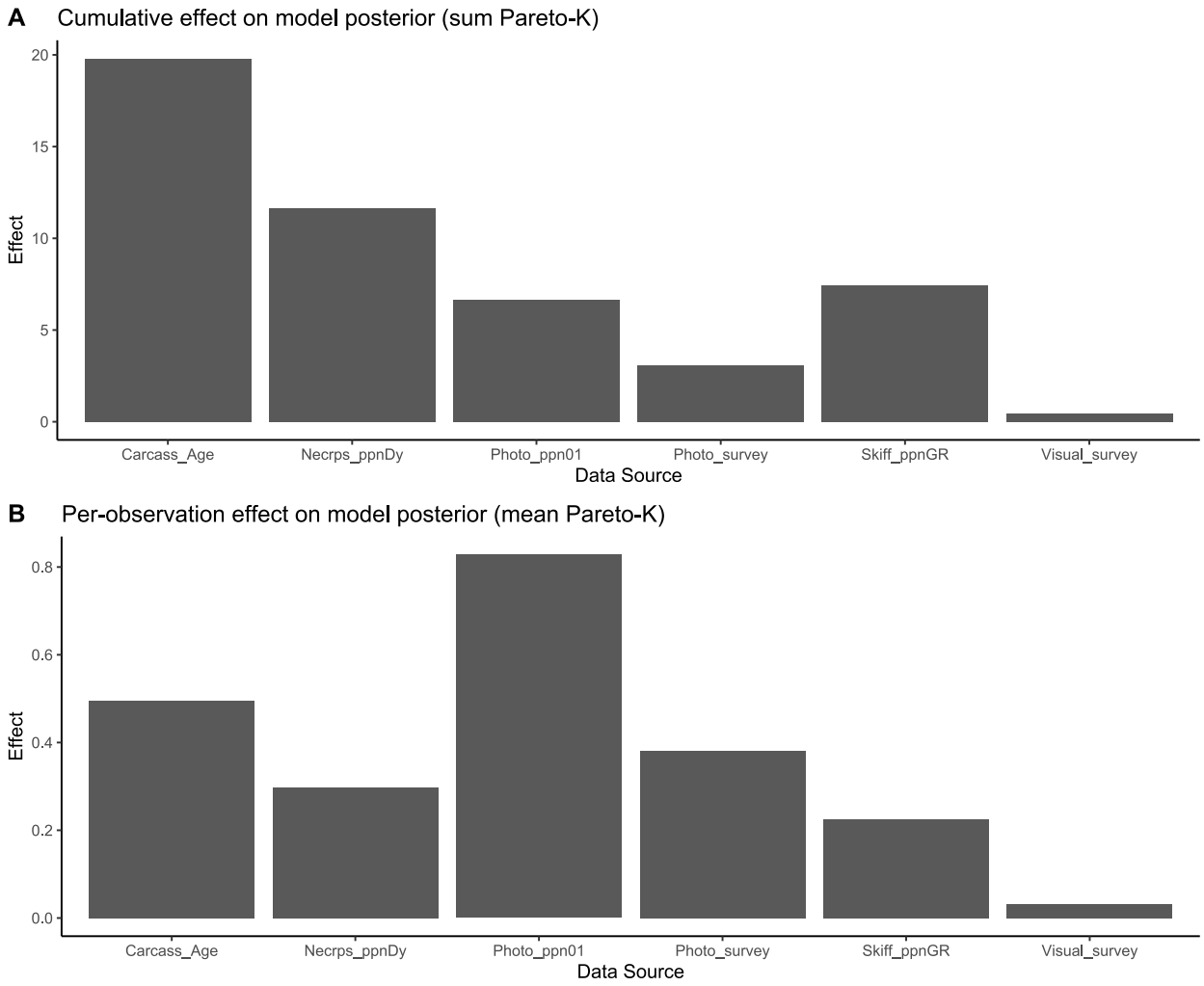

Figure S 4. Estimated influence of various data sources on the model posterior, based on contributions to total model likelihood. Panel A) shows the cumulative effect of data sources (reflecting both the per-data-point influence and the number of data points per data source), while panel B) shows the average influence for each data point for the specified data source.

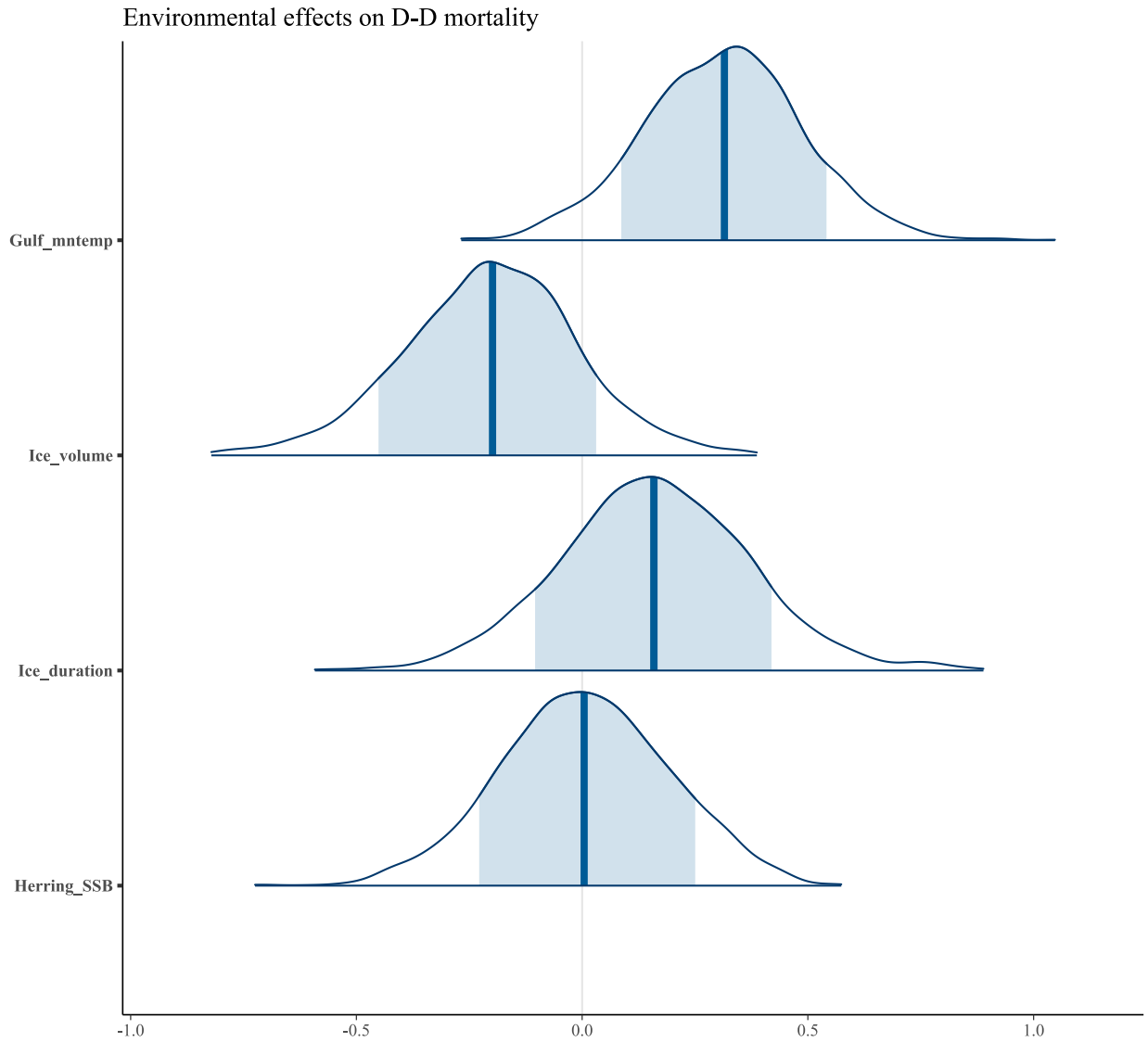

Figure S 5. Postrior distributions for the estimated effects of 4 environmental variables on the base hazard rate for calves, as estimated from an Integrated Population model fit to St. Lawrence Esturary beluga. Units on the horizontal axis represent log hazard ratio vaues, and the vertical axis shows the relative probability of a given value. The shaded areas under each curve designate 80% of the distribution (the 80% credible interval, or CI): if the shaded area does not overlap the 0 line then the effect is considered to be significant. Only the effect of Gulf mean temperature was signifant, although Ice Volume variable was only marginally nonsignificant. A 5th variable, mean Caplin biomass, is not show here but was also non significant with mean posterior centered on 0 (identical to posterior for Herring_SSB).

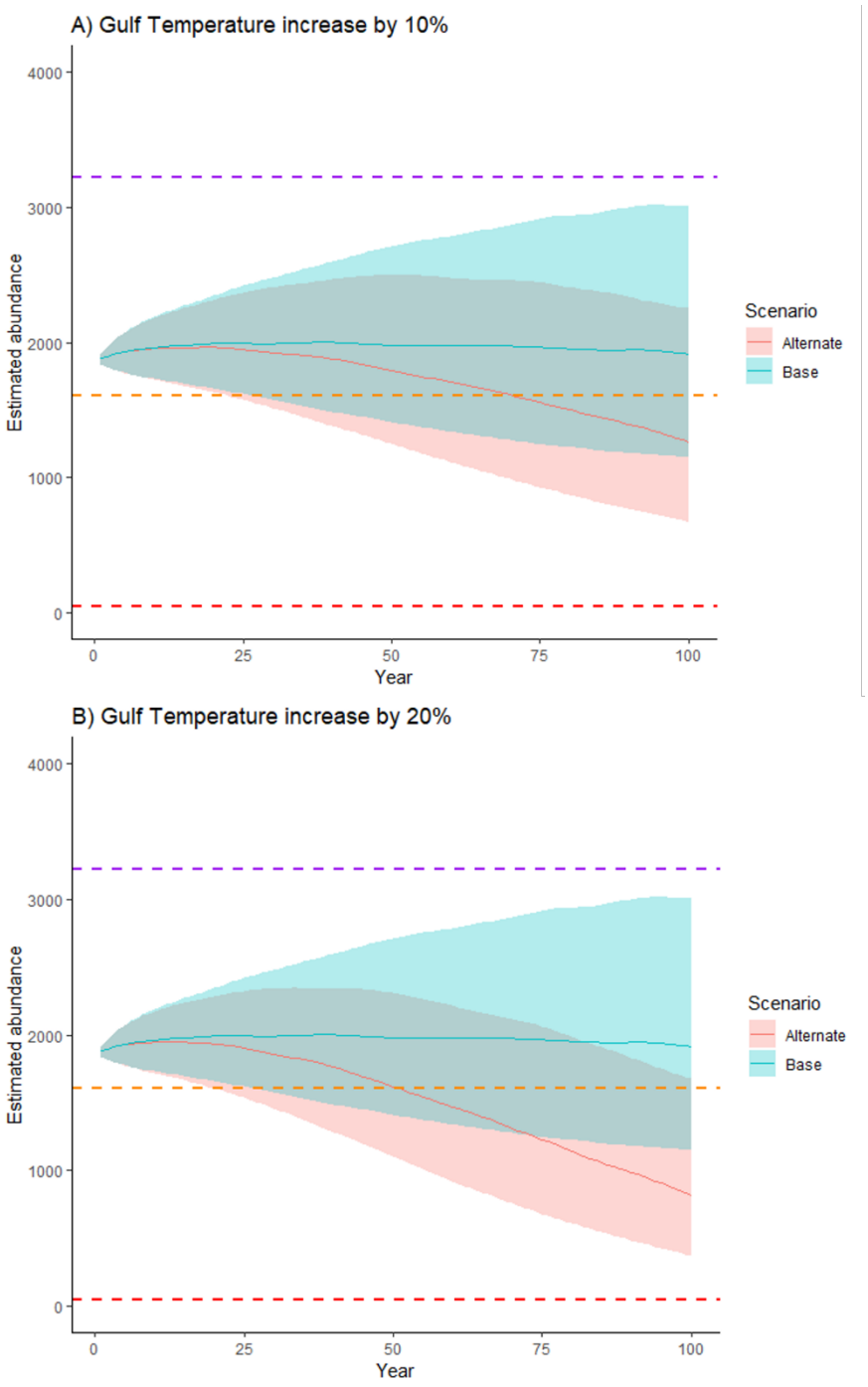
A) Gulf Temperature increase by 10%
Estimated abundance
4000
3000
2000
1000
0
0
25
50
75
100
Year
Scenario
Alternate
Base
B) Gulf Temperature increase by 20%
Estimated abundance
4000
3000
2000
1000
0
0
25
50
75
100
Year
Scenario
Alternate
Base

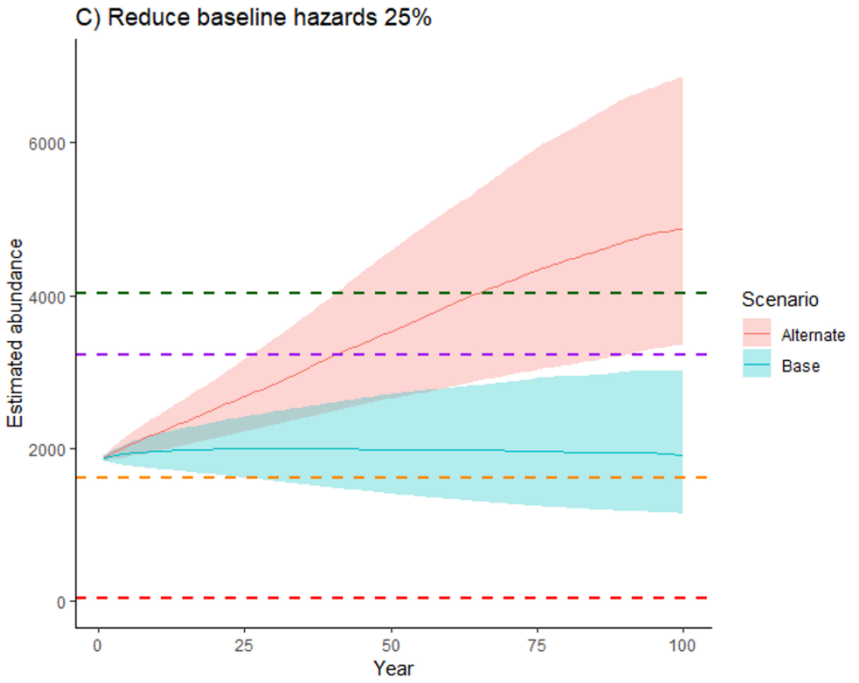
C) Reduce baseline hazards 25%
Estimated abundance
6000
4000
2000
0
0
25
50
75
100
Year
Scenario
Alternate
Base

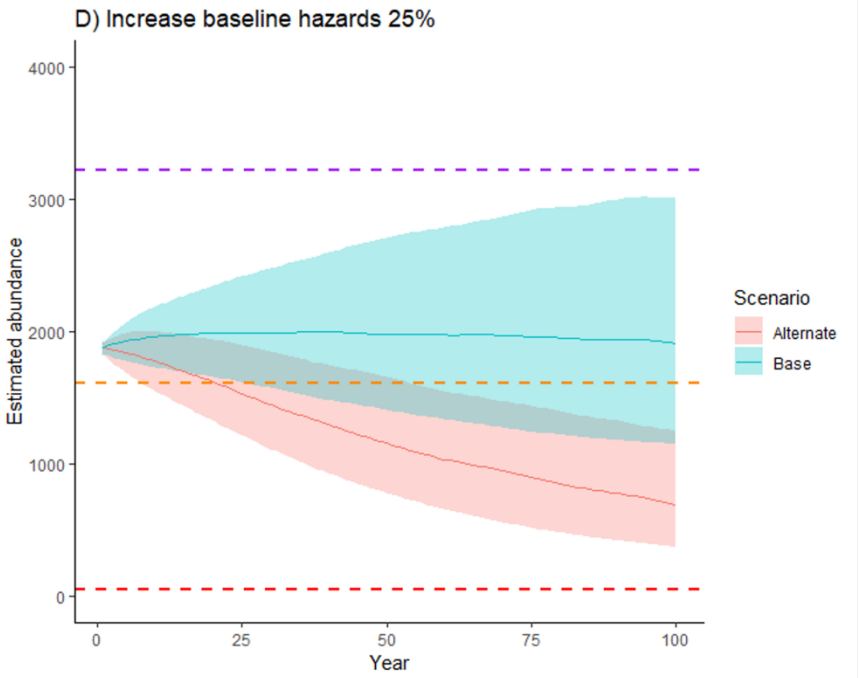
D) Increase baseline hazards 25%
Estimated abundance
4000
3000
2000
1000
0
0
25
50
75
100
Year
Scenario
Alternate
Base

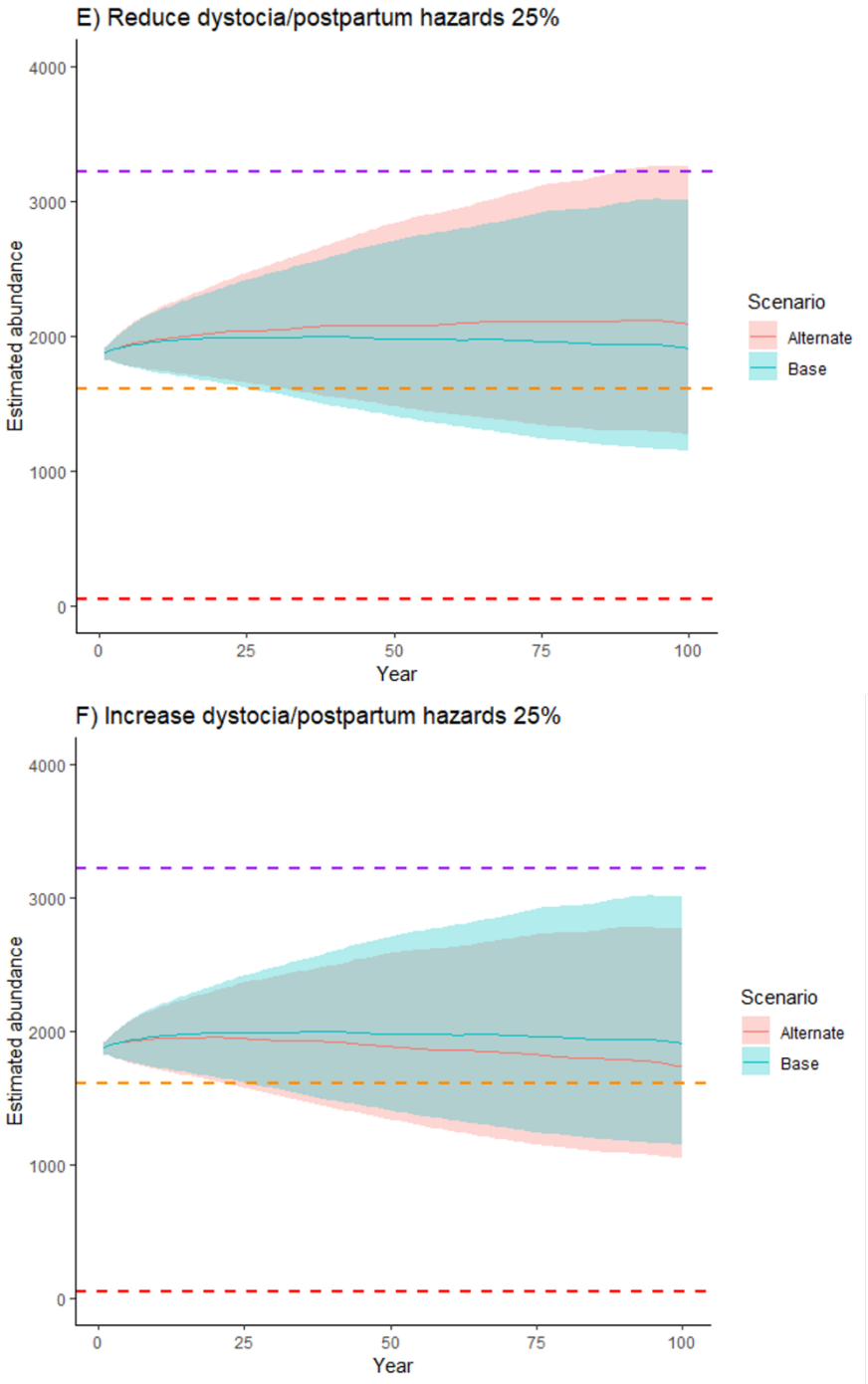

Figure S 6. Results from model projections of future population dynamics for St. Lawrence Estuary beluga. Plots A – F show simulated population dynamics for alternative scenarios of future conditions or management effects (light red) as compared to baseline scenario (light blue): the alternate scenario is described in the plot title (refer to Table 4 for details). Dashed lines show possible management thresholds: MNPL (green), PRL (purple), LRL (orange) and Quasi-extinction threshold (QE; red). Solid lines show mean of iterated simulations and shaded bands show the inter-quartile range.